

POLITECNICO DI MILANO

MSc in Building and Architectural Engineering

Major – Building Engineering



**EARTHQUAKE VULNERABILITY ASSESSMENT OF A  
MASONRY MONUMENT INCLUDING SOIL- FOUNDATION-  
STRUCTURE INTERACTION**

SUPERVISOR:

Prof. Maria Adelaide Vittoria Parisi

CO - SUPERVISOR:

Prof. Dimitrios Pitilakis

AUTHOR:

Eleonora Devetak

Matr. 896767

Academic year 2018 – 2019



# Abstract

The following dissertation analyses the structural behaviour of a masonry monument during an earthquake, taking into consideration the relation between soil, foundation and structure. The case study is Hagia Sophia Church in Thessaloniki, Greece.

The aim of the thesis is to obtain a clear view of the answers of the structure to the applied earthquake, through a linear analysis of the constructed model.

Two different models have been used to highlight the influence of a flexible base on the results, that appear to be more reliable respect to a fixed base case.

Starting from a modal analysis and then picturing the stresses distribution, the weaknesses of the building have been found out. To avoid the expected damages, a strengthening solution based on micropiles is proposed.

Therefore an analysis with the new characteristics of the building, once the micropiles are applied, is carried out to show how effective this technique is on the case study.



# Sommario

La seguente trattazione analizza il comportamento strutturale di un monumento in muratura durante un terremoto, tenendo in considerazione la relazione tra suolo, fondazione e struttura. Il caso studiato è la Chiesa di Hagia Sophia a Thessaloniki, in Grecia.

Lo scopo del lavoro è ottenere una immagine chiara della risposta della struttura all'imposizione di un sisma, attraverso una analisi lineari del modello costruito. Sono stati utilizzati due differenti modelli per sottolineare l'influenza di una base flessibile sui risultati, che appaiono maggiormente affidabili rispetto ad un caso con base fissa.

Partendo da una analisi modale e analizzando la distribuzione degli sforzi, sono stati identificati i punti deboli dell'edificio. Una soluzione di rinforzo strutturale, basata su micropali, viene quindi proposta con l'obiettivo di ridurre i danni previsti.

In conclusione, viene effettuata una analisi con il modello modificato tenendo conto dell'effetto benefico dei micropali, mostrando così quanto questa tecnica sia efficace per il caso studiato.



# Contents

LIST OF FIGURES .....	4
LIST OF TABLES .....	7
INTRODUCTION .....	9
<b>1 HISTORIC CONTEXT OF HAGIA SOPHIA CHURCH .....</b>	<b>11</b>
1.1 HISTORICAL ANALYSIS .....	11
1.2 CONSTRUCTION PHASES .....	13
1.3 EARTHQUAKES IN THESSALONIKI .....	20
<b>2 LOAD- BEARING STRUCTURE AND CONSTRUCTION MATERIALS.....</b>	<b>23</b>
2.1 GEOMETRY OF THE CHURCH.....	23
2.2 CONSTRUCTION OF THE CHURCH .....	25
2.3 CONSTRUCTION MATERIALS DESCRIPTION .....	26
2.4 MECHANICAL PROPERTIES OF THE CONSTRUCTION MATERIALS .....	27
<b>3 REGULATIONS AND DIGITAL MODELLING.....</b>	<b>28</b>
3.1 NORMATIVE.....	28
3.2 EUROCODE 6.....	28
3.2.1 KADET.....	31
3.3 SOIL- STRUCTURE INTERACTION - NIST .....	36
3.4 STRUCTURAL SIMULATION WITH THE SOFTWARE ETABS.....	43
3.4.1 ETABS SOFTWARE.....	43
3.4.2 ASSUMPTIONS FOR MODELLING SIMULATION .....	43
3.4.3 CONSTRUCTION MATERIALS SIMULATION.....	44
3.4.4 MODEL CREATION IN ETABS.....	50
3.4.5 FOUNDATION SIMULATION IN ETABS.....	53
<b>4 LOADS AND REACTIONS OF THE MODEL.....</b>	<b>63</b>
4.1 LOADING CONDITION .....	63
4.1.1 VERTICAL CONTRIBUTION OF DOME AND ROOF.....	63
4.1.2 WEIGHT OF THE LOAD- BEARING MASONRY .....	66
4.1.3 MODAL ANALYSIS.....	66
4.1.4 DYNAMIC LOAD .....	69
4.2 ANSWER OF THE STRUCTURE UNDER SEISMIC ACTION .....	70

<b>5</b>	<b>STRENGTHENING MEASURES .....</b>	<b>81</b>
<b>5.1</b>	<b>REINFORCEMENT OF THE FOUNDATIONS .....</b>	<b>81</b>
<b>5.2</b>	<b>REINFORCEMENT USING MICROPILES.....</b>	<b>84</b>
<b>5.3</b>	<b>SIMULATION OF MICROPILES AND REINFORCEMENT RESULTS OF THE ANALYSIS .....</b>	<b>89</b>
<b>6</b>	<b>CONCLUSIONS.....</b>	<b>96</b>
	<b>REFERENCES.....</b>	<b>98</b>





# List of Figures

Figure 1-1 - Plan of Hagia Sophia Church (K. Theoharidou. 1988).....	17
Figure 1-2 - North facade of Hagia Sophia Church (K. Theoharidou. 1988).....	18
Figure 1-3 -South facade of Hagia Sophia Church (K. Theoharidou. 1988).....	18
Figure 1-4 - East facade of Hagia Sophia Church (K. Theoharidou. 1988).....	19
Figure 1-5 - West facade of Hagia Sophia Church (K. Theoharidou. 1988).....	19
Figure 1-6 - Earthquake in Volvi on the 20 <sup>th</sup> of June 1978 (Mossiopoulos et al., 2008).....	21
Figure 1-7 - Response spectrum of the earthquake registered in Thessaloniki on the 20 <sup>th</sup> of June 1978 (Mossiopoulos et al., 2008).....	21
Figure 1-8 - Photo of Hagia Sophia Church during the 80's with repairs in development from the earthquake of 1978.....	22
Figure 2-1 - Metrical relations in the design of the church (plan view) (K. Theoharidou, 1988).....	24
Figure 3-1 - Vertical section of the foundation.....	33
Figure 3-2- Vertical section of the masonry of phase C.....	34
Figure 3-3 - Vertical section of the masonry of phase A and B .....	34
Figure 3-4 - Deflection caused by force applied to a single- degree- of- freedom structure represented by a simple oscillator: in case of: (a) fixed base structure; (b) structure with vertical, horizontal and rotational flexibility at its base.....	37
Figure 3-5 - Static stiffness of rigid footings at the ground surface .....	41
Figure 3-6 - Embedment correction factors for static stiffness of rigid footings.....	41
Figure 3-7 - Dynamic stiffness modifiers and radiation damping ratios for rigid footings .....	42
Figure 3-8 - Dynamic stiffness modifiers and radiation damping ratios for embedded footings .....	42
Figure 3-9 - Introduction of the foundation characteristics in ETABS .....	46
Figure 3-10 - Introduction of the A and B phase masonry characteristics in ETABS.....	47
Figure 3-11 - Introduction of the C phase masonry characteristics in ETABS.....	48
Figure 3-12 - Introduction of the marble characteristics in ETABS.....	49
Figure 3-13 - First phase of the model creation.....	50
Figure 3-14 - 3D model in ETABS.....	51
Figure 3-15 - Final model, including the assumptions made for the geometry of the building.....	51
Figure 3-16 - Openings creation in each wall of the monument .....	52
Figure 3-17 - Top view of the second level diaphragm.....	52
Figure 3-18 – Section of the soil under the Agia Sophia Church .....	53
Figure 4-1 - Vertical section of Hagia Sophia Church at the dome level.....	64
Figure 4-2 – Roof plan of Hagia Sophia Church .....	64
Figure 4-3 - Imposition of the covering loads on the perimeter of the building.....	66
Figure 4-4 - Modal analysis of the flexible model in x-axis direction. The displacements values [mm] are quantitatively (based on colour) shown in the horizontal axis at the bottom of the image.....	67
Figure 4-5 - Modal analysis of the flexible model in y-axis direction. The displacements values [mm] are quantitatively (based on colour) shown in the horizontal axis at the bottom of the image.....	67
Figure 4-6 - Modal analysis of the fixed- base model in x-axis direction. The displacements values [mm] are quantitatively (based on colour) shown in the horizontal axis at the bottom of the image.....	68
Figure 4-7 - Modal analysis of the fixed- base model in y-axis direction. The displacements values [mm] are quantitatively (based on colour) shown in the horizontal axis at the bottom of the image.....	68
Figure 4-8 - Geographical location of the City Hotel in Thessaloniki.....	69
Figure 4-9 - Seismic history along x direction.....	69

Figure 4-10 - Seismic history along y direction .....	70
Figure 4-11 - Floor plan of Hagia Sophia Church with orientation .....	70
Figure 4-12 – Maximum principal stresses distribution on the north wall of the flexible model. The principal stress values [MPa] are qualitatively shown based on colour in the horizontal axis at the bottom of the image. ....	73
Figure 4-13 – Maximum principal stresses distribution on the south wall of the flexible model. The principal stress values [MPa] are qualitatively shown based on colour in the horizontal axis at the bottom of the image. ....	73
Figure 4-14 – Maximum principal stresses distribution on the west wall of the flexible model. The principal stress values [MPa] are qualitatively shown based on colour in the horizontal axis at the bottom of the image. ....	74
Figure 4-15 - Maximum shear stress distribution on the north wall of the flexible model. The shear stress values [MPa] are qualitatively shown based on colour in the horizontal axis at the bottom of the image. 74	74
Figure 4-16 - Maximum shear stresses distribution on the south wall of the flexible model. The shear stress values [MPa] are qualitatively shown based on colour in the horizontal axis at the bottom of the image. ....	75
Figure 4-17 - Maximum shear stresses distribution on the west wall of the flexible model. The shear stress values [MPa] are qualitatively shown based on colour in the horizontal axis at the bottom of the image. 75	75
Figure 4-18 – Maximum principal stresses distribution on the north wall of the fixed- base model. The principal stress values [MPa] are qualitatively shown based on colour in the horizontal axis at the bottom of the image.....	76
Figure 4-19 - Maximum principal stresses distribution on the south wall of the fixed- base model. The principal stress values [MPa] are qualitatively shown based on colour in the horizontal axis at the bottom of the image. ....	76
Figure 4-20 - Maximum principal stresses distribution on the west wall of the fixed- base model. The principal stress values [MPa] are qualitatively shown based on colour in the horizontal axis at the bottom of the image. ....	77
Figure 4-21 - Maximum shear stresses distribution on the north wall of the fixed- base model. The shear stress values [MPa] are qualitatively shown based on colour in the horizontal axis at the bottom of the image. ....	77
Figure 4-22 - Maximum shear stresses distribution on the south wall of the fixed- base model. The shear stress values [MPa] are qualitatively shown based on colour in the horizontal axis at the bottom of the image. ....	78
Figure 4-23 - Maximum shear stresses distribution on the west wall of the fixed- base model. The shear stress values [MPa] are qualitatively shown based on colour in the horizontal axis at the bottom of the image. ....	78
Figure 4-24 - Maximum drift in the flexible model. The blue line represents the x-axis direction and the red line represents the y-axis direction. ....	79
Figure 4-25 - Maximum drift in the fixed- base model. The blue line represents the x-axis direction and the red line represents the y-axis direction.....	80
Figure 5-1 - Building and floor east plant of the Church (Pitilakis D.) .....	84
Figure 5-2 - Sections in position 1 and 2 and 8 of the Church (Pitilakis D.) .....	84
Figure 5-3 – Typical drilled micropiles construction sequence (Ir. Shong, F. Chew Chung, 2003).....	85
Figure 5-4 - Micropiles classification according to the types of grouting (A. Alnuaim, 2014).....	86
Figure 5-5 - Modalities of application of the micropiles without underpinning (top) and with underpinning (below) (T. R. S. Antunes, 2012).....	88

<i>Figure 5-6 - Maximum principal stresses distribution in the north wall of the flexible model with micropiles. The principal stress values [MPa] are qualitatively shown based on colour in the horizontal axis at the bottom of the image. ....</i>	<b>92</b>
<i>Figure 5-7 - Maximum principal stress distribution in the south wall of the flexible model with micropiles. The principal stress values [MPa] are qualitatively shown based on colour in the horizontal axis at the bottom of the image. ....</i>	<b>93</b>
<i>Figure 5-8 - Maximum principal stresses distribution in the west wall of the flexible model with micropiles. The principal stress values [MPa] are qualitatively shown based on colour in the horizontal axis at the bottom of the image. ....</i>	<b>93</b>
<i>Figure 5-9 - Maximum shear stresses distribution in the north wall of the flexible model with micropiles. The shear stress values [MPa] are qualitatively shown based on colour in the horizontal axis at the bottom of the image.....</i>	<b>94</b>
<i>Figure 5-10 - Maximum shear stresses distribution in the south wall of the flexible model with micropiles. The shear stress values [MPa] are qualitatively shown based on colour in the horizontal axis at the bottom of the image.....</i>	<b>94</b>
<i>Figure 5-11 - Maximum shear stresses distribution in the west wall of the flexible model with micropiles. The shear stress values [MPa] are qualitatively shown based on colour in the horizontal axis at the bottom of the image.....</i>	<b>95</b>

# List of Tables

Table 2-1 - Mechanical properties of the foundation's materials.....	27
Table 3-1 - Values of K for use with general purpose, thin layer and lightweight mortars.....	30
Table 3-2 - Compressive strength calculation for the three layers masonry.....	44
Table 3-3 – Final compressive strength and modulus of elasticity of the materials calculation.....	45
Table 3-4 - Ground type classification based on the stratigraphic profile.....	54
Table 3-5 - Shear wave velocity for layers.....	55
Table 3-6 - Segmentation of the foundation for the calculation of the spring constants.....	56
Table 3-7 - Spring constants calculation parameters.....	56
Table 3-8 - Elastic solutions for static stiffness.....	57
Table 3-9 - Embedment correction factors for static stiffness.....	57
Table 3-10 - Dynamic stiffness modifiers.....	57
Table 3-11 - Parameters to define the springs in ETABS software.....	59
Table 3-12 - Inserting values for translation along the x-axis for section $\tau\mu 1$ .....	60
Table 3-13 - Inserting values for translation along the y-axis for section $\tau\mu 1$ .....	61
Table 3-14 - Inserting values for translation along the z-axis for section $\tau\mu 1$ .....	62
Table 4-1 - Calculation of covering loads, including dome and roof.....	65
Table 4-2 - Maximum displacements at the four corners of the flexible model at the top of the building, at the ground level and at the lowest point of the foundation. The values are given in mm. ....	71
Table 4-3 - Maximum displacements in the middle of each side of the flexible model, except the side of the sanctuary. The values are given in mm. ....	71
Table 4-4 - Maximum displacements at the four corners of the fixed- base model at the top of the building and at the ground level. The values are given in mm. ....	72
Table 4-5 - Maximum displacements in the middle of each side of the fixed- base model, except the side of the sanctuary. The values are given in mm.....	72
Table 5-1 - Spring parameters after increasing the shear modulus G by 50%.....	89
Table 5-2 - Modal analysis of the flexible model in x-axis direction with micropiles. The displacements values [mm] are quantitatively (based on colour) shown in the horizontal axis at the bottom of the image. ....	90
Table 5-3 - Modal analysis of the flexible model in y-axis direction with micropiles. The displacements values [mm] are quantitatively (based on colour) shown in the horizontal axis at the bottom of the image. ....	91
Table 5-4 - Maximum displacements at the four corners of the flexible model with micropiles at the top of the building, at the ground level and at the lowest point of the foundation. The values are given in mm. 91	
Table 5-5 - Maximum displacements in the middle of each side of the flexible model with micropiles, except the side of the sanctuary. The values are given in mm. ....	92



# Introduction

Large magnitude earthquakes often affected Greece during the years, while small magnitude events are felt every couple of days. Some of them can be considered devastating for the whole country.

The long seismic history of the Hellenic Republic is particularly alarming, since this territory is rich of cultural heritage buildings, that are undergoing high stresses and risk to collapse under the influence of age, weather and earthquakes. A large number of these buildings undergoing damages are masonry monuments. This is the reason why studying the response of this kind of construction is so important. Safeguarding the Greek heritage is essential.

The present dissertation has been possible thanks to the Erasmus experience in the Aristotle University of Thessaloniki, in Greece, and the collaboration with Professor Dimitrios Pitilakis, expert in geotechnical earthquake engineering and soil- foundation- structure interaction, as well as seismic behaviour and rehabilitation of historical buildings and monuments.

During this international experience, a research work about seismic behaviour of masonry monuments has been carried out to picture the response of this kind of construction, considering not only the contribution of the material but also the age of the building, significantly affecting the behaviour of the structure.

The case study used to interpret the seismic behaviour of masonry monuments is the Hagia Sophia Church in Thessaloniki. It is one of the oldest, largest and most important examples of byzantine architecture in Greece.

This monument already underwent numerous damages since the construction in the early 7<sup>th</sup> century, caused by time, weather and earthquakes.

The aim of the dissertation is analysing this specific building under seismic influence, to estimate its response and to identify the weakest parts of the construction. For this purpose, the acceleration recorded during the earthquake on the 20<sup>th</sup> of June 1978 is used during the simulation. This data is particularly relevant for the analysis, since the strong earthquake caused serious damages to the whole city, causing the collapse of many buildings and destroying parts of the Hagia Sophia Church itself.

A second objective of the thesis is underlying the importance of considering the soil- foundation- structure interaction during the analysis. A flexible base model

can provide more accurate results than a fixed base one. To prove it, the analysis is carried out with two different models.

After analysing the behaviour of the structure in both the simulations, the possibility of applying a retrofitting strategy is considered. The choice falls on the micropiles technology, that seems to be the most valuable and suitable option for the specific case of masonry monument, which aesthetical appearance has to be preserved. To demonstrate its positive effect on the construction, a new analysis is carried out, considering new values obtained by applying the technology to strengthen the structure.

The thesis proposes a numerical simulation of the actual soil- foundation-structure system, following the provisions given by NIST2012 for the calculation of the impedance functions. The influence of soil- foundation- structure interaction is investigated using the software ETABS.

For what concerns the building materials properties, two codes have been used: the Eurocode EC6 (Design of masonry structures) and the Greek Regulation for the evaluation and structural intervention in masonry (KADET).

The dissertation is divided in five chapters.

The first chapter is about the Hagia Sophia Church history and construction, with a reference to the seismic events affecting the city of Thessaloniki.

In the second chapter the Church is described by a geometrical point of view. The materials used in the construction are discussed and their mechanical properties are listed.

From the third chapter the modelling begins. This chapter regards the normative and theory on which the analysis is based. The design of the model realized in ETABS software is discussed.

The fourth chapter sees the calculation of the loads used for the analysis and the reaction of the model to their application.

In the fifth and last chapter a proposal to strengthen the foundation using micropiles is made. An analysis with the new properties is then executed.



# Chapter 1

## Historic context of Hagia Sophia Church

### 1.1 Historical analysis

Hagia Sophia, or officially the Temple of the Wisdom of God, is one of the oldest early Christian Byzantine temple in the city of Thessaloniki, Greece.

The Church of Hagia Sophia at Thessaloniki is the largest and most important monument in the whole group of Byzantine architecture buildings. It is generally believed to have preserved its original form to a much greater extent than any of the others.

It is located in the city centre, right in front of the Hagia Sophia square, and it is still used today as cathedral of the city. It was built in the 7th century in the place of a large early Christian basilica, that was probably destroyed by an earthquake at the beginning of the century and which foundations still lie under the actual building.

The earliest written reference to Hagia Sophia is from the year 795, in a letter sent from his exile in Thessaloniki by St Theodore Studites to his uncle Plato. The saint reports that upon his arrival the city's overlord sent him to the Archbishop, advising him to pray first in the Church of Hagia Sophia.

The next reference is in John Cameniates's account of the city's siege at the hands of the Saracens in 904; the monument is mentioned as one of the city's three principal churches, together with the Churches of the Theotokos and of St Demetrius.

In two of the oldest Anthonine codices (dating from 942 and 1097) Hagia Sophia is referred to as the "Great Church of Thessaloniki", which may mean that it was the city's cathedral church.

During the Latin occupation of the city (1205-24), Hagia Sophia was appropriated by the conquerors and became their cathedral church, as we learn from three

letters written by the Pope Innocent III dating from 1208, 1209 and 1212. After the city's liberation, the church remained the cathedral of the Orthodox community. The fact that the Archbishop of Thessaloniki, and later Saint, Gregory Palamas was buried inside the church in 1359 indicates that it had the status of cathedral in the years which followed.

During the ottoman period, after the Turkish conquest in 1430, Hagia Sophia was transformed in a mosque in 1524, as many other religious sites.

In 1864 Texier and Pullan made the first drawings of the building in their book on Byzantine Architecture. Their study also provides the first information about the date of the church's conversion into a mosque (their suggestion being AH 993), based on their reading of a now lost inscription originally placed by the Turks over the main entrance.

After the fire of 1890, which also destroyed the church's immediate environs, Hagia Sophia was abandoned in a semi-ruined state until the early years of the twentieth century. Between 1908 and 1910 the Turkish administration carried out drastic restoration work on the mosque.

The Greek army managed to liberate the city in 1912 and Hagia Sophia was restored to its original Christian worship.

Four years later, in 1917 the building was extensively damaged by the great fire and then gradually restored.

In August 1941, a bomb fell on the north-west part of the dome, also destroying the small onion dome of the bell-tower and part of the west portico. The latter was eventually demolished in 1948, as the archives of the 9th Ephorate of the Byzantine Antiquities in Thessaloniki attest.

The restoration of the dome was completed in 1980.

In a city like Thessaloniki, which is in an extremely earthquake-prone region, this kind of information is particularly valuable, especially when the building in question, like Hagia Sophia, has such a long history and shows evidence of having undergone numerous interventions.

The Church of Hagia Sophia stands in the south-east part of the city, not far from the sea. It is north-west of the Galerian complex and 120 meters south of Egnatia Street. In the immediate vicinity of the church's foundations the remains of a succession of buildings have been found, dating from Roman times to the period of Ottoman rule. This shows that this area has been in constant use throughout the centuries.

Today the Church has a ponderous cubic shaped body with an almost squared plan (the internal dimensions are 30,92 m, 28,90 m length without the apse and 40,06 m with it) from which the tripartite sanctuary protrudes to the east.

Outside the body of the church, as its north- west corner, there is a tower, which now gives access to the galleries. It is addition dating from the Ottoman rule.

The interior of the church has a cruciform nucleus, the centre of which is covered by a large dome on pendentives, supported by four barrel- vaults of unequal length. Lateral aisles and a narthex, with galleries above them, surround the naos on three sides.

## 1.2 Construction phases

As said in K. Theoharidou's "The architecture of Hagia Sophia, Thessaloniki", the removal of the external plaster in 1975 from the north, south and east walls brought successive construction phases to light. Then removing the plaster from the west wall and from the galleries, a more precise picture of these phases was made.

The main construction phases of the Hagia Sophia Church are described in the following paragraphs, underling the difference between Hagia Sophia and the basilica that previously occupied the site. Parts of this building have been wrongly attributed to the present church during the past.

Today the previous church masonry is visible and accessible at only two points. One is the low foundation 70 cm from the church west wall and the other is part of the basilica north outer wall, which survives to a height of 1,3 m above the ground. They both are 1,25 m thick.

The masonry of these sections consists of alternating bands of brick and rubble stone, the green schist quarried from the hills around the city. The method of construction of the basilica dates back in Thessaloniki to the Late Roman period. The connecting medium is a strong white lime mortar containing an aggregate of gravel and coarse brick pieces, the latter in relatively small proportions. Quite large pebbles up to the size of a walnut and pieces of brick up to 3 cm long characterize the mortar.

Most of the bricks measure 3 -3,5 x 28- 30 x 39- 40 cm, though some are a little bigger and thicker. Inside the clay there may be coarse grains of aggregate, mainly quartz.

- Phase A – Erection of the church

The original masonry consists of alternate layers of roughly dressed limestone (four or five courses) and bricks (usually five courses), held together with strong, pink, crushed tile mortar.

This phase comprises:

- the whole ground floor up to and including the springing of the barrel-vaults over the north and south aisles and of the strainer arches in the narthex;
- most of the tripartite sanctuary;
- at the gallery level, the basis features of the cruciform nucleus.

On the west wall, the A phase reaches various heights, from a maximum of 6,5 m to a minimum of 5,7 m above the present floor level.

At the west façade the seven openings originally reached down to the base of the wall. Four of them were converted into windows and their lower sections were blocked up with rough mud- built mixture of stone and broken bricks. Originally the narthex had five entrances on the west side.

On the south level the first phase ends at a horizontal line level 5,3 m above the ground.

On the north façade the upper level of the first phase is extremely irregular, reaching a maximum height of 5,6 m and a minimum of 4,4 m from the ground. In the east walls the first phase survived to a higher level than the other facades and include much of the masonry of the tripartite sanctuary. The three- sided central apse survives in its original form.

The cruciform nucleus is found to belong to the first phase, both at the ground and the gallery levels (up to a height of 3,9- 4 m above the marble cornice marking the floor of the galleries).

In the east wall of both the south and north gallery, in the section where it encounters the cruciform nucleus, part of the masonry of the first phase survives up to 2 m.

The pendentive dome over the north- west part of the narthex belongs to the A phase, being coherent with the base of the original wall of the cruciform nucleus at gallery level.

The original masonry forms successive horizontal bands of bricks (usually five courses) and four or five courses of ashlar stones bound with a very strong crushed- tile mortar. A band of five bricks courses is 45 cm high, while a band of

four or five stone courses is usually 1,15 m high, but neither of them is constant. The larger stones are in the lowest bands.

The ashlar stones used in the building are for the most part a mixture of limestone and a smaller proportion of sandstone, which is characterized by a high content of shells. The stone, which is not generally considered to make good building material because of its admixtures of organic origin, is very probably from Chalkidiki. It is soft and easy to quarry and hew.

The bricks measure 40 x 30- 32 x 4- 4,5 cm and half bricks measure 40 x 15- 18 cm. They are of very good quality, solid and with a high proportion of aggregates mixed in with the clay. Thinner bricks measuring 3- 3,5 cm are to be found only in a horizontal band from the first phase, mainly on the east façade.

The mortar is a strong, pink, crushed- tile lime mortar.

The material used for jointing has the same composition of the regular building mortar, but much more fine- grained. It contains a small proportion of sand, while the mostly used aggregate is broken brick, with occasional fine gravel. The presence of brick dust gives the mortar exceptional hydraulic properties, while the porous brick helps the mortar to set rapid and it makes it lighter than if gravel was used instead. These combined qualities make for a quicker building process, even when using very thick joints.

#### ▪ Phase B

The B phase is characterized by masonry which is likewise constructed in bands of brick and stone, but in this case the brick courses are less uniform in height, consisting of six, five, four and even fewer rows, and the stone is the green gneiss quarried in the surrounding hills. The mortar is a strong, pink crushed- tile mortar very similar to the one of the first phase.

The construction style is similar to the first phase one, but it is a cheaper method. Instead of limestone ashlar, the unworked green stone from the local hills is used.

This phase is found exclusively above the ground floor and forms:

- the outer gallery walls above the surviving sections of the first phase and up to 2,55 m above the gallery floors;
- the chambers over the corner bays in the galleries;
- the tympana of the arms of the cross at the gallery level;
- the whole square base of the dome;
- part of the north and south sides of the recessed top of the sanctuary apse.

On the east façade it is present high up to the right and left sanctuary apse, forming the east walls of the two chambers above the first- phase east corner bays in the galleries, so it starts at about 4 m above the gallery floors.

- Phase C

The third phase is present in the outer wall of the west gallery between the two transverse walls of the previous phase, from which it is separate by joints. It extends from the highest surviving level of the first phase in the west wall of the church up as far as 2,2 m above the present floor of the west gallery.

Its masonry of green rubble with plenty of whitish mortar has a rather makeshift appearance, particularly outside where no jointing was found. The mortar is whitish and consists chiefly of lime and sand with a very small proportion of crushed tile.

- Phase D

The fourth phase is characterized by imperfect cloisonné masonry, that is present at the top of the east and north outer walls of the north gallery, in part of the east wall of the south gallery and probably in a narrow band at the top of the walls enclosing the chambers high up above the second- phase corner bay at gallery level.

The walls built in the course of these middle Byzantine repairs consist of irregular stone and bricks in a kind of imperfect cloisonné system in which courses of brick and stone alternate separated by usually three horizontal layers of brick pieces. The connecting medium is a pink crushed- tile mortar containing lime, brick dust, sand and relatively fine- grained ceramic aggregates. It contains less brick dust and has finer- grained aggregates than the mortar of the first two construction phases.

- Later phases

The later phases cannot be determined in time.

In a later phase the exterior walls and the apses of the parabemata were elevated, as well as parts of the recessed top of the main sanctuary apse.

An extensive phase is evident in the east, south and west walls of the south gallery, which replaced the middle Byzantine elevation of this area with a blind wall. The masonry of this phase is mixed rubble with horizontal bricks.

The west wall of the north gallery and the west end of its north wall is due to Turkish repairs.

The gallery roof must have been lowered by at least 60 cm and other small scale interventions were also carried out (for instance some openings were blocked up and others were created in their stead).

The following images show the floor plan and all the facades elevations of the building, as shown in “The Architecture of Hagia Sophia, Thessaloniki. From its erection up to the Turkish conquest” written by K. Theoharidou (1988).

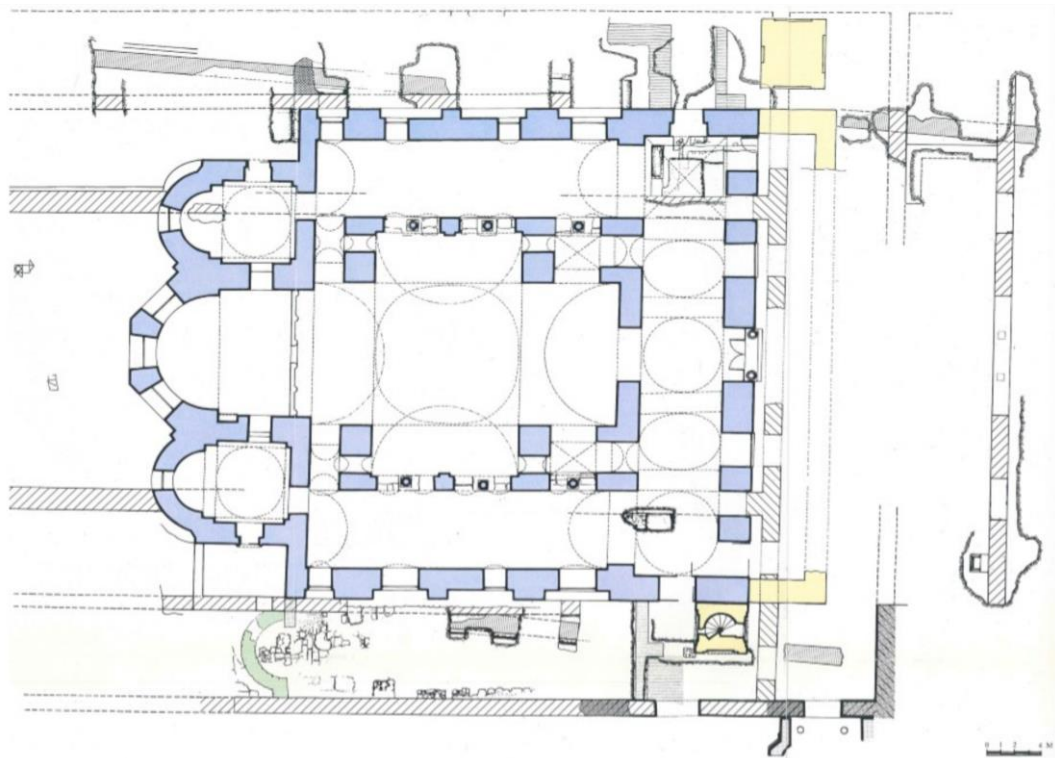


*Figure 1-1 - Plan of Hagia Sophia Church  
(K. Theoharidou. 1988)*

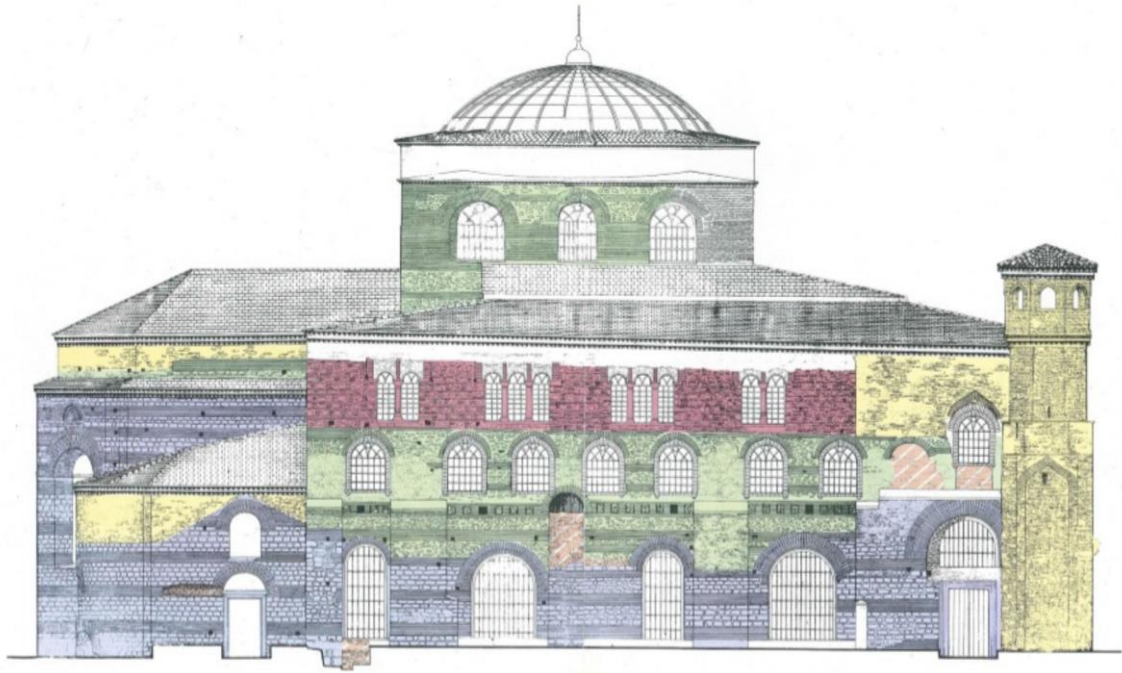


*Figure 1-2 - North facade of Hagia Sophia Church  
(K. Theoharidou. 1988)*

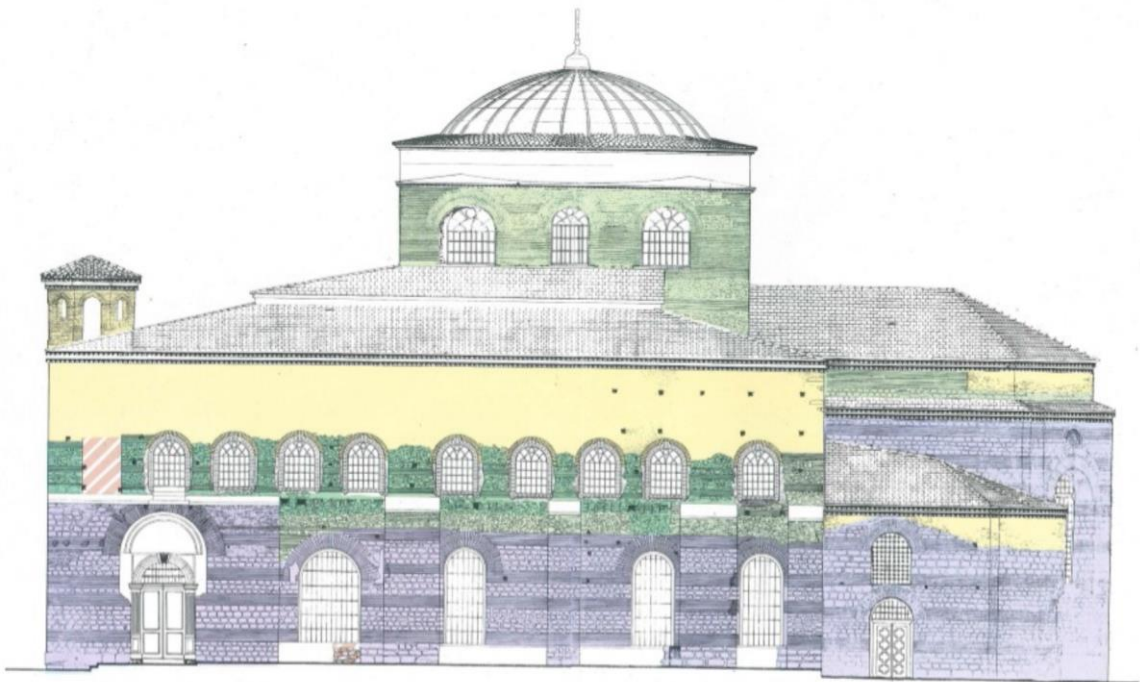


*Figure 1-3 -South facade of Hagia Sophia Church  
(K. Theoharidou. 1988)*



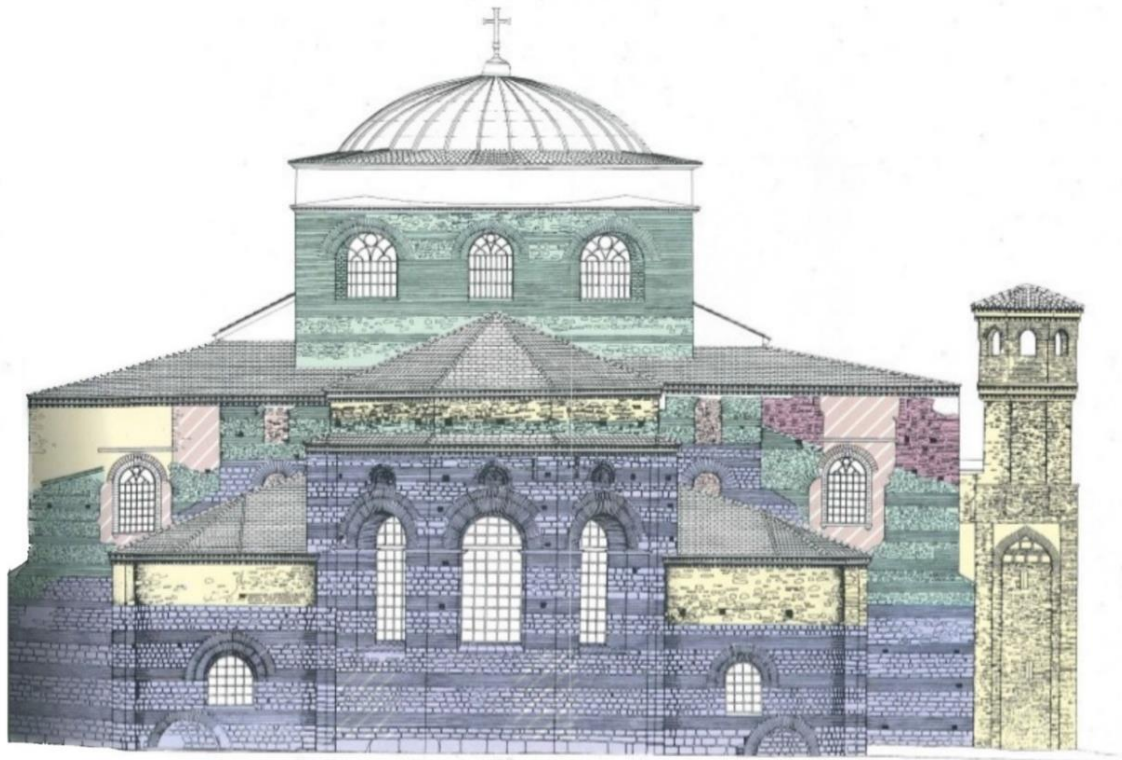


*Figure 1-4 - East facade of Hagia Sophia Church  
(K. Theoharidou. 1988)*



*Figure 1-5 - West facade of Hagia Sophia Church  
(K. Theoharidou. 1988)*

## 1.3 Earthquakes in Thessaloniki

Although the area of Thessaloniki has low seismicity, the risk is high. The focal depth of the earthquakes in the area is superficial, making strong surface earthquakes more destructive. This is due to the many active faults existing around the area of Thessaloniki.

The city is located on the Axios- Vardar seismogenic zone. It is adjacent to the Servomacedonian massif, that is considered the most active zone of the north Helladic area.

Numerous earthquakes have been registered in the area. The great historical earthquakes that caused significant damages to the city of Thessaloniki are mainly three:

- the first one was registered in 1430 and was probably 6.0 on the Richter scale;
- the second one was registered in 1542 and was 6.2 on the Richter scale;
- the third one was in 1759 and was 6.5 on the Richter scale.

According to the Geodynamics Observatory Institute, for the most recent devastating earthquakes in Thessaloniki there are three time periods of exacerbation.

The first period of seismic sequences:

- seismic sequence with magnitude 6,6 in 1902 in Assiros;
- earthquake with magnitude 7,3 in 1904 in Bulgaria;
- seismic sequence in Athos peninsula with the main one of magnitude 7,5 in 1905.

The second seismic sequences:

- seismic sequence in Former Yugoslav Republic of Macedonia with a bigger event in Valandovo in 1931 with magnitude 6,6;
- a strong earthquake measuring magnitude 7 in Lerissos in 1932.

The third period was located in the area of Lagkada and Volvi lakes, with a major earthquake measuring 6,5 on the Richter scale in June 1978.

The most important of these earthquakes is known as the Great Earthquake of Thessaloniki. It was registered on the 20<sup>th</sup> of June 1978, with epicentre 20 km at the east side of Thessaloniki, between the Koroneia and Volvi lakes, in the village of Stivos.

It was registered by the accelerometer installed in the City Hotel in Thessaloniki. It had a peak ground acceleration of 0,15 g and a vibration period from 0,4 to 0,5

s. After the several failures during the earthquake, 28 restoration works were carried out. Some of the monuments were in danger of collapsing because of the high static problems. The biggest challenges were Rotunda, Hagia Sophia Church, Church of Acheiropoietos and Church of Saint Panteleimon.

It was preceded by a series of earthquakes, which strongest one was on the 23<sup>rd</sup> of may 1978, measuring 5,8 on the Richter scale, from the same epicentre.

A series of aftershocks followed with the strongest being on the 5th of July 1978 with magnitude of 5,0 and epicentre at around 10 km from Thessaloniki.

The intensity of these catastrophes is estimated at level VIII of the Mercalli 12-levels scale.

Extensive damages were found in the city monuments, mostly due to the deterioration of existing damages due to seismic events.

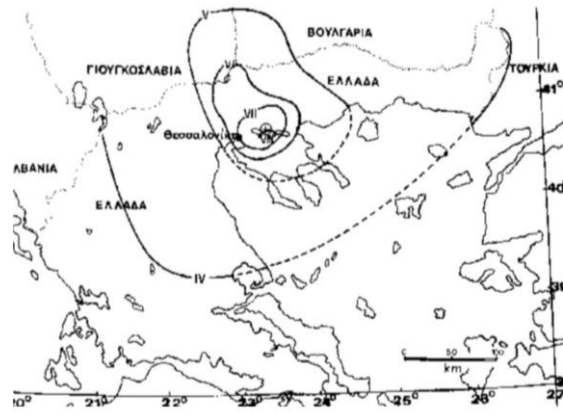


Figure 1-6 - Earthquake in Volvi on the 20<sup>th</sup> of June 1978  
(Mossiopoulos et al., 2008)

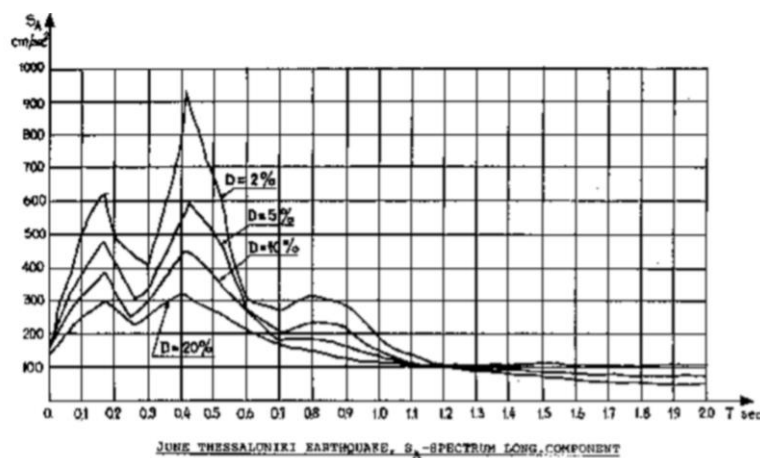
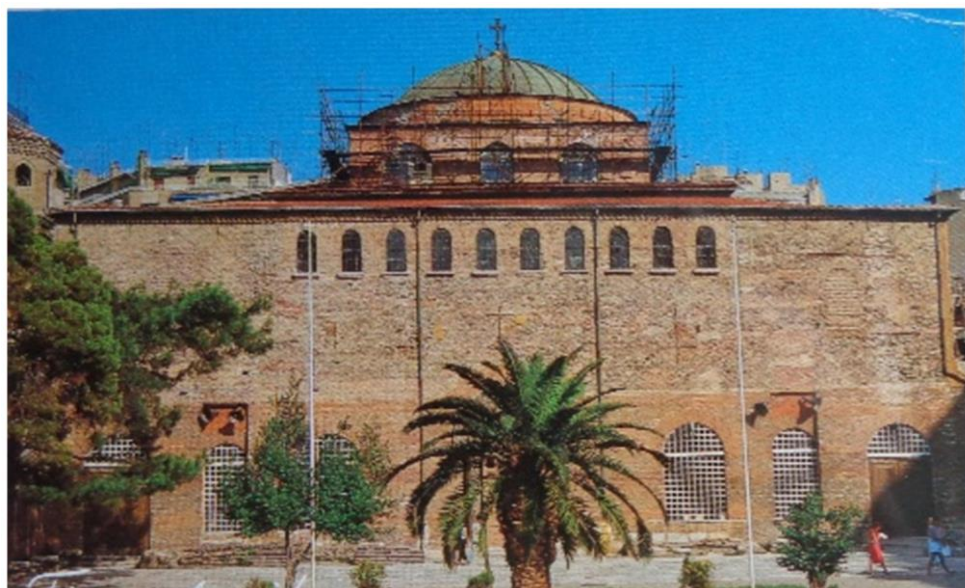


Figure 1-7 - Response spectrum of the earthquake registered in Thessaloniki on the 20<sup>th</sup> of June 1978  
(Mossiopoulos et al., 2008)

After the earthquake in 1978, Hagia Sophia Church suffered many damages. The earthquake revealed also already existing damages caused by time, previous seismic events and interventions.

The big challenge while repairing and strengthening a monument is that the old must be kept with care, without changing the aesthetic of the building, but at the same time fixing all the problems. The most problematic part involved the mosaics and murals, that required a delicate work to be maintained. The works done on the monument revealed new archaeological evidences. Important murals and data from the past came to light.

The earthquake in 1978 gave the opportunity to study the building, restore and strengthen it.



*Figure 1-8 - Photo of Hagia Sophia Church during the 80's with repairs in development from the earthquake of 1978*

## Chapter 2

# Load-bearing structure and construction materials

### 2.1 Geometry of the Church

The entrance to the church is through the narthex, a rectangular chamber measuring 31,72 x 5,74 m internally and extending across the whole of the west side of the building. Its sides project about 65 cm beyond the side of the church, forming shallow towers up to the level of the gallery floor.

At the north and south ends the narthex gives direct access to the lateral aisles, which are each about the same width as the narthex. These three aisles together form a U-shaped ambulatory around the cruciform nucleus of the church. Access from the narthex to the nave is effected through three arches: the largest, on the main axis of the church, leads into the naos and hence to the sanctuary door, while the two smaller archways on either side communicate with the western groin-vaulted corner bays formed between the arms of the cross.

There are seven openings in the west façade, three of which now serve as entrances, while the other openings were converted into windows.

Four strainer arches divide the roof of the narthex into five unequal parts, covered by five dissimilar vaults. A flattered pendentive dome in the centre is flanked by two elliptical vaults, while the differentiation is even more marked at either extremity, since at the north end there is a pendentive dome and at the south a cross-vault. The strainer arches are not quite semi-circular, but somewhat flattened and the two at either end present problems with respect to their position and to the form of the arches leading from the narthex to the lateral aisles, since the former essentially spring from part of the latter's fronts.

The form of the roof of the narthex is a consequence of problems in the original architectural design (which was preordained by the layout of the foundations of

the previous basilica beneath) and of changes introduced in the building's later phases.

The centre of the church comprises cruciform nucleus topped by a dome. Four barrel- vaults with an average span of 10,16 m, but of unequal length, cover the arms of the cross, and the spaces in between the arms of the cross have been developed into corner bays, enclosed within the massive piers.

An arcade with three columns on raised pedestals pierces the tympanum of the west arm of the cross, which separates the gallery from the space of the naos.

On the east wall of the west gallery there is a row of marble corbels. These are 90 cm higher than those in the lateral galleries.

The dome rests upon a low drum with twelve windows. The exterior of the drum is cubic in shape, while its interior surface is far from circular in plan: its north-south diameter is 11,60 m and its east- west diameter is 10,95 m. A narrow balcony is formed at the base of the drum.

The twelve windows are disposed equally around the massive drum, three on each side, with the result that those at the extremities of each side are very deep. In the north- east corner of the drum, within the masonry between the two windows, there is a narrow staircase which may be reached from the easternmost window on the north side and which leads to the roof of the square drum. Above this level there is a second, low, cylindrical drum.

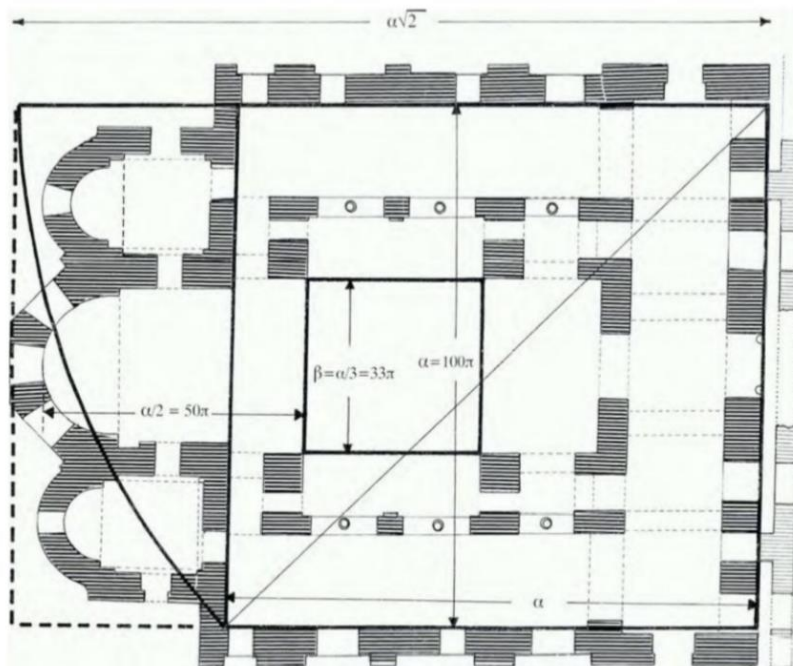


Figure 2-1 - Metrical relations in the design of the church (plan view)  
(K. Theoharidou, 1988)

## 2.2 Construction of the church

The ground floor of the church is constructed with masonry which comprises (usually five) courses of bricks alternating with four or five rows of roughly squared limestone jointed with a bright red crushed- tile mortar.

In the upper storey, the first zone, which is 2,5 m above the gallery floor, is constructed with alternating courses of brick and rubble masonry using local green stone. The mortar again is of bright red crushed rille. This masonry is mainly observed in the north and south exterior facades, in various parts of the east and west facades at gallery level and in the square base of the dome. Inside the building, it is likewise encountered in the galleries, in the transverse walls of the west gallery, and in the upper zone of the central nucleus.

In the upper part of the north façade, in the area occupied by the double and triple windows, there is a third style of masonry, comprising alternating single rows of brick and stone separated by usually three horizontal layers of brick pieces, forming a kind of imperfect cloisonné. The mortar is again crushed tile but has a pale red colour. This style of masonry is seen in the upper zone of the east façade of the north gallery and in a small section of the interior of the east wall of the south gallery. Similar masonry is encountered in the upper zone containing the single- light windows in the centre of the west façade. This corresponds to the section of the west gallery divided off by the two transverse walls inside.

Above the ground floor level, the west wall of the church is constructed of plain rubble masonry consisting of horizontal layers of undressed stone interspersed with smaller stones and pieces of brick. White lime mortar is used here. The masonry in this section of the church is badly damaged and has undergone frequent repairs. Plain rubble masonry is also encountered in the upper zone of the south exterior wall and part of the east faced of the south gallery, as also at the west end of the church north façade at gallery level.

The arches are built of single or double rows of brick and all the various types of vault used in the church are exclusively of bricks.

## 2.3 Construction materials description

As mentioned above, Hagia Sofia Church is divided in phases based on the construction period. In each phase the used construction materials are different.

The foundation of the first phase was built with gneiss of a local stone coming from the Thessaloniki- Chalkidiki area. It is a rock with slate shape and a mineralogical composition similar to the one of igneous rocks as granite. It is very resistant to use and meteorological conditions, while it guarantees a reduced workability thanks to its silicone components.

The masonry of the first phase was built with limestone and sandstone. These stones can be easily carved. Cause of their organic impurity they are not considered good construction materials. They have been used with irregular cut and dimensions around 14-18 x 24-30 x 37-40 cm. The limestone, characterized by the high presence of mollusc fossils, is predominant.

Byzantine bricks have been used during both the first and second construction phases, with many impurities and irregular shapes (changes of thickness, edges, texture and curvature). The usual dimension is about 40 x 30-32 x 4,5-5 cm.

During the second construction phase, in addition to the byzantine bricks, the slate has been used. It is a raw green stone coming from the surrounding hills.

In all the construction phases the predominant material is the mortar. It is made of: mortar, sand, water, crushed tiles, quartz sand, prairie soil and other minor aggregates. It is used both as construction material and as joining material.

The capitals and the base of the columns are made of white marble. The trunk of the pillars is made of a variety of marbles (green stone from Thessaloniki or Atracian marble from Atracia) or granite.



## 2.4 Mechanical properties of the construction materials

The mechanical properties of the materials change along the years. The properties used in the simulation cannot be considered equal to the ones of a new construction.

The empirical values have been given by the Department of Civil Engineering of the Aristotle University. These values are shown in the following tables.

### Foundation

Material	E [GPa]	$\gamma$ [KN/m <sup>3</sup> ]	$\rho$ [t/m <sup>3</sup> ]	$\nu$ [%]	$f_b$ [MPa]	$f_m$ [MPa]
Gneiss	30	27	2,25	15	40	
Mortar	5		1,5	30		2

Table 2-1 - Mechanical properties of the foundation's materials

### Indoor columns

Material	E [GPa]	$\gamma$ [KN/m <sup>3</sup> ]	$\rho$ [t/m <sup>3</sup> ]	$\nu$ [%]	$f_b$ [MPa]	$f_m$ [MPa]
Marble	80	26,4 ÷ 28,6	2,7	20	80	

Table 2-2 - Mechanical properties of the internal columns material

### Masonry

Material	E [GPa]	$\gamma$ [KN/m <sup>3</sup> ]	$\rho$ [t/m <sup>3</sup> ]	$\nu$ [%]	$f_b$ [MPa]	$f_m$ [MPa]
Phase A						
Limestone	30	18,7 ÷ 26,9	1,8	15	40	
Sandstone	20	22 ÷ 27			30	
Brick		20	1,5	16	40	
Mortar	5					2
Phase B						
Slate	50	28		20	60	
Brick	40	20	1,5	16	30	
Mortar	5					2

Table 2-3 - Mechanical properties of the masonry materials

# Chapter 3

## Regulations and digital modelling

### 3.1 Normative

The loading capacity of the materials has to be defined to create the model of the church. The modelling part is based on two regulations:

Eurocode 6 - Design of masonry structures;

KADET - Greek Regulation of the structural intervention and evaluation of masonry.

### 3.2 Eurocode 6

The Eurocode 6 is used to design buildings and civil engineering works, or parts of them, made of unreinforced, reinforced, prestressed and confined masonry. It concerns only the requirements for resistance, serviceability and durability of the structures. Other requirements, as thermal and acoustic insulation, are not considered.

It uses the ultimate limit state (ULS) and the serviceability limit state (SLS) for designing the masonry buildings.

It consists of four parts:

EN 1996- 1-1: general rules for reinforced and unreinforced masonry;

EN 1996- 1-2: structural fire design;

EN 1996- 2: design considerations, materials selection and execution of masonry;

EN 1996- 3: simplified calculation methods for unreinforced masonry structures.

The aim of the Eurocode 6 is the construction of buildings suitable for use (depending on durability and costs of the project), able to resist to fixed conditions.

Equilibrium check:

$$E_d \leq R_d$$

The characteristic resistance is determined from results of tests on masonry specimens and empirical equations.

The general equation to calculate the characteristic compressive strength of masonry is:

$$f_k = K \cdot f_b^\alpha \cdot f_m^\beta$$

Where:

- $f_k$  is the characteristic compressive strength of masonry [N/mm<sup>2</sup>]
- $K$  is a constant depending on the following table [/]
- $\alpha, \beta$  are constants [/]
- $f_b$  is the normalised mean compressive strength of a masonry unit [N/mm<sup>2</sup>]
- $f_m$  is the compressive strength of the mortar [N/mm<sup>2</sup>]

The empirical relations depend on the composition of the masonry:

$$f_k = K \cdot f_b^{0.7} \cdot f_m^{0.3} \quad (\text{general purpose mortar and lightweight mortar})$$

$$f_k = K \cdot f_b^{0.85} \quad (\text{layer of mortar, in bed joints of thickness 0,5 to 3 mm, and clay units, calcium silicate, aggregate, concrete and autoclaved aerated concrete units})$$

$$f_k = K \cdot f_b^{0.7} \quad (\text{layer of mortar, in bed joints of thickness 0,5 to 3 mm, and clay units})$$

Masonry Unit		General purpose mortar	Thin layer mortar (bed joint $\geq 0,5$ mm and $\leq 3$ mm )	Lightweight mortar of density	
				$600 \leq \rho_d \leq 800$ kg/m <sup>3</sup>	$800 < \rho_d \leq 1300$ kg/m <sup>3</sup>
Clay	Group 1	0,55	0,75	0,30	0,40
	Group 2	0,45	0,70	0,25	0,30
	Group 3	0,35	0,50	0,20	0,25
	Group 4	0,35	0,35	0,20	0,25
Calcium Silicate	Group 1	0,55	0,80	‡	‡
	Group 2	0,45	0,65	‡	‡
Aggregate Concrete	Group 1	0,55	0,80	0,45	0,45
	Group 2	0,45	0,65	0,45	0,45
	Group 3	0,40	0,50	‡	‡
	Group 4	0,35	‡	‡	‡
Autoclaved Aerated Concrete	Group 1	0,55	0,80	0,45	0,45
Manufactured Stone	Group 1	0,45	0,75	‡	‡
Dimensioned Natural Stone	Group 1	0,45	‡	‡	‡
‡ Combination of mortar/unit not normally used, so no value given.					

Table 3-1 - Values of K for use with general purpose, thin layer and lightweight mortars (Eurocode 6, pp 37)

To control all the boundary conditions, the simulation should be based on the following elements:

- a detailed description of the structure, the materials and the environment of its location;
- the behaviour of the whole structure;
- the actions and how they are applied to the structure.

Appropriate stability and robustness during construction and use should be guaranteed. Depending on it, the general arrangement of the structure and the interaction and connection of its parts should be chosen.

The Eurocode 6 alone is not covering all the requirements of this study. Although it is still an important reference document, it does not cover what concerns the evaluation and structural interventions of existing masonry buildings. It needs to be combined with Eurocode 8 (Design for structure for earthquake resistance).

The results of the analysis is not reliable if Eurocode 6 is used to calculate the mechanical properties of the materials. So the KADET (Greek Regulation for the evaluation and structural intervention in masonry) has been used.

### 3.2.1 KADET

KADET is the Greek Regulation for the evaluation and structural intervention in masonry.

The aim of this document is to establish criteria for the evaluation of the bearing capacity of load-bearing masonry structures of existing buildings.

The objectives are:

- providing criteria to assess the seismic behaviour of existing buildings;
- describing the method for the selection of the necessary corrective action;
- setting criteria to plan the intervention measures.

A structural intervention is a work that involves the alteration of existing mechanical components, the addition of new components or the removal of them. Every restoration is a structural intervention.

The selection of the appropriate strategy and the type of intervention should be based on the evaluation of the existing structure. The main aspect to be considered is the overall behaviour of the building, with attention to its weak points. They could be for instance the lack of resistance or rigidity or plasticity, an unfavourable morphology, inadequate individual characteristics etc.

In Hagia Sophia Church the walling is made only of masonry and mortar.

The cracking of a walling subjected to compressive loads depends on the mechanical properties of the materials and on the morphology of the structure (both the shape and the thickness):

- single layer masonry: the failure is manifested by approximately vertical cracks on the facades, which penetrate the mortar joints or even in the masonry;
- two layers masonry: the failure is manifested at the two sides, in addition to a vertical crack along the intermediate mortar inside the wall;
- three layers masonry: when there is a clear intermediate area made of infill materials between the two external sides of the wall, the failure is manifested by approximately vertical cracks on the facades of the wall and

in its thickness. Both the types of crack penetrate the mortar joints, the infill material and the masonry. The infill materials consist of pieces of stone and mortar mixed together and spaced in height, so it isn't a uniform material, it has a large number of gaps and very poor mechanical properties.

Hagia Sophia Church is structured with three layers masonry, as found in bibliographical study.

The factors that influence the compressive strength of the masonry are:

- mechanical properties of the constituent materials;
- parameters as the thickness of the mortar joints, the construction technique, the roughness and the deformability of masonry and mortar;
- the behavioural eccentricity that occurs when vertical load is applied, depending on how the masonry is structured. The two sides of the masonry are structured in different ways, so they behave differently respect to the load, having different compressive strength;
- how the stones are working together in the masonry.

To estimate the compressive strength of the three layers masonry, the geometry (façade area and thickness), the mechanical properties of the two sides and the ones of the infill material have to be known. Taking into account all the parts is necessary because even if the external side of the wall is strong, the overall resistance is going to decrease due to the infill material, that has lower quality.

It can be estimated with the following equation:

$$f_{wc} = \frac{1}{\gamma_{Rd}} (2 \lambda_e \delta f_{c,e} + \lambda_i f_{c,i}) \div (1 + 2\delta)$$

Where:

- $\delta$  is the ratio between the external side thickness and the internal one [/]
- $f_{c,e}$  is the compressive strength of the external sides of the masonry [MPa]
- $f_{c,i}$  is the compressive strength of the intermediate area of the masonry [MPa]

$\lambda_e, \lambda_i$  are empirical factors depending on the interaction between the external sides of the masonry and the intermediate area ( $\lambda_e < 1,00$  and  $\lambda_i > 1,00$ ) [/]

$\gamma_{Rd}$  is the uncertainty factor, taken as 1,50 [/]

The value of the uncertainty factor is taken equal to 1,25 as personally suggested by Professor Christos Ignatakis from the School of Civil Engineering of Aristotle University of Thessaloniki, Greece.

The ratio between the external side thickness and the internal one is now calculated, following the directions of Professor Ignatakis.

Foundation:

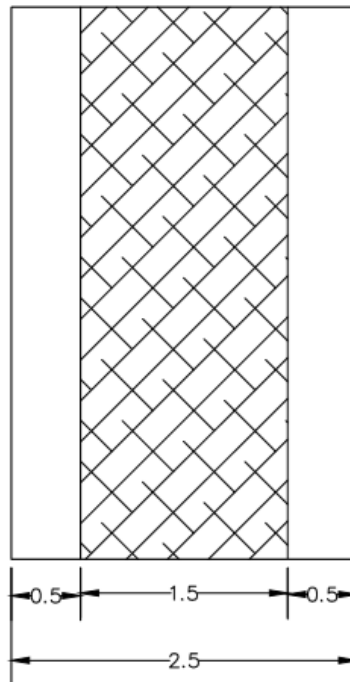


Figure 3-1 - Vertical section of the foundation

$$\frac{\text{external side}}{\text{intermediate area}} = \frac{0,5}{1,5} = 0,333$$

Masonry of phase A, B and C:

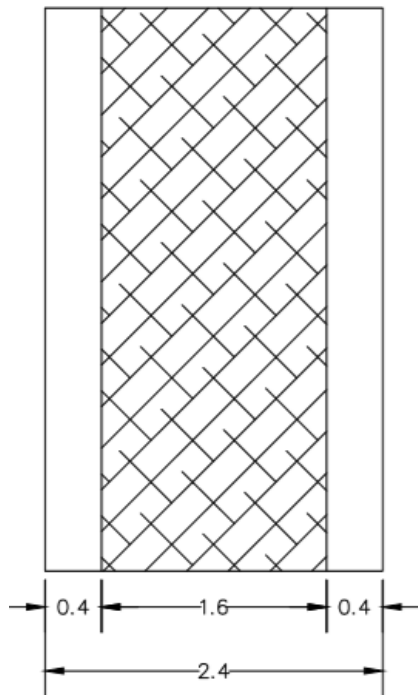


Figure 3-3 - Vertical section of the masonry of phase A and B

$$\frac{\text{external side}}{\text{intermediate area}} = \frac{0,4}{1,6} = 0,25$$

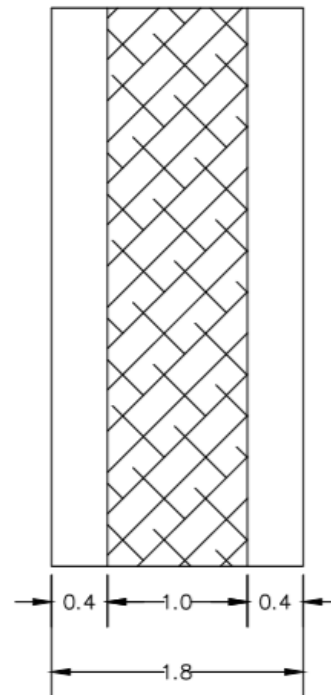


Figure 3-2- Vertical section of the masonry of phase C

$$\frac{\text{external side}}{\text{intermediate area}} = \frac{0,4}{1,0} = 0,4$$

The final compressive strength of the masonry is the average of the values of the two walls (with thickness 2,4 m and 1,8 m). It is equal to 0,325.

For what concerns the infill material compressive strength, the norm takes into account the low resistance materials which mechanical properties can't be examined in vitro. The value may be equal to 0,15 MPa. For greater accuracy of calculation, in this situation the compressive strength of the infill material is taken as 2/3 of the compressive strength of the external side, as suggested by Professor Ignatakis.



Therefore for the low resistance stones, the compressive strength is found with the following equation:

$$f_{wc} = \xi \cdot \left\{ \left[ \frac{2}{3} \sqrt{f_{bc}} - f_0 \right] + \lambda f_{mc} \right\}$$

Where:

- $f_{bc}$  is the compressive strength of the masonry [MPa]
- $f_{mc}$  is the compressive strength of the mortar [MPa]
- $\lambda$  is the masonry-mortar affinity coefficient, which is equal to 0,50 for rough stones and equal to 0,1 for smooth ones [/]
- $f_0$  is a coefficient that takes into account the degree of carving of the stones and has the value [MPa]:
  - 0,00 for carved stones;
  - 0,50 – 1,00 for semi- regular stones;
  - 1,50 – 2,50 depending on the quality of construction.
- $\xi$  is the coefficient which takes into account the influence of the thickness of the mortar joints. It is equal to 1,00 if  $V_m / V_w \leq 0,30$  where  $V_m$  is the volume of the mortar and  $V_w$  is the volume of the masonry [/]

The calculated compressive strength values are average values. The characteristic value required is:

$$f_{wc}^K = f_{wc} - 1,645 \cdot S \approx f_{wc} - 1,645 \cdot (0,2 f_{wc}) \approx 0,67 f_{wc}$$

Where S is the mean squared deviation of 100 trials and it is approximately equal to  $0,2 f_{wc}$ , while 1,1645 is the Gauss distribution coefficient.

### 3.3 Soil- Structure interaction - NIST

NIST is the National Institute of Standards and Technology in the USA. In September 2012 it published a guidance for implementing soil structure interaction in response history analyses. This chapter aims at displaying these indications.

Structure, foundation and soil underlying and surrounding the foundation are directly affecting the response to earthquake. So their interaction is analysed to evaluate the response to seismic events.

The seismic soil- structure interaction analysis is made with a specific free- field ground motion, that means the motion is not affected by structural vibrations or the scattering of waves at and around the foundation. There is not interaction in the theoretical case of a rigid foundation on rigid soil.

The interaction analysis describes the variation of the answer of a structure when finite rigidity is taken into account both for foundation and surrounding soil.

The soil- structure interaction effects are categorized in:

- inertial interaction effects: they refer to the effect of the mass on the phenomenon and provoke displacements and rotations at the foundation level caused by the inertia- driven forces, such as base shear and moment, during the oscillation. These movements are due to the finite rigidity of the soil.
- kinematic interaction effects: they are consequence of the presence of stiff foundation elements on or in the soil. They cause motions at the foundation to deviate from free- field motions;
- soil- foundation flexibility effects.

The following image shows a simple oscillator representing a single- degree- of- freedom structure with stiffness  $k$  and mass  $m$ . In the (a) case the base is fixed, while in the (b) case the springs represent the soil flexibility against a rigid foundation.

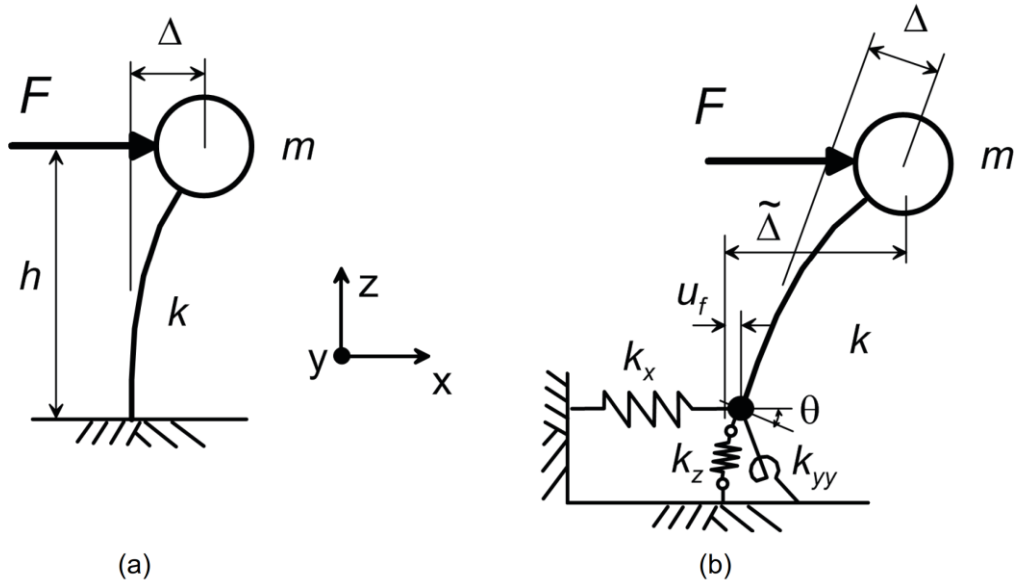


Figure 3-4 - Deflection caused by force applied to a single- degree- of- freedom structure represented by a simple oscillator: in case of: (a) fixed base structure; (b) structure with vertical, horizontal and rotational flexibility at its base  
(NIST GCR 12-917-21 (2012))

In both cases a static force  $F$  is applied, generating a deflection.  
In the (a) case the deflection  $\Delta$  is equal to:

$$\Delta = \frac{F}{k}$$

With square of period equal to:

$$T^2 = (2\pi)^2 \frac{m}{(F/\Delta)} = (2\pi)^2 \frac{m\Delta}{F}$$

In the (b) case the deflection  $\tilde{\Delta}$  is like the one of the fixed base system, but with two more contributions:

- $u_f$  : deflection of the rotational spring caused by the base shear  $F$ ;
- $\theta$ : deflection of the rotational spring caused by the base moment  $F \cdot h$ .

$$\tilde{\Delta} = \frac{F}{k} + u_f + \theta \cdot h$$

$$\tilde{\Delta} = \frac{F}{k} + \frac{F}{k_x} + \left( \frac{F \cdot h}{k_{yy}} \right) h$$

With square period equal to:

$$\tilde{T}^2 = (2\pi)^2 \frac{m\tilde{\Delta}}{F} = (2\pi)^2 m \left( \frac{1}{k} + \frac{1}{k_x} + \frac{h^2}{k_{yy}} \right)$$

The springs at the base level, so the soil flexibility, increase the inertial forces at the foundation level. Moreover, they increase the overall damping of the system. This is because at the foundation level there is a geometrical dumping of the waves reflected by the superstructure. When the base is rigid the waves undergo continuous reflections from the top of the superstructure to the foundation, being trapped. Inertia and flexibility always cause wave propagation.

In general, the overall damping of the system is a function of three factors: the hysteretic soil damping, radiation damping and superstructure material damping (usually referred as viscoelastic damping).

The hysteretic damping is due to the non- elastic behaviour of the soil materials. The radiation damping is due to weakening of the waves as they move away from the source, giving rise to energy dissipation.

The viscoelastic damping is due to the elasticity of the material in the superstructure and to the friction between different materials.

The principal dimensionless parameters that influence the period lengthening are:

$$\frac{h}{V_s T}, \quad \frac{h}{B}, \quad \frac{B}{L}, \quad \frac{m}{\rho_s 4BLh}, \quad \nu$$

Where:

- $h$  is the structure height [m]
- $V_s$  is the shear wave velocity, depending on the soil shear modulus  $G$ , according to the relation  $V_s = \sqrt{G / \rho_s}$  [m/s]
- $T$  is the structural first mode period [s]
- $B$  is the half- width of the foundation [m]
- $L$  is the half- length of the foundation [m]

- $m$  is the mass (or effective modal mass) of the structure [g]
- $\rho_s$  is the soil mass density [g/m<sup>3</sup>]
- $\nu$  is the Poisson's ratio of the soil [/]

The term  $h/(V_s T)$  represents the structure- to- soil stiffness ratio and it is the most important to determine the influence of the interaction. Period lengthening increases with  $h/(V_s T)$ .

The ratio  $h/T$  quantifies the stiffness of the superstructure. This value is higher for stiff lateral force resisting systems (such as shear walls), while it is smaller for flexible systems (such as moment frames).

The terms  $h/B$  and  $B/L$  describe the geometry of the soil- structure system. Increasing the ratio  $h/B$ , the period lengthening increases due to the increment of overturning moment and foundation rotation. For a fixed value of  $h/B$ , period lengthening decreases with  $B/L$  cause of the increased foundation size (so the stiffness) normal to the direction of loading.

The term  $m/\rho_s 4BLh$  is the ratio of the structure mass to the soil mass in a volume extending to a depth equal to the structure height  $h$ .

The Poisson's ratio of the soil affects the stiffness and damping characteristics of the foundation.

The stiffness and damping characteristics of the soil- foundation interaction are simulated using impedance function models or springs and dashpots.

The impedance functions represent the frequency- dependent stiffness and damping characteristics of soil- foundation interaction. They are complex equations describing the finite stiffness of the foundation (assuming that for each degree of freedom of the foundation, there is a spring with finite stiffness) and damping of the foundation (assuming that for each degree of freedom there is a damper).

Most of the solutions proposed can be written as:

$$\bar{k}_j = k_j + i\omega c_j$$

Where:

- $\bar{k}_j$  is the impedance function
- $j$  is the mode of translational displacement or rotation [/]
- $k_j$  is the frequency- dependent foundation stiffness

- $c_j$  is the dashpot coefficient [/]
- $\omega$  is the circular frequency [rad/s]

The imaginary part of the complex impedance represents a phase difference between harmonic excitation and response at a given frequency.

The dynamic stiffness of the springs  $k_j$  depends on the soil shear modulus  $G$ , Poisson's ratio  $\nu$ , foundation dimensions, dynamic stiffness modifiers  $\alpha_j$  and embedment modifiers  $\eta_j$ .

The stiffness of a static foundation is increased by the embedment of the foundation below the ground surface.

An alternative form to describe the impedance is:

$$\bar{k}_j = k_j (1 + 2i\beta_j)$$

With damping  $\beta$ :

$$\beta_j = \frac{\omega c_j}{2k_j} \quad (\text{defined for } k_j > 0)$$

The other values are found as:

$$k_j = K_j \times \alpha_j \times \eta_j$$

$$K_j = GB^m f\left(\frac{B}{L}, \nu\right)$$

$$\alpha_j = f\left(\frac{B}{L}, \alpha_o\right)$$

$$\eta_j = f\left(\frac{B}{L}, \frac{D}{B}, \frac{d_w}{B}, \frac{A_w}{BL}\right)$$

Where  $K_j$  is the static foundation stiffness at zero frequency for mode  $j$ ,  $m=1$  for translation and  $m=3$  for rotation,  $\alpha_o$  is the dimensionless frequency and it is equal to  $\alpha_o = \omega B / V_s$ .

The equations to find the parameters to calculate the impedance are shown in the following images.

Elastic Solutions for Static Stiffness of Rigid Footings at the Ground Surface		
Degree of Freedom	Pais and Kausel (1988)	Gazetas (1991); Mylonakis et al. (2006)
Translation along z-axis	$K_{z, sur} = \frac{GB}{1-\nu} \left[ 3.1 \left( \frac{L}{B} \right)^{0.75} + 1.6 \right]$	$K_{z, sur} = \frac{2GL}{1-\nu} \left[ 0.73 + 1.54 \left( \frac{B}{L} \right)^{0.75} \right]$
Translation along y-axis	$K_{y, sur} = \frac{GB}{2-\nu} \left[ 6.8 \left( \frac{L}{B} \right)^{0.65} + 0.8 \left( \frac{L}{B} \right) + 1.6 \right]$	$K_{y, sur} = \frac{2GL}{2-\nu} \left[ 2 + 2.5 \left( \frac{B}{L} \right)^{0.85} \right]$
Translation along x-axis	$K_{x, sur} = \frac{GB}{2-\nu} \left[ 6.8 \left( \frac{L}{B} \right)^{0.65} + 2.4 \right]$	$K_{x, sur} = K_{y, sur} - \frac{0.2}{0.75-\nu} GL \left( 1 - \frac{B}{L} \right)$
Torsion about z-axis	$K_{zz, sur} = GB^3 \left[ 4.25 \left( \frac{L}{B} \right)^{2.45} + 4.06 \right]$	$K_{zz, sur} = GJ_i^{0.75} \left[ 4 + 11 \left( 1 - \frac{B}{L} \right)^{10} \right]$
Rocking about y-axis	$K_{yy, sur} = \frac{GB^3}{1-\nu} \left[ 3.73 \left( \frac{L}{B} \right)^{2.4} + 0.27 \right]$	$K_{yy, sur} = \frac{G}{1-\nu} (I_y)^{0.75} \left[ 3 \left( \frac{L}{B} \right)^{0.15} \right]$
Rocking about x-axis	$K_{xx, sur} = \frac{GB^3}{1-\nu} \left[ 3.2 \left( \frac{L}{B} \right) + 0.8 \right]$	$K_{xx, sur} = \frac{G}{1-\nu} (I_x)^{0.75} \left( \frac{L}{B} \right)^{0.25} \left[ 2.4 + 0.5 \left( \frac{B}{L} \right) \right]$

Notes:

Axes should be oriented such that  $L \geq B$ .  
 $I_i$  = area moment of inertia of soil-foundation contact,  $i$  denotes which axis to take the surface around.  
 $J_i = I_x + I_y$ , polar moment of inertia of soil-foundation contact surface.  
 $G$  = shear modulus (reduced for large strain effects, e.g., Table 2-1).

Figure 3-5 - Static stiffness of rigid footings at the ground surface  
(NIST GCR 12-917-21 (2012))

Embedment Correction Factors for Static Stiffness of Rigid Footings		
Degree of Freedom	Pais and Kausel (1988)	Gazetas (1991); Mylonakis et al. (2006)
Translation along z-axis	$\eta_z = \left[ 1.0 + \left( 0.25 + \frac{0.25}{L/B} \right) \left( \frac{D}{B} \right)^{0.8} \right]$	$\eta_z = \left[ 1 + \frac{D}{21B} \left( 1 + 1.3 \frac{B}{L} \right) \right] \left[ 1 + 0.2 \left( \frac{A_w}{4BL} \right)^{2/3} \right]$
Translation along y-axis	$\eta_y = \left[ 1.0 + \left( 0.33 + \frac{1.34}{1+L/B} \right) \left( \frac{D}{B} \right)^{0.8} \right]$	$\eta_y = \left( 1 + 0.15 \sqrt{\frac{D}{B}} \right) \left[ 1 + 0.52 \left( \frac{z_w A_w}{BL^2} \right)^{0.4} \right]$
Translation along x-axis	$\eta_x \approx \eta_y$	Same equation as for $\eta_y$ , but $A_w$ term changes for $B \neq L$
Torsion about z-axis	$\eta_{zz} = \left[ 1 + \left( 1.3 + \frac{1.32}{L/B} \right) \left( \frac{D}{B} \right)^{0.9} \right]$	$\eta_{zz} = 1 + 1.4 \left( 1 + \frac{B}{L} \right) \left( \frac{d_w}{B} \right)^{0.9}$
Rocking about y-axis	$\eta_{yy} = \left[ 1.0 + \frac{D}{B} + \left( \frac{1.6}{0.35 + (L/B)^4} \right) \left( \frac{D}{B} \right)^2 \right]$	$\eta_{yy} = 1 + 0.92 \left( \frac{d_w}{B} \right)^{0.6} \left[ 1.5 + \left( \frac{d_w}{D} \right)^{1.9} \left( \frac{B}{L} \right)^{-0.6} \right]$
Rocking about x-axis	$\eta_{xx} = \left[ 1.0 + \frac{D}{B} + \left( \frac{1.6}{0.35 + L/B} \right) \left( \frac{D}{B} \right)^2 \right]$	$\eta_{xx} = 1 + 1.26 \frac{d_w}{B} \left[ 1 + \frac{d_w}{B} \left( \frac{d_w}{D} \right)^{-0.2} \sqrt{\frac{B}{L}} \right]$

Notes:

$d_w$  = height of effective side wall contact (may be less than total foundation height)  
 $z_w$  = depth to centroid of effective sidewall contact  
 $A_w$  = sidewall-solid contact area, for constant effective contact height,  $d_w$ , along perimeter.  
For each degree of freedom, calculate  $K_{emb} = \eta K_{sur}$

Coupling Terms:  $K_{emb,rx} = \left( \frac{D}{3} \right) K_{emb,x}$   
 $K_{emb,ry} = \left( \frac{D}{3} \right) K_{emb,y}$

Figure 3-6 - Embedment correction factors for static stiffness of rigid footings  
(NIST GCR 12-917-21 (2012))

Dynamic Stiffness Modifiers and Radiation Damping Ratios for Rigid Footings (adapted from Pais and Kausel, 1988)		
Degree of Freedom	Surface Stiffness Modifiers	Radiation Damping
Translation along z-axis	$\alpha_z = 1.0 - \left[ \frac{\left(0.4 + \frac{0.2}{L/B}\right) a_0^2}{\left(\frac{10}{1+3(L/B-1)}\right) + a_0^2} \right]$	$\beta_z = \left[ \frac{4\psi(L/B)}{(K_{z,sur}/GB)} \right] \left[ \frac{a_0}{2\alpha_z} \right]$
Translation along y-axis	$\alpha_y = 1.0$	$\beta_y = \left[ \frac{4(L/B)}{(K_{y,sur}/GB)} \right] \left[ \frac{a_0}{2\alpha_y} \right]$
Translation along x-axis	$\alpha_x = 1.0$	$\beta_x = \left[ \frac{4(L/B)}{(K_{x,sur}/GB)} \right] \left[ \frac{a_0}{2\alpha_x} \right]$
Torsion about z-axis	$\alpha_{zz} = 1.0 - \left[ \frac{\left(0.33 - 0.03\sqrt{L/B-1}\right) a_0^2}{\left(\frac{0.8}{1+0.33(L/B-1)}\right) + a_0^2} \right]$	$\beta_{zz} = \left[ \frac{(4/3) \left[ (L/B)^3 + (L/B) \right] a_0^2}{(K_{zz,sur}/GB^3) \left[ \left(\frac{1.4}{1+3(L/B-1)^{0.7}}\right) + a_0^2 \right]} \right] \left[ \frac{a_0}{2\alpha_{zz}} \right]$
Rocking about y-axis	$\alpha_{yy} = 1.0 - \left[ \frac{0.55a_0^2}{\left(0.6 + \frac{1.4}{(L/B)^3}\right) + a_0^2} \right]$	$\beta_{yy} = \left[ \frac{(4\psi/3)(L/B)^3 a_0^2}{\left(\frac{K_{yy,sur}}{GB^3}\right) \left[ \left(\frac{1.8}{1+1.75(L/B-1)}\right) + a_0^2 \right]} \right] \left[ \frac{a_0}{2\alpha_{yy}} \right]$
Rocking about x-axis	$\alpha_{xx} = 1.0 - \left[ \frac{\left(0.55 + 0.01\sqrt{L/B-1}\right) a_0^2}{\left(2.4 - \frac{0.4}{(L/B)^3}\right) + a_0^2} \right]$	$\beta_{xx} = \left[ \frac{(4\psi/3)(L/B) a_0^2}{(K_{xx,sur}/GB^3) \left[ \left(2.2 - \frac{0.4}{(L/B)^3}\right) + a_0^2 \right]} \right] \left[ \frac{a_0}{2\alpha_{xx}} \right]$
Notes:	Orient axes such that $L \geq B$ . Soil hysteretic damping, $\beta_s$ , is additive to foundation radiation damping, $\beta$ . $a_0 = \omega B / V_s$ ; $\psi = \sqrt{2(1-\nu)/(1-2\nu)}$ ; $\psi \leq 2.5$	

Figure 3-7 - Dynamic stiffness modifiers and radiation damping ratios for rigid footings (NIST GCR 12-917-21 (2012))

Dynamic Stiffness Modifiers and Radiation Damping Ratios for Embedded Footings (adapted from Pais and Kausel, 1988)		
Degree of Freedom	Radiation Damping	
Translation along z-axis	$\beta_z = \left[ \frac{4[\psi(L/B) + (D/B)(1+L/B)]}{(K_{z,emb}/GB)} \right] \left[ \frac{a_0}{2\alpha_z} \right]$	
Translation along y-axis	$\beta_y = \left[ \frac{4[L/B + (D/B)(1+\psi L/B)]}{(K_{y,emb}/GB)} \right] \left[ \frac{a_0}{2\alpha_y} \right]$	
Translation along x-axis	$\beta_x = \left[ \frac{4[L/B + (D/B)(\psi + L/B)]}{(K_{x,emb}/GB)} \right] \left[ \frac{a_0}{2\alpha_x} \right]$	
Torsion about z-axis	$\beta_{zz} = \left[ \frac{(4/3) \left[ 3(L/B)(D/B) + \psi(L/B)^3(D/B) + 3(L/B)^2(D/B) + \psi(D/B) + (L/B)^3 + (L/B) \right] a_0^2}{\left(\frac{K_{zz,emb}}{GB^3}\right) \left[ \left(\frac{1.4}{1+3(L/B-1)^{0.7}}\right) + a_0^2 \right]} \right] \left[ \frac{a_0}{2\alpha_{zz}} \right]$	
Rocking about y-axis	$\beta_{yy} = \left[ \frac{(4/3) \left[ \left(\frac{L}{B}\right)^3 \left(\frac{D}{B}\right) + \psi \left(\frac{D}{B}\right)^3 \left(\frac{L}{B}\right) + \left(\frac{D}{B}\right)^3 + 3 \left(\frac{D}{B}\right) \left(\frac{L}{B}\right)^2 + \psi \left(\frac{L}{B}\right)^3 \right] a_0^2}{\left(\frac{K_{yy,emb}}{GB^3}\right) \left[ \left(\frac{1.8}{1+1.75(L/B-1)}\right) + a_0^2 \right]} + \left[ \frac{\left(\frac{4}{3}\right) \left(\frac{L}{B} + \psi\right) \left(\frac{D}{B}\right)^3}{\left(\frac{K_{yy,emb}}{GB^3}\right)} \right] \right] \left[ \frac{a_0}{2\alpha_{yy}} \right]$	
Rocking about x-axis	$\beta_{xx} = \left[ \frac{(4/3) \left[ \left(\frac{D}{B}\right) + \left(\frac{D}{B}\right)^3 + \psi \left(\frac{L}{B}\right) \left(\frac{D}{B}\right)^3 + 3 \left(\frac{D}{B}\right) \left(\frac{L}{B}\right) + \psi \left(\frac{L}{B}\right) \right] a_0^2}{\left(\frac{K_{xx,emb}}{GB^3}\right) \left[ \left(\frac{1.8}{1+1.75(L/B-1)}\right) + a_0^2 \right]} + \left[ \frac{\left(\frac{4}{3}\right) \left(\psi \frac{L}{B} + 1\right) \left(\frac{D}{B}\right)^3}{\left(\frac{K_{xx,emb}}{GB^3}\right)} \right] \right] \left[ \frac{a_0}{2\alpha_{xx}} \right]$	
Notes:	Soil hysteretic damping, $\beta_s$ , is additive to foundation radiation damping, $\beta$ . $\alpha_{emb} = \alpha_{sur}$ ; from Table 2-3a $a_0 = \omega B / V_s$ ; $\psi = \sqrt{2(1-\nu)/(1-2\nu)}$ ; $\psi \leq 2.5$	

Figure 3-8 - Dynamic stiffness modifiers and radiation damping ratios for embedded footings (NIST GCR 12-917-21 (2012))



## 3.4 Structural simulation with the software ETABS

In order to perform the static and dynamic calculation, an accurate study of the geometry and the mechanical properties of the actual construction has to be carried out. The model realised with the software has to be as much similar as possible to the real building as possible. The spatial simulation of the construction is required for the application of any calculation method.

The static model includes the geometric and elastic characteristics of the construction.

The dynamic calculation requires also the inertial characteristics, as the masses of the construction, in the dynamic model.

### 3.4.1 ETABS software

ETABS is an engineering software used for building structural analysis and design. It offers the possibility of masonry structure simulation since it allows the definition of the properties of the materials and the design of various configurations at multiple levels. Moreover it takes into account the non-linear properties of each layer.

The software allows to perform different loading scenarios and the soil conditions through spring constants.

### 3.4.2 Assumptions for modelling simulation

ETABS offers the ability to create the model, but its tools are limited respect to those of a design software. For this reason, some simplifying assumptions have been made to create a simplified model. The assumptions and simplifications lead to a vaguer description of the body of the building, however faithful enough to rule out significant errors during the simulation.

The assumptions are the following ones:

- 1- Absence of the dome. Its weight and mass are calculated, and the load is imposed on the perimeter walls of the building.
- 2- Absence of the roof. Its impact on the construction is calculated and taken into account.

- 3- The curved surfaces are simulated as the sum of straight elements.
- 4- The foundation of the previous construction laying under the Hagia Sophia Church is not considered. The foundation is assumed laying directly on the soil.
- 5- The live loads are neglected. The construction itself is very heavy so the presence of live loads would not change the situation.
- 6- The masonries of the A and B phases are considered equal, due to the similar mechanical characteristics of the materials. So during the design process the two phases are considered together as one.

### 3.4.3 Construction materials simulation

To obtain a model efficiently simulating the behaviour of the construction, four materials have been created: one for the foundation of the building, two for the two different considered construction phases of the building and one for the marble internal columns.

Using the KADET regulation, the mechanical characteristic has been calculated as follows.

The compressive resistance is calculated for

	Compressive strength of the external side of the masonry	Compressive strength of the infill material	Average compressive strength
	$f_{wc} = \xi \cdot \left\{ \left[ \frac{2}{3} \sqrt{f_{bc}} - f_0 \right] + \lambda f_{mc} \right\}$ <p style="text-align: center;">[MPa]</p>	$f_{c,i}$ <p style="text-align: center;">[MPa]</p>	$f_{wc} = \frac{1}{\gamma_{Ra}} \frac{(2 \lambda_e \delta f_{c,e} + \lambda_i f_{c,i})}{(1 + 2\delta)}$ <p style="text-align: center;">[MPa]</p>
Foundation	2,966370214	1,98	1,90
Masonry A and B phases	2,694053189	1,80	1,72
Masonry C phase	1,73142397	1,15	1,11

Table 3-2 - Compressive strength calculation for the three layers masonry

	Compressive strength	Modulus of elasticity	Final modulus of elasticity
	$0,67 f_{wc}$ [MPa]	$E_{wc} = 1000 \cdot f_{wc}$ [MPa]	$E_{wc} = 1/2 \cdot E_{wc}$ [MPa]
Foundation	1,27	1271,98	635,99
Masonry A and B phases	1,16	1155,21	577,61
Masonry C phase	0,74	742,43	371,22

*Table 3-3 – Final compressive strength and modulus of elasticity of the materials calculation*

The compressive strength of a three layers masonry is calculated as indicated in the chapter 3.1.2 about the Greek Regulation for the evaluation and structural intervention in masonry (KADET).

The modulus of elasticity is considered empirically equal to 1000 times the compressive strength of the wall. The modulus of elasticity used in the software is taken equal to half of the one calculated, due to the reduction of strength of the materials due to the age of construction, as suggested by Professor Ignatakis.

Calculating the modulus of elasticity of marble is not necessary, cause it is a compact material and the mechanical characteristics are already known. The mechanical characteristics listed in the chapter 2.2 are directly inserted in the software.

The following images are taken from the ETABS software and show the creation of the previously analysed materials. The materials behaviour is considered elastic.

The specific weight and the Poisson ratio of the prevailing materials are considered for each formation.

Material Property Data

**General Data**

Material Name: Foundation

Material Type: Masonry

Directional Symmetry Type: Isotropic

Material Display Color:  Change...

Material Notes: Modify/Show Notes...

**Material Weight and Mass**

Specify Weight Density       Specify Mass Density

Weight per Unit Volume: 22,065 kN/m<sup>3</sup>

Mass per Unit Volume: 2250 kg/m<sup>3</sup>

**Mechanical Property Data**

Modulus of Elasticity, E: 635,99 MPa

Poisson's Ratio, U: 0,15

Coefficient of Thermal Expansion, A: 0,0000081 1/C

Shear Modulus, G: 276,52 MPa

**Design Property Data**

Modify/Show Material Property Design Data...

**Advanced Material Property Data**

Nonlinear Material Data...      Material Damping Properties...

Time Dependent Properties...

OK      Cancel

Figure 3-9 - Introduction of the foundation characteristics in ETABS

**Material Property Data**

**General Data**

Material Name: Masonry A,B

Material Type: Masonry

Directional Symmetry Type: Isotropic

Material Display Color:

Material Notes:

**Material Weight and Mass**

Specify Weight Density       Specify Mass Density

Weight per Unit Volume: 19,6133 kN/m<sup>3</sup>

Mass per Unit Volume: 2000 kg/m<sup>3</sup>

**Mechanical Property Data**

Modulus of Elasticity, E: 577,61 MPa

Poisson's Ratio, U: 0,15

Coefficient of Thermal Expansion, A: 0,0000081 1/C

Shear Modulus, G: 251,13 MPa

**Design Property Data**

**Advanced Material Property Data**

Figure 3-10 - Introduction of the A and B phase masonry characteristics in ETABS


**Material Property Data**

**General Data**

Material Name: Masonry C

Material Type: Masonry

Directional Symmetry Type: Isotropic

Material Display Color:  Change...

Material Notes: Modify/Show Notes...

**Material Weight and Mass**

Specify Weight Density       Specify Mass Density

Weight per Unit Volume: 19,6133 kN/m<sup>3</sup>

Mass per Unit Volume: 2000 kg/m<sup>3</sup>

**Mechanical Property Data**

Modulus of Elasticity, E: 371,22 MPa

Poisson's Ratio, U: 0,16

Coefficient of Thermal Expansion, A: 0,0000081 1/C

Shear Modulus, G: 160,01 MPa

**Design Property Data**

Modify/Show Material Property Design Data...

**Advanced Material Property Data**

Nonlinear Material Data...      Material Damping Properties...

Time Dependent Properties...

OK      Cancel

Figure 3-11 - Introduction of the C phase masonry characteristics in ETABS

**Material Property Data** [X]

**General Data**

Material Name:

Material Type:

Directional Symmetry Type:

Material Display Color:

Material Notes:

**Material Weight and Mass**

Specify Weight Density       Specify Mass Density

Weight per Unit Volume:  kN/m<sup>3</sup>

Mass per Unit Volume:  kg/m<sup>3</sup>

**Mechanical Property Data**

Modulus of Elasticity, E:  MPa

Poisson's Ratio, U:

Coefficient of Thermal Expansion, A:  1/C

Shear Modulus, G:  MPa

**Design Property Data**

**Advanced Material Property Data**

Figure 3-12 - Introduction of the marble characteristics in ETABS

### 3.4.4 Model creation in ETABS

ETABS software enables the creation of different components with specific geometry and mechanical properties. Thus, five different masonry sections with different dimensions (the thickness of the wall varies depending on the side of the building) and a frame cross section for the simulation of the marble columns have been created.

After the creation of the sections, the design of the building is realised, according to the simplifying assumptions mentioned in the 3.3.2 chapter. The curved surfaces at the apse side have been converted in polygonal surfaces.

The model is divided in three levels:

- foundation;
- first level;
- second level.

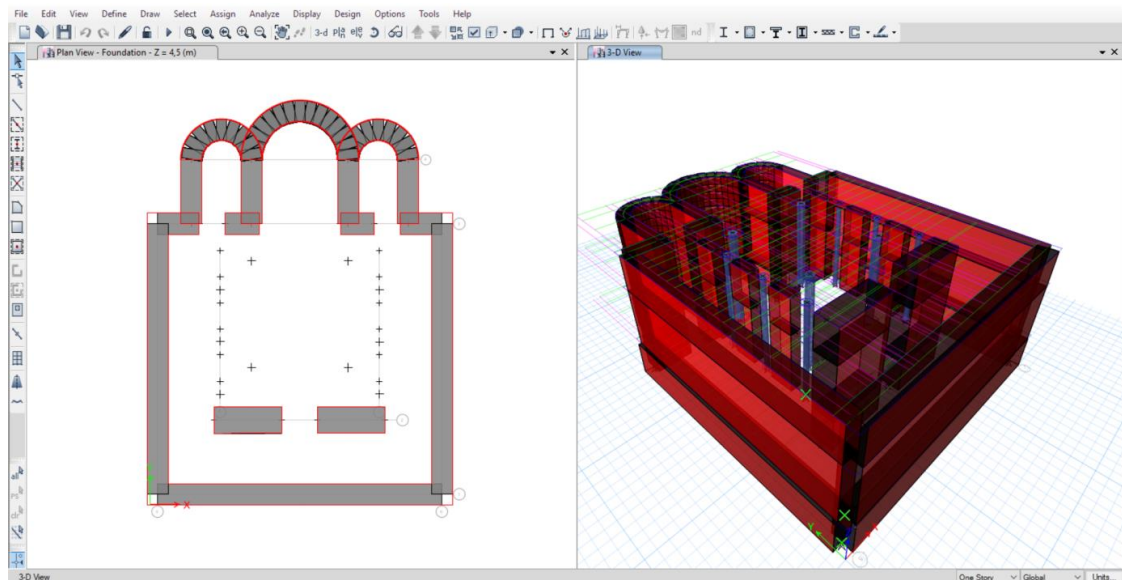


Figure 3-13 - First phase of the model creation



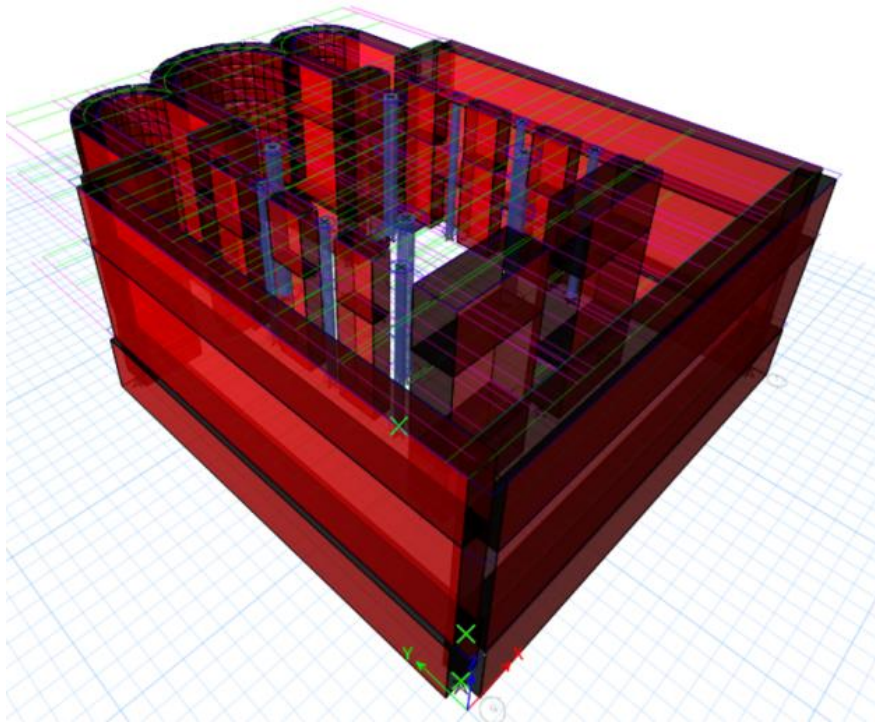


Figure 3-14 - 3D model in ETABS

The elements have then been considered separately and the openings have been designed in each wall of the building.

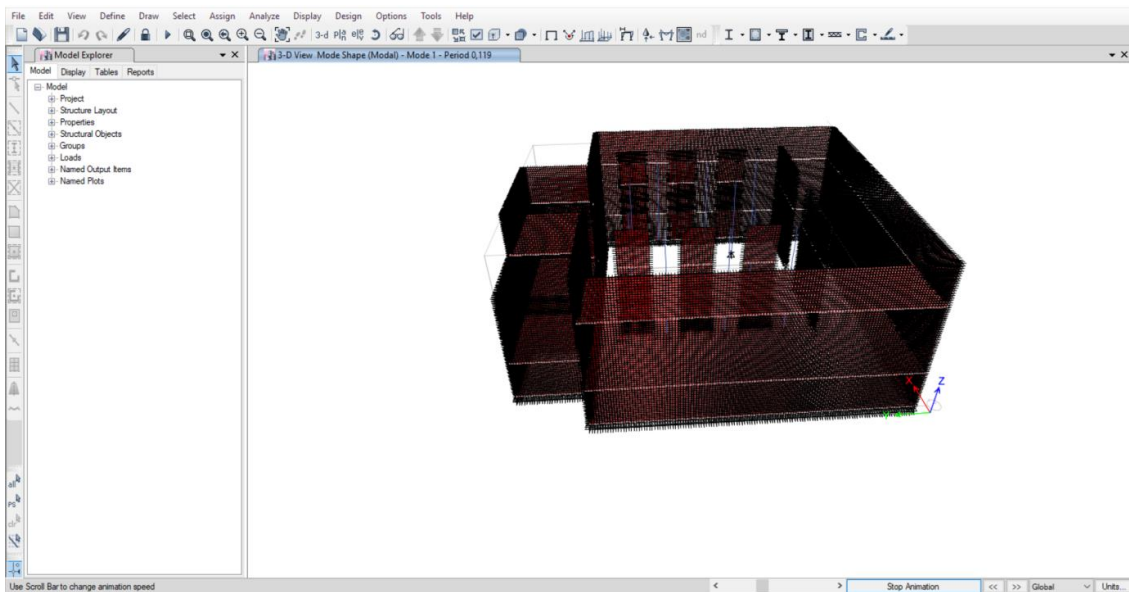


Figure 3-15 - Final model, including the assumptions made for the geometry of the building

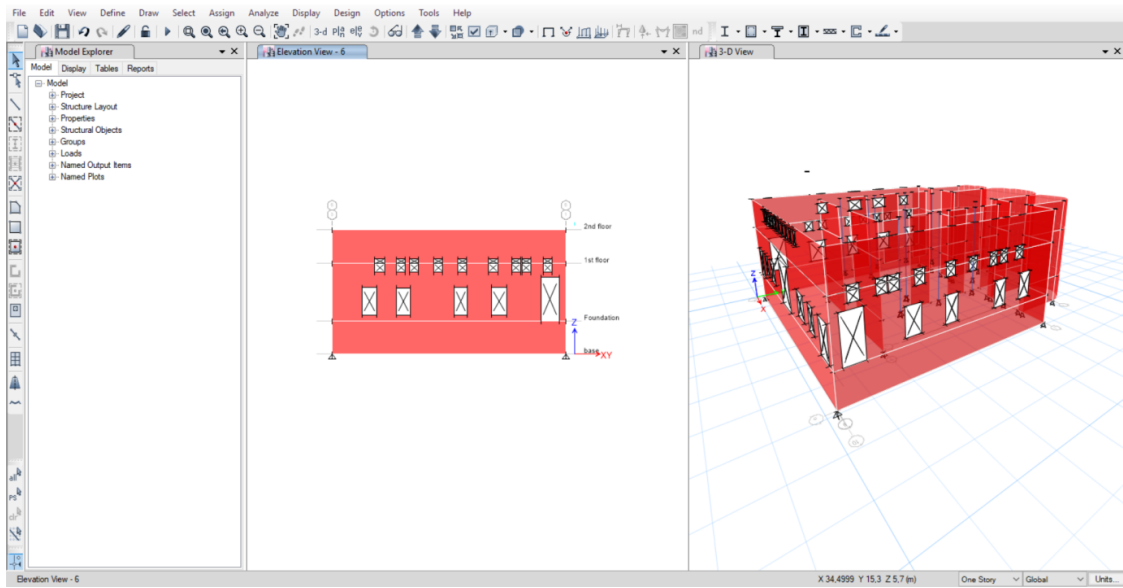


Figure 3-16 - Openings creation in each wall of the monument

The dome and the roof are absent as previously assumed. Their influence is simulated using diaphragms at the end of the first and second levels. And their loads are added as extra forces.

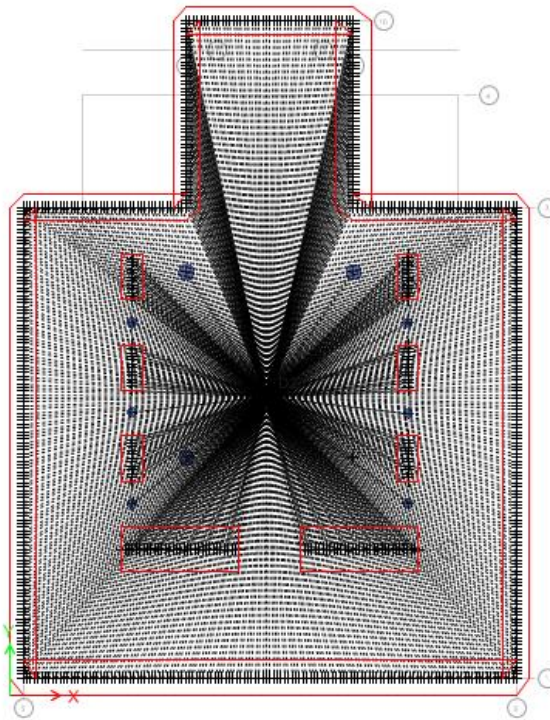


Figure 3-17 - Top view of the second level diaphragm

### 3.4.5 Foundation simulation in ETABS

In the fixed- base model the soil- foundation- structure interaction was not considered.

In the flexible model the foundation has been simulated through vertical and horizontal springs applied along the entire length and height of the foundation of the construction.

To calculate the spring constants, the properties of the underlying soil have been studied. These studies have been made both in the area surrounding the Church and under a close historical building (in Agia Sophia 31 street).

Under the foundation of the Church, the following layers are distinguished:

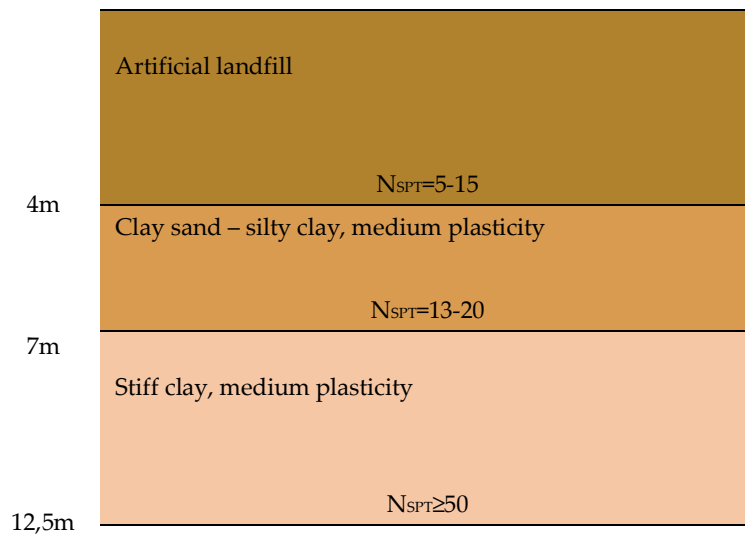


Figure 3-18 – Section of the soil under the Agia Sophia Church

$N_{SPT}$  is an experimental way of measuring the strength of the soil. SPT stands for Standard Penetration Test, that is used to measure the in situ density and angle of shearing resistance of cohesion- less soils and the strength of cohesive soils.

The ground at the foundation level, until a depth of about 4,5 m, is classified in category “D” according to the EN 1998-1. This category is characterized by the deposits of loose- to- medium cohesionless soil or of predominantly soft- to- firm cohesive soil. This results in an average shear wave velocity  $v_{s,30}$  lower than 180 m/s.

The ground types are described by the stratigraphic profiles. The classification can be used to measure the influence of local ground conditions on the seismic action.

The table with the detailed classification taken from the norm EN 1998-1 is shown below.

Ground type	Description of stratigraphic profile	Parameters		
		$v_{s,30}$ (m/s)	$N_{SPT}$ (blows/30cm)	$c_u$ (kPa)
A	Rock or other rock-like geological formation, including at most 5 m of weaker material at the surface.	> 800	–	–
B	Deposits of very dense sand, gravel, or very stiff clay, at least several tens of metres in thickness, characterised by a gradual increase of mechanical properties with depth.	360 – 800	> 50	> 250
C	Deep deposits of dense or medium-dense sand, gravel or stiff clay with thickness from several tens to many hundreds of metres.	180 – 360	15 - 50	70 - 250
D	Deposits of loose-to-medium cohesionless soil (with or without some soft cohesive layers), or of predominantly soft-to-firm cohesive soil.	< 180	< 15	< 70
E	A soil profile consisting of a surface alluvium layer with $v_s$ values of type C or D and thickness varying between about 5 m and 20 m, underlain by stiffer material with $v_s > 800$ m/s.			
$S_1$	Deposits consisting, or containing a layer at least 10 m thick, of soft clays/silts with a high plasticity index ( $PI > 40$ ) and high water content	< 100 (indicative)	–	10 - 20
$S_2$	Deposits of liquefiable soils, of sensitive clays, or any other soil profile not included in types A – E or $S_1$			

Table 3-4 - Ground type classification based on the stratigraphic profile  
(Eurocode 8)

Using the soil classification method, the results are conservative, so a new method is used.

Considered the results of the Standard Penetration Test and according to the article published by Professor Pitilakis in 1999, the shear wave velocity is given by the equation:

$$v_s = 132 (N_{60})^{0,271} \quad [\text{m/s}]$$

Where  $N_{60}$  is the energy corrected SPT blow count. The subscript 60 indicates the percentage of the theoretical free- fall hammer energy. It may be normalised to an effective overburden pressure of 100 kPa, which produces the  $N_{1,60}$  value. The shear wave velocity value is calculated for each layer:

$v_s$ [m/s]	
$v_{s1}$	231,91
$v_{s2}$	274,98
$v_{s3}$	358,70

*Table 3-5 - Shear wave velocity for layers*

The final average value for the foundation soil is  $v_s = 280$  m/s .

The shear modulus is calculated as:

$$G = \rho (v_s)^2$$

The value of the shear modulus  $G$  is used to estimate the stiffness of the springs in ETABS software.

Since in this case the foundation is a thicker wall, the walls are considered lying directly on the soil.

For the calculation of the spring constants, the foundation has been segmented in 11 sections, as shown below.

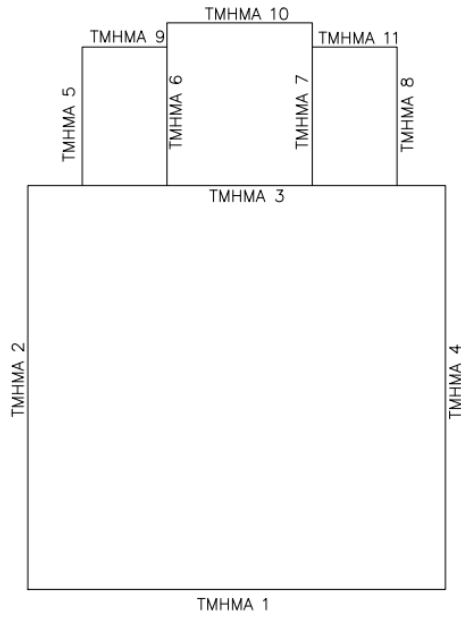


Table 3-6 - Segmentation of the foundation for the calculation of the spring constants

The spring constants are now calculated using the equations taken from NIST documentation and shown in the 3.2 chapter.

$\alpha_o$	$\omega \cdot B/v_s$
$\Psi$	$\sqrt{2(1 - \nu)/(1 - 2\nu)}$
$v_s$	280 m/s
$G$	$E/2(\nu + 1)$
$G$	$\rho (v_s)^2$
$T$	0,487
$\omega$	12,9018
$N_{SPT,avg}$	10
$N_{SPT,w,avg}$	12,1609
$N_{60(1)}$	11,2
$N_{60(2)}$	8,1
$N_{60(3)}$	9,77471

Table 3-7 - Spring constants calculation parameters

Static stiffness		
Translation along z-axis	$K_{z,sur}$	$\frac{GB}{1-\nu} \left[ 3,1 \left( \frac{L}{B} \right)^{0,75} + 1,6 \right]$
Translation along y-axis	$K_{y,sur}$	$\frac{GB}{2-\nu} \left[ 6,8 \left( \frac{L}{B} \right)^{0,65} + 0,8 \left( \frac{L}{B} \right) + 1,6 \right]$
Translation along x-axis	$K_{x,sur}$	$\frac{GB}{2-\nu} \left[ 6,8 \left( \frac{L}{B} \right)^{0,65} + 2,4 \right]$

Table 3-8 - Elastic solutions for static stiffness

[NIST GCR 12-917-21 (2012)- Soil Structure Interaction for Building Structures. NEHRP Consultants Joint Venture]

Embedment correction factors		
Translation along z-axis	$\eta_z$	$\left[ 1,0 + \left( 0,25 + \frac{0,25}{L/B} \right) \left( \frac{D}{B} \right)^{0,8} \right]$
Translation along y-axis	$\eta_y$	$\left[ 1,0 + \left( 0,33 + \frac{1,34}{1+L/B} \right) \left( \frac{D}{B} \right)^{0,8} \right]$
Translation along x-axis	$\eta_x$	$\eta_x \approx \eta_y$

Table 3-9 - Embedment correction factors for static stiffness

[NIST GCR 12-917-21 (2012)- Soil Structure Interaction for Building Structures. NEHRP Consultants Joint Venture]

Dynamic stiffness modifiers		
Translation along z-axis	$\alpha_z$	$1,0 - \frac{\left( 0,4 + \frac{0,2}{L/B} \right) \alpha_0^2}{\left( \frac{10}{1+3(L/B-1)} \right) + \alpha_0^2}$
Translation along y-axis	$\alpha_y$	$\alpha_y = 1,0$
Translation along x-axis	$\alpha_x$	$\alpha_x = 1,0$

Table 3-10 - Dynamic stiffness modifiers

[NIST GCR 12-917-21 (2012)- Soil Structure Interaction for Building Structures. NEHRP Consultants Joint Venture]

From the shear wave velocity, the other mechanical characteristics of the soil are found.

The final parameters used to define the springs in ETABS software are shown in the following tables.

Section	B	L	D	G <sub>1</sub>	G <sub>2</sub>	G <sub>3</sub>	v	ρ	α <sub>0</sub>	Ψ
τμ1	1,25	16,8	4,5	2,69	1,63	2,21	0,3	2,03874	0,38881	1,87
τμ2	1,25	16	4,5	2,69	1,63	2,21	0,3	2,03874	0,38881	1,87
τμ3	1,25	16,8	4,5	2,69	1,63	2,21	0,3	2,03874	0,38881	1,87
τμ4	1,25	16	4,5	2,69	1,63	2,21	0,3	2,03874	0,38881	1,87
τμ5	1,25	5,35	4,5	2,69	1,63	2,21	0,3	2,03874	0,38881	1,87
τμ6	1,25	6,35	4,5	2,69	1,63	2,21	0,3	2,03874	0,38881	1,87
τμ7	1,25	6,35	4,5	2,69	1,63	2,21	0,3	2,03874	0,38881	1,87
τμ8	1,25	5,35	4,5	2,69	1,63	2,21	0,3	2,03874	0,38881	1,87
τμ9	1,25	3,55	4,5	2,69	1,63	2,21	0,3	2,03874	0,38881	1,87
τμ10	1,25	5,7	4,5	2,69	1,63	2,21	0,3	2,03874	0,38881	1,87
τμ11	1,25	3,55	4,5	2,69	1,63	2,21	0,3	2,03874	0,38881	1,87

Section	K <sub>z,sur</sub>	K <sub>y,sur</sub>	K <sub>x,sur</sub>	η <sub>z</sub>	η <sub>y</sub>	η <sub>x</sub>	α <sub>z</sub>	α <sub>y</sub>	α <sub>x</sub>
τμ1	6667514	5777895	4608265	1,748	2,178	2,178	0,99479	1	1
τμ2	6444352	5582674	4473218	1,751	2,190	2,190	0,99504	1	1
τμ3	6667514	5777895	4608265	1,748	2,178	2,178	0,99479	1	1
τμ4	6444352	5582674	4473218	1,751	2,190	2,190	0,99504	1	1
τμ5	3089572	2646752	2338361	1,859	2,627	2,627	0,9984	1	1
τμ6	3450654	2964248	2580639	1,834	2,534	2,534	0,99808	1	1
τμ7	3450654	2964248	2580639	1,834	2,534	2,534	0,99808	1	1
τμ8	3089572	2646752	2338361	1,859	2,627	2,627	0,9984	1	1
τμ9	2392383	2030150	1857150	1,942	2,892	2,892	0,99898	1	1
τμ10	3217727	2759546	2424828	1,849	2,591	2,591	0,99829	1	1
τμ11	2392383	2030150	1857150	1,942	2,892	2,892	0,99898	1	1



Section	$k_z$	$k_y$	$k_x$	$k_{z, \text{uploaded}}$	$k_{y, \text{uploaded}}$	$k_{x, \text{uploaded}}$
$\tau\mu 1$	11596955	12584716,33	10037169	85903,4	5566	295211
$\tau\mu 2$	11228225,7	12226456,07	9796668	88411,2	5663,02	288137
$\tau\mu 3$	11596955	12584716,33	10037169	85903,4	5401,17	295211
$\tau\mu 4$	11228225,7	12226456,07	9796668	88411,2	5663,02	288137
$\tau\mu 5$	5735412,61	6952119,722	6142081	136557	9736,86	361299
$\tau\mu 6$	6315386,67	7510261,319	6538345	123831	9015,92	384609
$\tau\mu 7$	6315386,67	7510261,319	6538345	123831	9015,92	384609
$\tau\mu 8$	5735412,61	6952119,722	6142081	136557	9736,86	361299
$\tau\mu 9$	4641000,66	5870875,314	5370587	165750	12790,6	315917
$\tau\mu 10$	5940542,28	7150118,419	6282850	126395	9346,56	184790
$\tau\mu 11$	4641000,66	5870875,314	5370587	165750	12790,6	315917

*Table 3-11 - Parameters to define the springs in ETABS software*

After the calculation of the spring constants, the parameters are applied along the entire length and height of the foundation of the building.

The procedure is shown for below for the section  $\tau\mu 1$  since it is the same for all the elements.

Point Spring Property Data

**General Data**

Property Name:

Display Color:

Property Notes:

**Spring Stiffness Options**

User Specified/Link Properties  Based on Soil Profile and Footing Dimensions

**Simple Spring Stiffness in Global Directions**

Translation X:  kN/m

Translation Y:  kN/m

Translation Z:  kN/m

Rotation about X-Axis:  kN-m/rad

Rotation about Y-Axis:  kN-m/rad

Rotation about Z-Axis:  kN-m/rad

**Single Joint Links at Point**

Link Property	Axial Direction	Axis 2 Angle

Table 3-12 - Inserting values for translation along the x-axis for section  $\tau\mu 1$

Point Spring Property Data

**General Data**

Property Name:

Display Color:

Property Notes:

**Spring Stiffness Options**

User Specified/Link Properties  Based on Soil Profile and Footing Dimensions

**Simple Spring Stiffness in Global Directions**

Translation X:  kN/m

Translation Y:  kN/m

Translation Z:  kN/m

Rotation about X-Axis:  kN-m/rad

Rotation about Y-Axis:  kN-m/rad

Rotation about Z-Axis:  kN-m/rad

**Single Joint Links at Point**

Link Property	Axial Direction	Axis 2 Angle

Table 3-13 - Inserting values for translation along the y-axis for section  $\tau\mu 1$

Point Spring Property Data

General Data

Property Name:

Display Color:

Property Notes:

Spring Stiffness Options

User Specified/Link Properties  Based on Soil Profile and Footing Dimensions

Simple Spring Stiffness in Global Directions

Translation X:  kN/m

Translation Y:  kN/m

Translation Z:  kN/m

Rotation about X-Axis:  kN-m/rad

Rotation about Y-Axis:  kN-m/rad

Rotation about Z-Axis:  kN-m/rad

Single Joint Links at Point

Link Property	Axial Direction	Axis 2 Angle

Table 3-14 - Inserting values for translation along the z-axis for section  $\tau\mu 1$

# Chapter 4

## Loads and reactions of the model

### 4.1 Loading condition

The paragraph analyses the types of loading conditions applied to the model and how they are performed. There are two subcategories: static loads and dynamic loads.

The static loads category includes the weight of the dome and the roof and the one of the load-bearing masonry.

For the dynamic loads we impose the seismic acceleration along the x and y directions.

#### 4.1.1 Vertical contribution of dome and roof

As explained in 3.3.2 chapter, two of the simplifying assumptions are the absence of the dome and the roof. They are replaced with equivalent loads, masses and stiffnesses.

The loads they transmit to the building have been calculated and applied along the perimeter of the church as vertical forces.



Figure 4-1 - Vertical section of Hagia Sophia Church at the dome level  
(K. Theoharidou, 1988)

The geometry of the dome is visible in the vertical section above. It is reinforced at the external base (including the mosaics and the bronze cladding). For the calculation, a thickness of 40 cm is chosen for the entire dome.

For the base of the dome, so the stairs made of green stone, brick and mortar, the thickness is chosen equal to 50 cm.

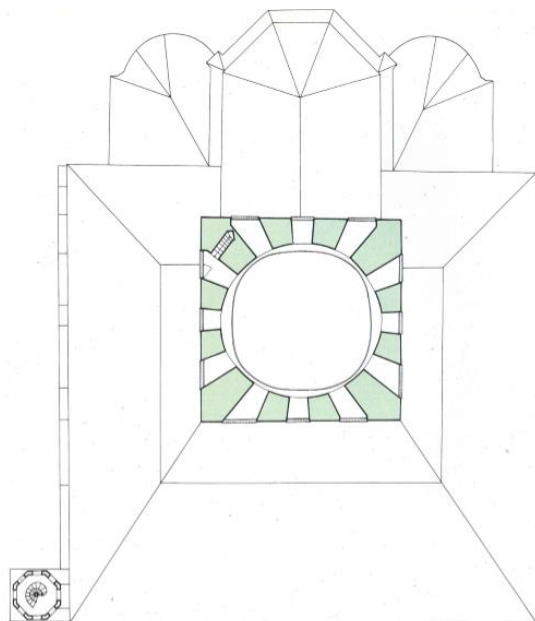


Figure 4-2 – Roof plan of Hagia Sophia Church  
(K. Theoharidou, 1988)

The rest of the cover is made of bricks and it is considered to have a thickness of 30 cm for the calculations.

The loads of the roof and the dome are shown in the following table.

Covering loads calculation						
	Area [m <sup>2</sup> ]	Volume [m <sup>3</sup> ]	$\gamma$ [kN/m <sup>3</sup> ]	G [m/s <sup>2</sup> ]	Mass [kg]	Weight [kN]
Central dome	199,157	119,4942	20	9,81	243,6171	2389,884
Square perimeter of the dome	101,947	50,9735	20	9,81	103,9215	1019,47
Dome ramp	122,036	61,018	28	9,81	174,1594	1708,504
Central square perimeter	170,71	85,355	20	9,81	174,0163	1707,1
Total roof area without the elevated sanctuary	702,964	351,482	20	9,81	716,579	7029,64
Central sanctuary	130,835	65,4175	20	9,81	133,369	1308,35
Right sanctuary	70,561	35,2805	20	9,81	71,92762	705,61
Left sanctuary	70,561	35,2805	20	9,81	71,92762	705,61

*Table 4-1 - Calculation of covering loads, including dome and roof*

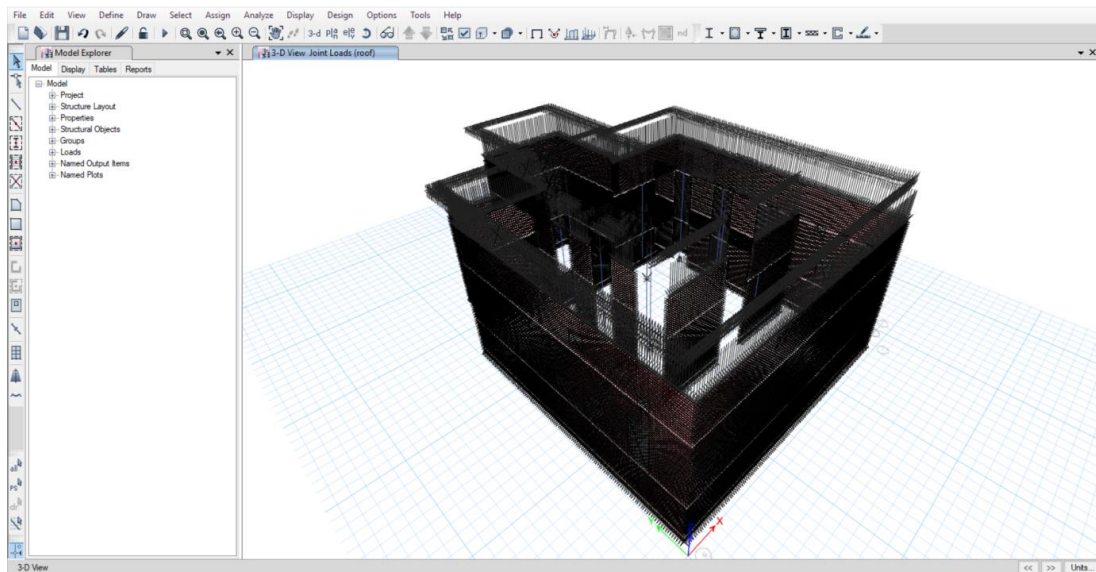


*Figure 4-3 - Imposition of the covering loads on the perimeter of the building*

## 4.1.2 Weight of the load- bearing masonry

The perimeter and the interior masonry walls produce loads uniformly distributed over the entire surface. Calculating these loads is not necessary, since they are directly calculated by ETABS software, after inserting the mechanical characteristics of the materials and the geometry of each elements.

## 4.1.3 Modal analysis

Thanks to the modal analysis done with ETABS software, the natural periods of vibration are found both in x and y directions, both for the model with springs and the one with fixed- base.

This analysis shows the dynamic characteristics of the structure. Knowing the basic characteristics of vibration leads to understand how the building is going to react when an earthquake load is applied, so if the structure is stiff or flexible. The natural periods and the shape of deformation are found, and the most influential ones are shown below.



For the flexible model, the periods are 0,43 s in the x-axis direction and 0,379 s in the y-axis direction. In this case the values are higher cause of the model is more flexible. This model is more precise since also the soil effect is considered.

For the fixed- base model, the periods are 0,291 s in the x-axis direction and 0,271 s in the y-axis direction.

- Flexible model: modal analysis

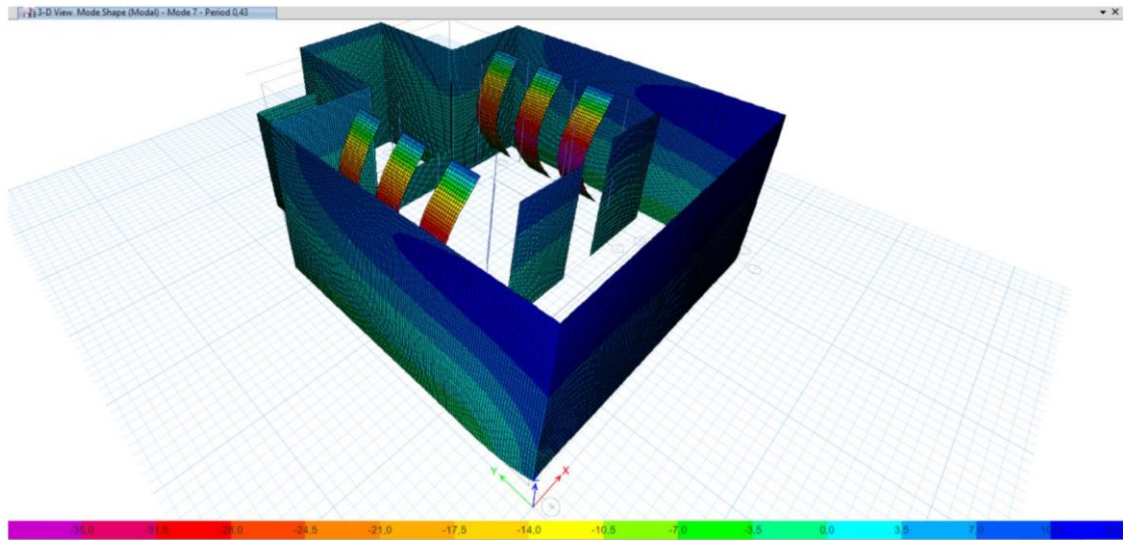


Figure 4-4 - Modal analysis of the flexible model in x-axis direction. The displacements values [mm] are quantitatively (based on colour) shown in the horizontal axis at the bottom of the image.

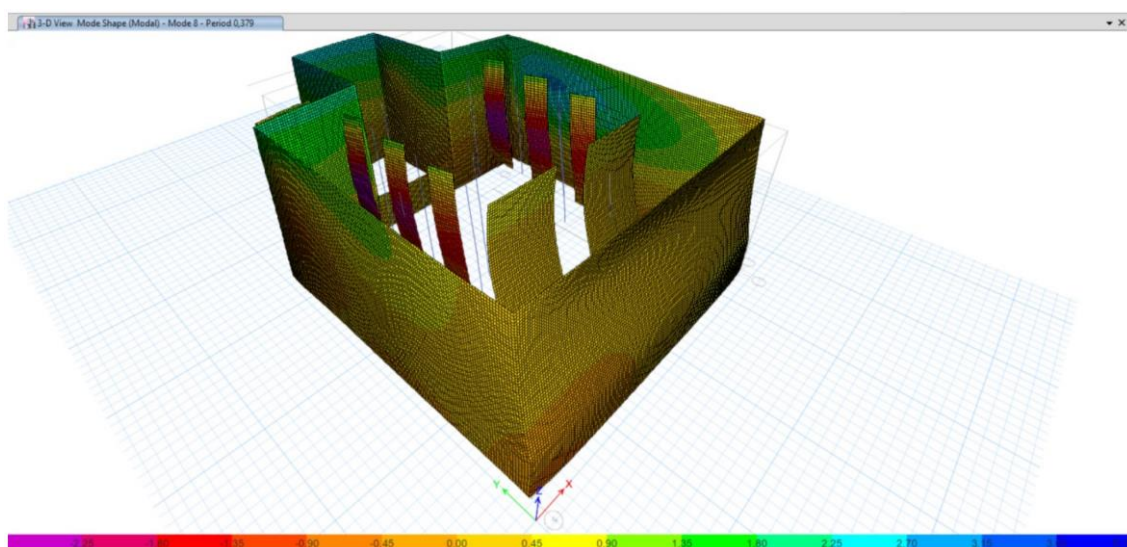


Figure 4-5 - Modal analysis of the flexible model in y-axis direction. The displacements values [mm] are quantitatively (based on colour) shown in the horizontal axis at the bottom of the image.

- Fixed- base model: modal analysis

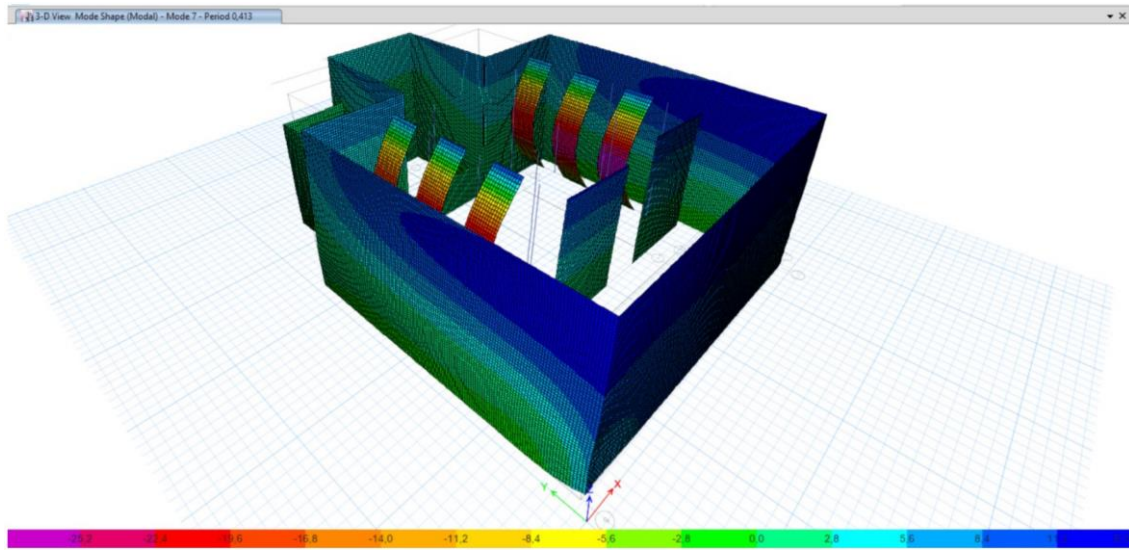


Figure 4-6 - Modal analysis of the fixed- base model in x-axis direction. The displacements values [mm] are quantitatively (based on colour) shown in the horizontal axis at the bottom of the image.

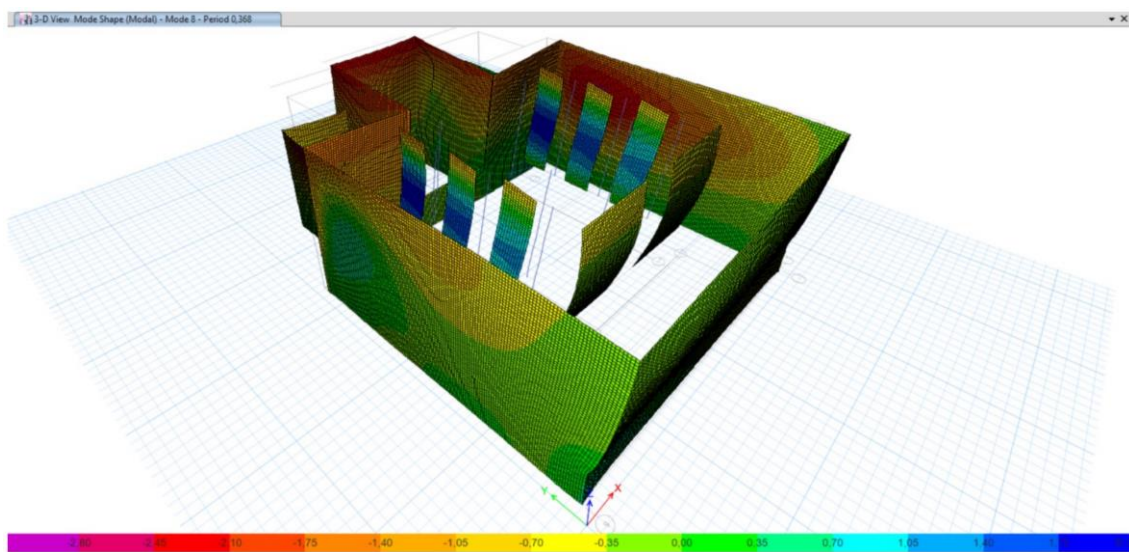


Figure 4-7 - Modal analysis of the fixed- base model in y-axis direction. The displacements values [mm] are quantitatively (based on colour) shown in the horizontal axis at the bottom of the image.

## 4.1.4 Dynamic load

The analysis is performed first for the dead loads, since the live loads are neglected as assumption, as previously said. Then the seismic load is applied. The simulation of the seismic action is based on the acceleration recorded by the accelerometers at the City Hotel in Thessaloniki, during the earthquake on the 20<sup>th</sup> of June 1978.

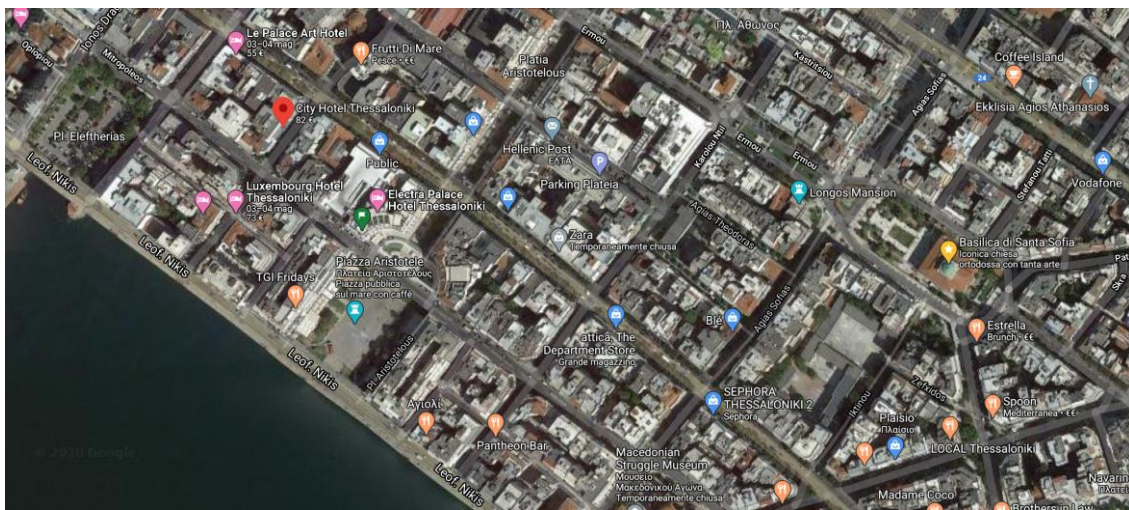


Figure 4-8 - Geographical location of the City Hotel in Thessaloniki

The following figures show the time history of the earthquake. A time step of 0,01 is set and a total of 3000 steps are selected.

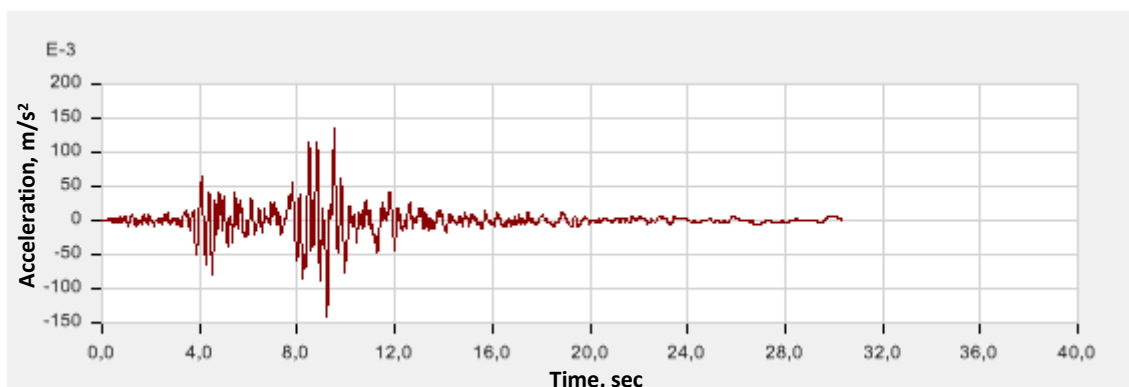


Figure 4-9 - Seismic history along x direction

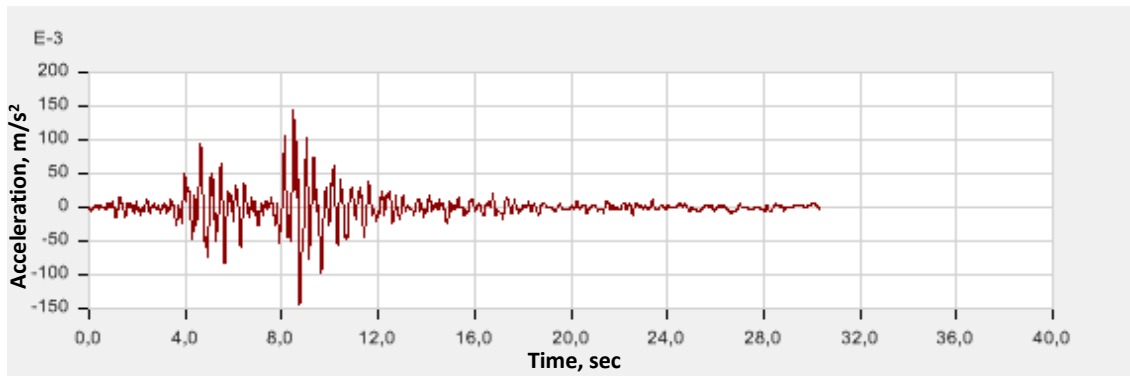


Figure 4-10 - Seismic history along y direction

## 4.2 Answer of the structure under seismic action

The following tables show the displacements that occur after the analysis made with ETABS software in the four corners of the masonry of both the flexible model and the fixed- base one. These values are the maximum displacements at non simultaneous times.

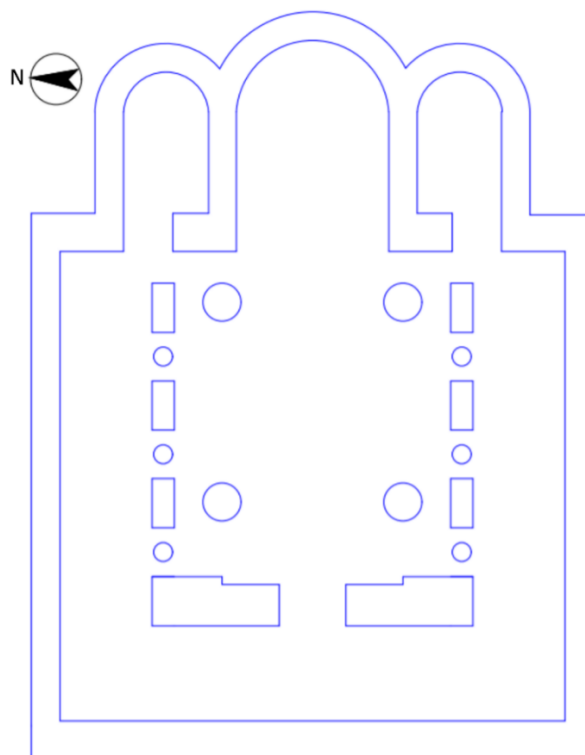


Figure 4-11 - Floor plan of Hagia Sophia Church with orientation

Flexible model							
North - West				North - East			
Elevation	x	y	z	Elevation	x	y	z
12,5	-14,453	19,077	-3,344	12,5	-9,642	19,077	-2,914
0	-9,653	4,682	-3,78	0	-1,52	-9,528	-1,725
-4,5	-7,711	1,371	-1,766	-4,5	-0,513	-7,715	-0,851
South - West				South - East			
Elevation	x	y	z	Elevation	x	y	z
12,5	-14,453	20,573	3,345	12,5	-9,642	20,573	4,731
0	-8,204	2,395	2,535	0	1,714	3,257	3,033
-4,5	-6,61	-0,95	1,42	-4,5	-1,297	1,081	1,351

Table 4-2 - Maximum displacements at the four corners of the flexible model at the top of the building, at the ground level and at the lowest point of the foundation. The values are given in mm.

Flexible model			
Side	x	y	z
North (middle)	-7,37	-13,342	-0,632
West (middle)	-12,607	13,644	0,395
South (middle)	-6,463	11,344	0,225

Table 4-3 - Maximum displacements in the middle of each side of the flexible model, except the side of the sanctuary. The values are given in mm.

For the fixed- base model at the -4,5 m elevation, the values of expected deformation are zero. So in the following tables the displacements in -4,5 m are not shown.

Fixed- base model							
North - West				North - East			
Elevation	x	y	z	Elevation	x	y	z
12,5	7,214	4,265	-2,494	12,5	10,539	4,265	2,01
0	0,099	-0,029	0,133	0	0,138	0,059	0,171
South - West				South - East			
Elevation	x	y	z	Elevation	x	y	z
12,5	7,214	-5,333	-2,466	12,5	10,539	-5,333	1,729
0	0,102	-0,08	-0,198	0	0,149	-0,074	-0,146

Table 4-4 - Maximum displacements at the four corners of the fixed- base model at the top of the building and at the ground level. The values are given in mm.

Fixed- base model			
Side	x	y	z
North (middle)	11,735	1,789	0,067
West (middle)	3,272	-5,722	-0,03
South (middle)	15,716	-2,392	-0,083

Table 4-5 - Maximum displacements in the middle of each side of the fixed- base model, except the side of the sanctuary. The values are given in mm.

The images below depict the maximum stresses on the walls. They are the maximum values recorded during the seismic analysis. They happen at different times, so these are not actual snapshots of the movement.

The purpose is defining which part of the structure suffer the most during a seismic activity.

For what concerns the principal stresses, the positive values correspond to traction, while the negative ones to compression.

The distributions are recorded in the three walls at north, south and west, both for the flexible model and the fixed- base one.

- Flexible model: Principal stresses

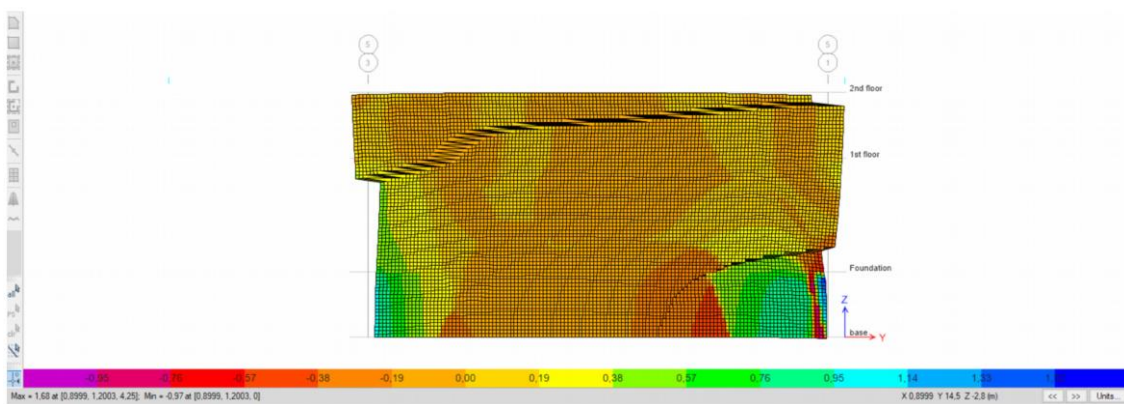


Figure 4-12 – Maximum principal stresses distribution on the north wall of the flexible model. The principal stress values [MPa] are qualitatively shown based on colour in the horizontal axis at the bottom of the image.

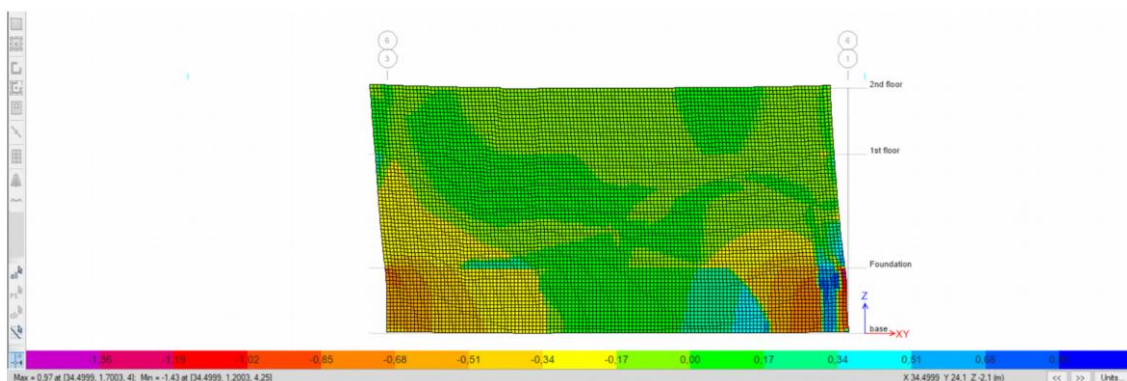


Figure 4-13 – Maximum principal stresses distribution on the south wall of the flexible model. The principal stress values [MPa] are qualitatively shown based on colour in the horizontal axis at the bottom of the image.

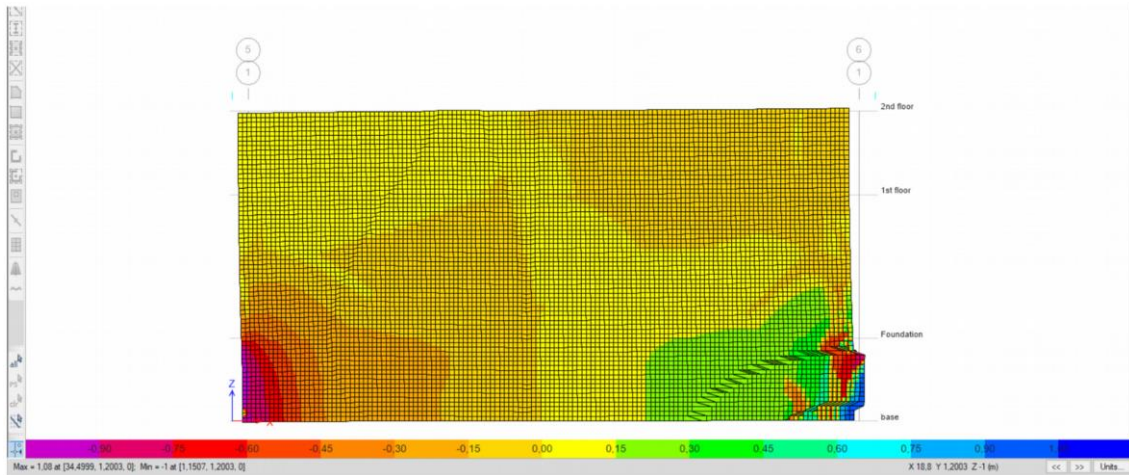


Figure 4-14 – Maximum principal stresses distribution on the west wall of the flexible model. The principal stress values [MPa] are qualitatively shown based on colour in the horizontal axis at the bottom of the image.

In the majority of the north wall, mainly negative principal stresses (traction) are observed (orange colour), while there are small positive trends (compression) mostly at the two sides (green and blue colour). The south wall is mainly dominated by traction (green colour), with negative values in small areas (orange and yellow). On the west wall, the highest absolute values are observed to appear at the height of the foundation, at the joints with the other walls (red and blue colour), while the rest of the wall is subjected to small compression.

- Flexible model: Shear stresses

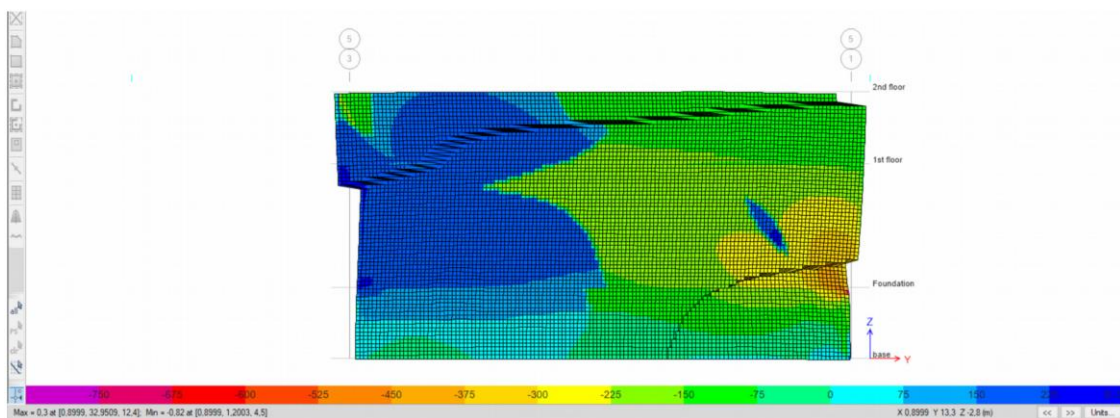


Figure 4-15 - Maximum shear stress distribution on the north wall of the flexible model. The shear stress values [MPa] are qualitatively shown based on colour in the horizontal axis at the bottom of the image.



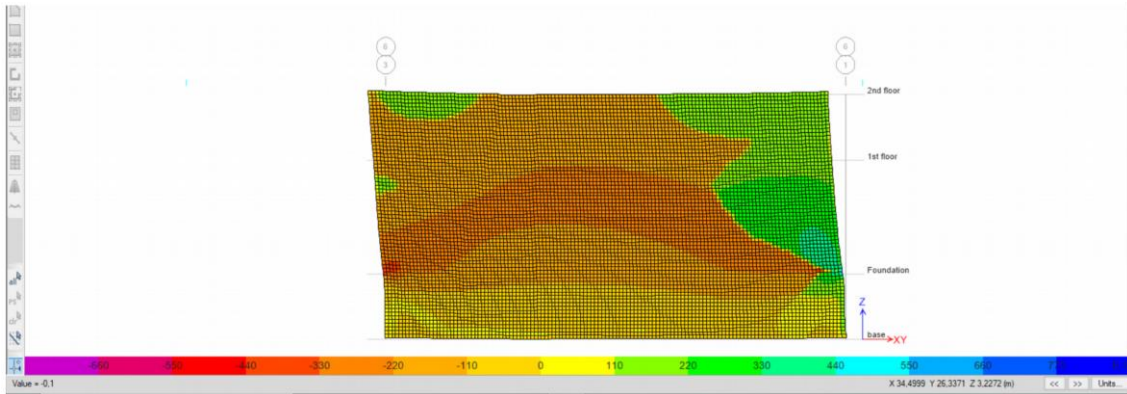


Figure 4-16 - Maximum shear stresses distribution on the south wall of the flexible model. The shear stress values [MPa] are qualitatively shown based on colour in the horizontal axis at the bottom of the image.

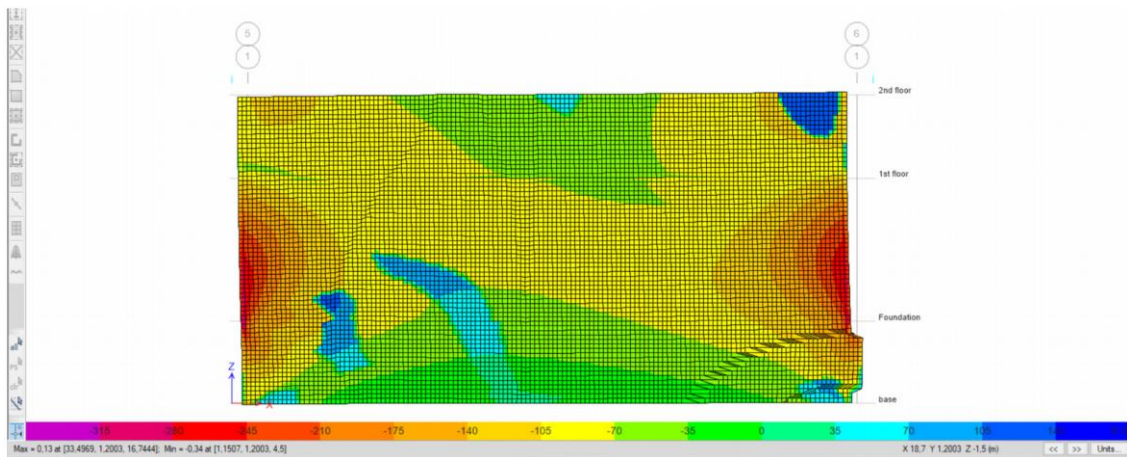


Figure 4-17 - Maximum shear stresses distribution on the west wall of the flexible model. The shear stress values [MPa] are qualitatively shown based on colour in the horizontal axis at the bottom of the image.

On the north wall of the church high positive shear stresses are registered at the left side (blue colour), while the rest of the wall is dominated by negative values (green colour), increasing at the right side (yellow and orange colour). On the south wall there are mainly negative values (orange colour), with small positive ones one the sides (green colour) and in the foundation (yellow colour). On the west wall there are mainly negative values (green and yellow colour), increasing at the two sides (red colour), with small spots of positive stress (blue colour).

- Fixed- base model: Principal stresses

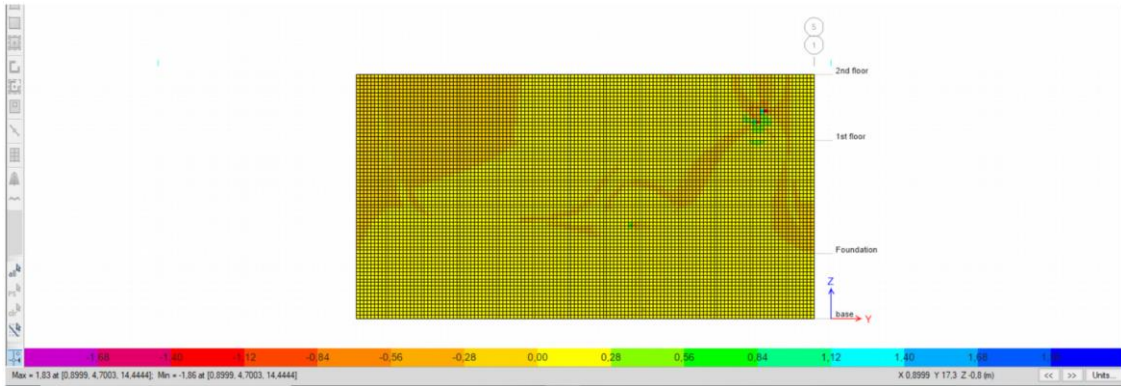


Figure 4-18 – Maximum principal stresses distribution on the north wall of the fixed- base model. The principal stress values [MPa] are qualitatively shown based on colour in the horizontal axis at the bottom of the image.

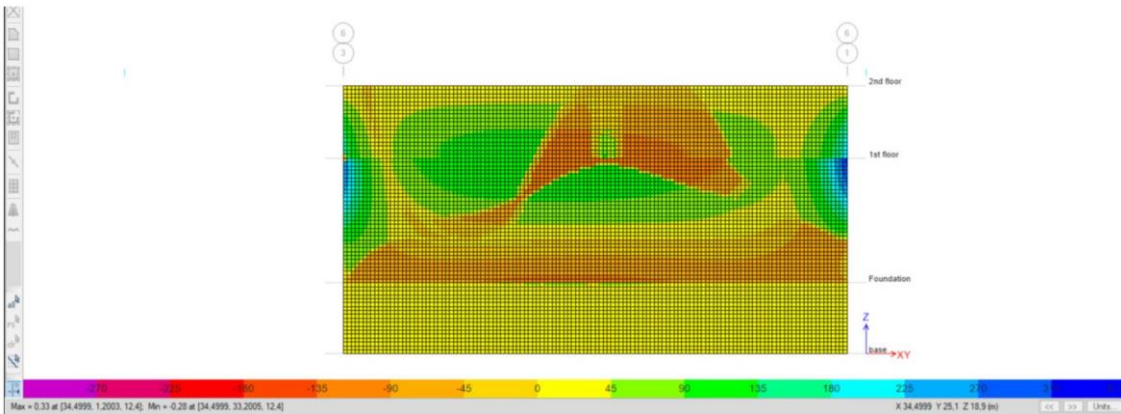


Figure 4-19 - Maximum principal stresses distribution on the south wall of the fixed- base model. The principal stress values [MPa] are qualitatively shown based on colour in the horizontal axis at the bottom of the image.

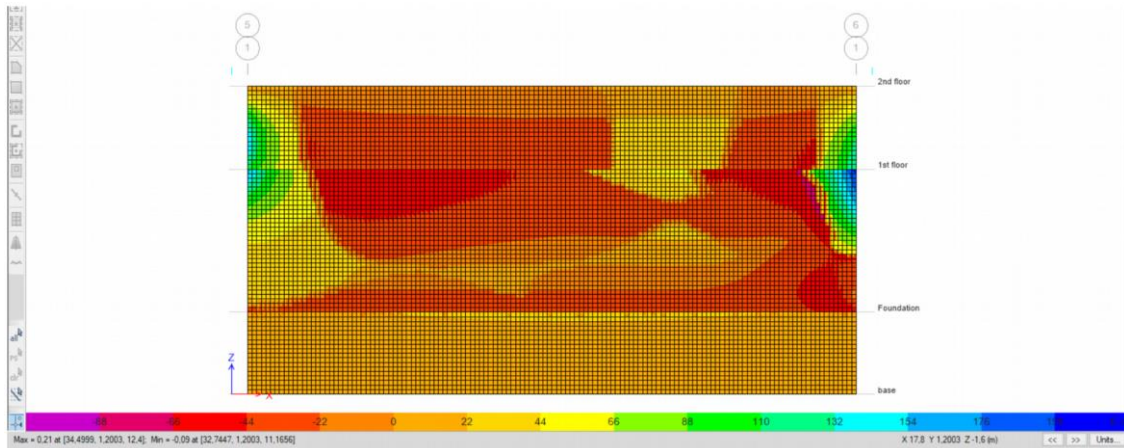


Figure 4-20 - Maximum principal stresses distribution on the west wall of the fixed- base model. The principal stress values [MPa] are qualitatively shown based on colour in the horizontal axis at the bottom of the image.

Throughout the length and height of the foundation of the three walls, the trend of principal stress is small (yellow and light orange colour). The same for the entire length of the north wall. In the south wall in the central area, the increment of the principal stresses is observed (light orange and green colour), especially on the sides (green and blue colour). On the west wall the upper part is dominated by a high value of negative stresses so compression (red colour), while the foundation is subjected to small positive ones so traction (orange colour).

- Fixed- base model: Shear stresses

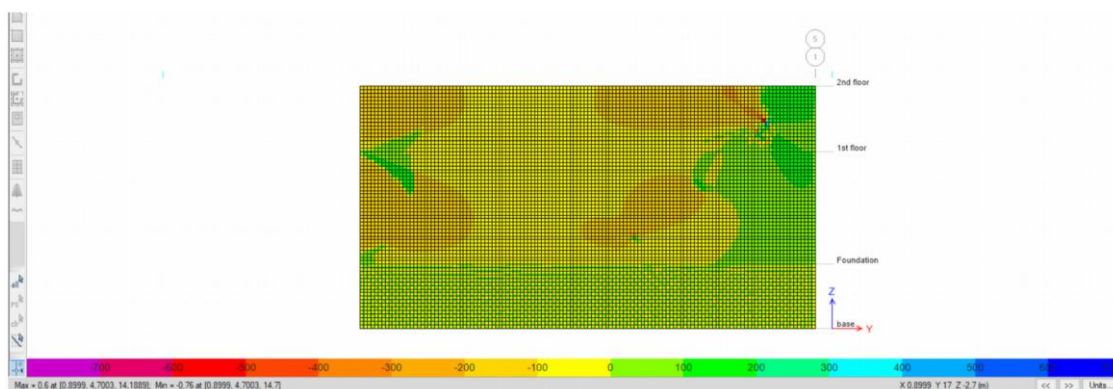


Figure 4-21 - Maximum shear stresses distribution on the north wall of the fixed- base model. The shear stress values [MPa] are qualitatively shown based on colour in the horizontal axis at the bottom of the image.

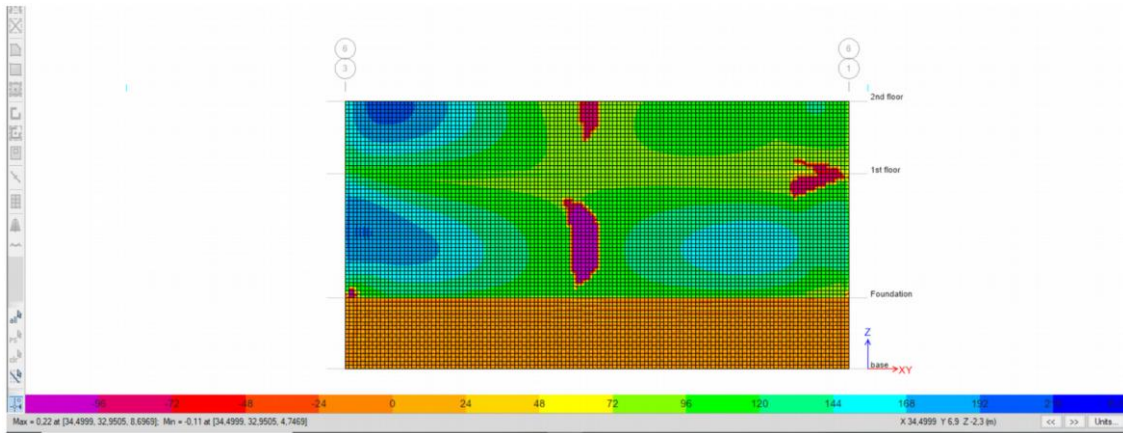


Figure 4-22 - Maximum shear stresses distribution on the south wall of the fixed- base model. The shear stress values [MPa] are qualitatively shown based on colour in the horizontal axis at the bottom of the image.

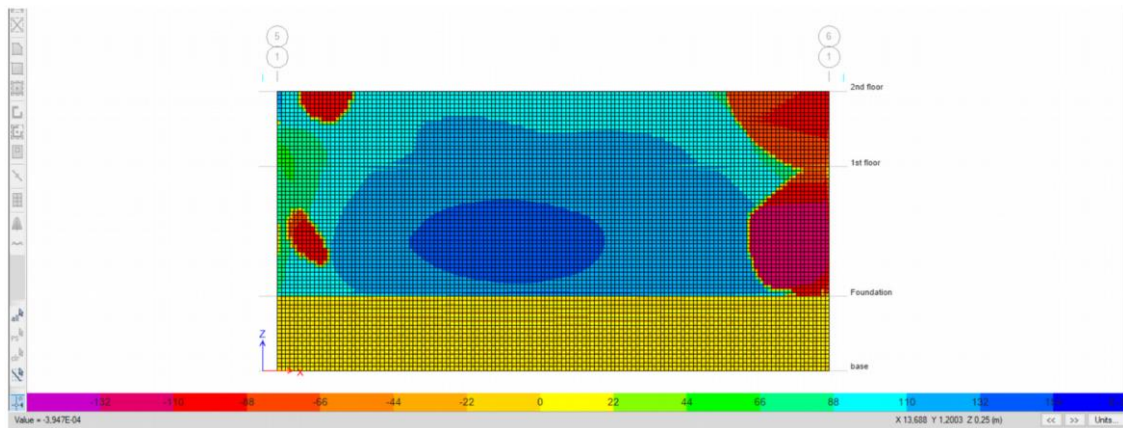


Figure 4-23 - Maximum shear stresses distribution on the west wall of the fixed- base model. The shear stress values [MPa] are qualitatively shown based on colour in the horizontal axis at the bottom of the image.

Throughout the foundation of the three walls, exclusively positive shear stresses are observed (yellow, orange and green colour). At the left side of the north wall mainly negative trends are registered, while at the right side there is a development of positive trends. A positive trend is registered in the whole south wall (from green to blue colour), but the central area and close to the joints with

other walls (red and violet colour). In the central part of the west wall there are only positive shear stresses (blue colour) with a peak in the centre, while on the join with the south wall the predominant stress is negative (red colour).

The maximum drift is shown in the following diagrams. The drift is the displacement at the top minus the displacement at the bottom, divided by the distance between the two points, so the height. It represents the rotation of the wall.

The maximum drift for the flexible model is 0,64% along the x-axis direction and 0,26% along the y-axis direction. For the fixed- base model the maximum drift is 0,52% along the x-axis direction and 0,0751% along the y-axis direction.

The model with springs has bigger drift, so maybe it is more damaged and the strengthening

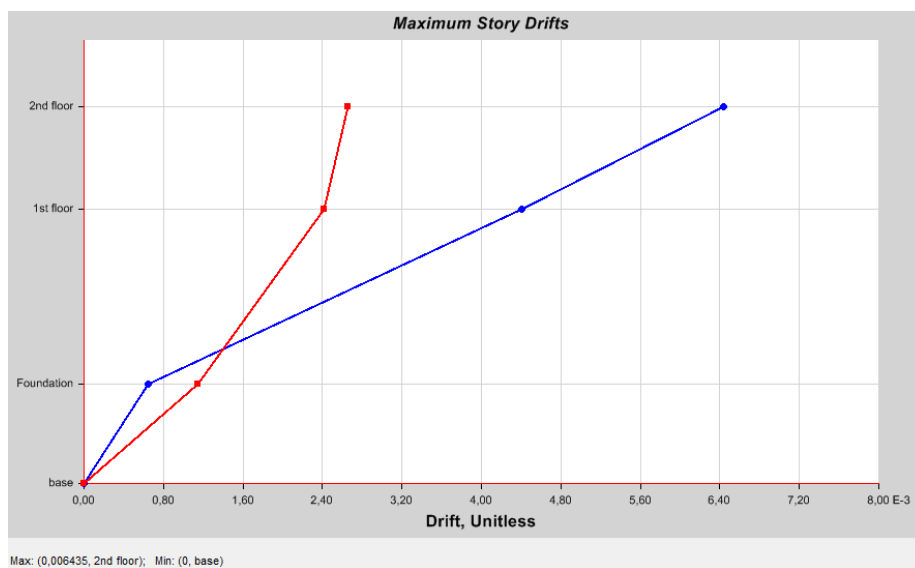


Figure 4-24 - Maximum drift in the flexible model. The blue line represents the x-axis direction and the red line represents the y-axis direction.

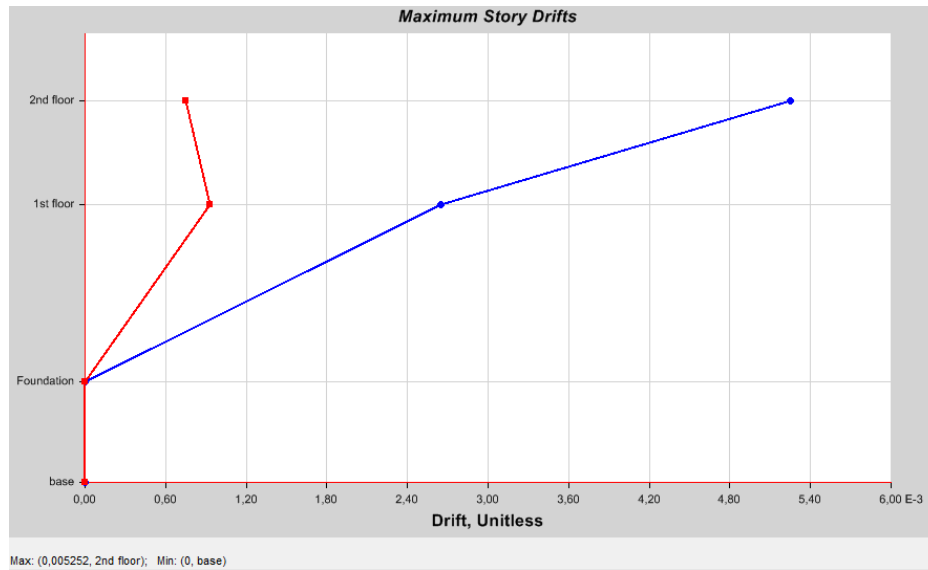


Figure 4-25 - Maximum drift in the fixed- base model. The blue line represents the x-axis direction and the red line represents the y-axis direction.

Comparing the two models, there is an increase of the drift of the construction in the flexible model with springs.

The maximum displacements do not appear in any of the four studied corners. For the flexible model they are 35,89 mm in the x-axis direction and 21,118 mm in the y-axis direction, while for the fixed- base model they are 22,318 mm in the x-axis direction and 7,97 mm in the y-axis direction.

The maximum out- of- plane displacements occur in the middle of almost every wall cause here there are not constraints, which are at the extreme points of the structure.

Due to the introduction of springs, so the influence of the soil, the displacements increase by 60% along the x-axis direction and by 175% along the y-axis direction. The influence of soil is visible even in the increase of the oscillation periods of the flexible model respect to the fixed- base one.

In areas such as the bases of the walls and the joints with other walls, which are sensitive parts of the building, increased trends are observed in both the models. In the flexible model, these increased trends seem to be higher than the ones in the fixed- base model. This indicates a higher risk of failure in the flexible simulation, so when the influence of the soil is taken into account.

# Chapter 5

## Strengthening measures

The main purpose of this dissertation is to investigate the strain of Hagia Sophia in Thessaloniki, focusing on the foundations of the building and then proposing the most appropriate measures to strengthen them.

In this chapter these strengthening measures are analysed and at the end a proposal for the most appropriate one for the Hagia Sophia Church is made.

The most important parameters that will affect the choice of the proposed reinforcement measure are the characteristics of the building and the ground, the historic importance of the construction and the financial burden.

### 5.1 Reinforcement of the foundations

Reinforcement is defined as the set of measures for upgrading the mechanical characteristics (strength, stiffness) of a structural element or building, up to a desired or required level (as for seismic design actions imposed by the current regulation).

The reinforcement is not only matter of repairing a damage, but it can also be applied as a preventive strengthening without any occurred accident. The level and measures of reinforcement are determined by a specific study.

The interventions aim at removing the pathology of the construction from a structural point of view and increasing its capacity to sustain static and seismic loads.

Two important factors that influence the choice of the reinforcement measure are the possible alteration of the architectural aspect and the degree of reversibility of the intervention.

To strengthen the foundations of a construction, the following techniques are listed:

- enlargement of the existing foundations;
- construction of new foundation next to the existing ones;
- underpinning construction;
- soil improvement;
- base isolation;
- centercore strengthening.

The studied building belongs to the category of historical load-bearing masonry constructions. This peculiarity greatly limits the possible intervention measures because each historic construction is a unique case of structural behaviour and requires a well-thought-out strategy based on specific rules. The main concern is the prevention of the architectural identity of the building.

The most common retrofit techniques for this kind of building are:

- **Enlargement of existing foundation:**  
It is the most widespread foundation retrofit technique, especially for common buildings, due to its low cost and fast application compared to the other interventions listed below. It is mainly applied in cases where the foundations need to be strengthened but no soil issues are observed. It essentially reduces the size of the strain on the foundation-soil joint thanks to the widening of the paddle pad, obtaining a reduction of the displacements and differential settlements at the foundation level.  
The load-bearing capacity improvement of the structure depends on the quality of the connection between the new reinforced concrete elements and the existing foundation. This connection requires a meticulous and extensive work, especially in case of bilateral reinforcement.
- **Deep injection using micropiles:**  
This technique is recommended to improve the bearing capacity of both the soil and the foundation. It is mainly applied in cases where working only on the foundation is not possible (eg problematic soil, high aquifer etc).  
The main advantages of using the micropiles are the immediate application and the fast construction, the avoidance of excavation work, and their ability to gradually receive part of the loads and lead to the



stabilization of the displacements. It requires the disposal of a flexible and powerful drilling rig, capable of perforating any type of soil and foundation.

The symmetrical position of the micropiles on both sides of the wall increases the efficiency. However drilling inside the building is rarely possible and the cost of application of the technique is high.

- Soil improvement:

It is the most suitable method to guarantee the harmony of the building. It is applied by inserting a stabilizing fluid under high pressure. It increases the bearing surface, when improving the bearing capacity of the ground is needed (eg soils with low initial bearing capacity, adding floors which increase ground stresses, case of excavation next to the foundations that causes relative soil instability below the construction).

It is applied to both cohesive and non-cohesive soils, as well as to rock (if it is cracked with the cracking connected to each other). It cannot be applied to soils with low permeability, as clay. The injected substance closes the gaps and improves the strength.

The efficiency of the technique depends on the uniformity of the dispersion of the grout under the foundation. In cases of non-homogeneous soils, the uniform dispersion of the grout is particularly difficult and can have significant economical consequences, especially using a low quality and price material.

## 5.2 Reinforcement using micropiles

Taking into account the historical and cultural value of Hagia Sophia Church, as well as the territorial conditions prevailing in the studied area (ancient sand embankments with pebbles and tiles combined with a very loose sand- clay mixture), the micropiles method has been chosen.

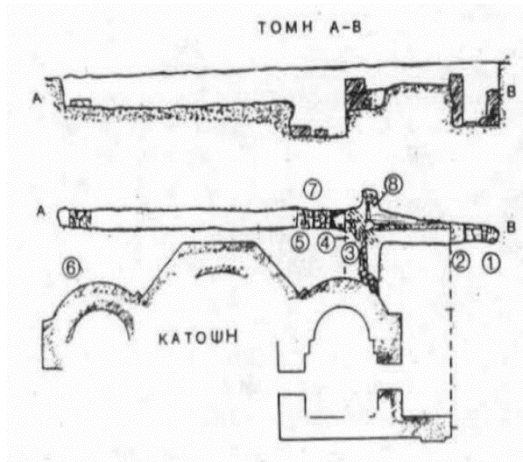


Figure 5-1 - Building and floor east plant of the Church (Pitilakis D.)

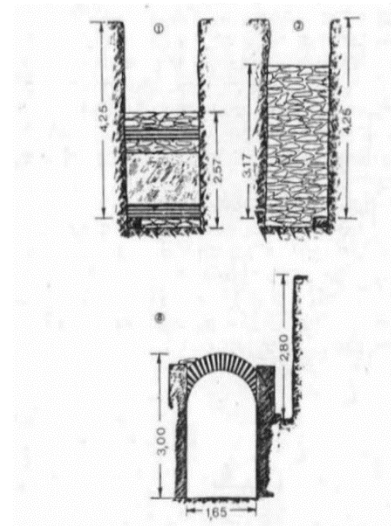


Figure 5-2 - Sections in position 1 and 2 and 8 of the Church (Pitilakis D.)

The micropiles method was conceived in Italy in the early 1950's as an innovative technique to face the damages the buildings are subjected to. It involves the drilling the pile shaft to the required depth, placing the steel reinforcement, initial grouting by tremie and placing additional grout under pressure, where applicable.

Some advantages of this technique are the high carrying capacity, speed of realization, less site constraint problems and self-sustained operation. The only disadvantage is the high cost compared to other methods.

The micropiles are small diameter pipes (from 100 mm to 250 mm), drilled, sealed and/ or injected with cement mortar and reinforced steel elements. They can reach a length of up to 20- 30 m.

These elements withstand a higher percentage of all design loads compared to conventional pipes. The loads are mainly supported by the steel part and transmitted through the mortar to the surrounding soil mostly by friction on the side.

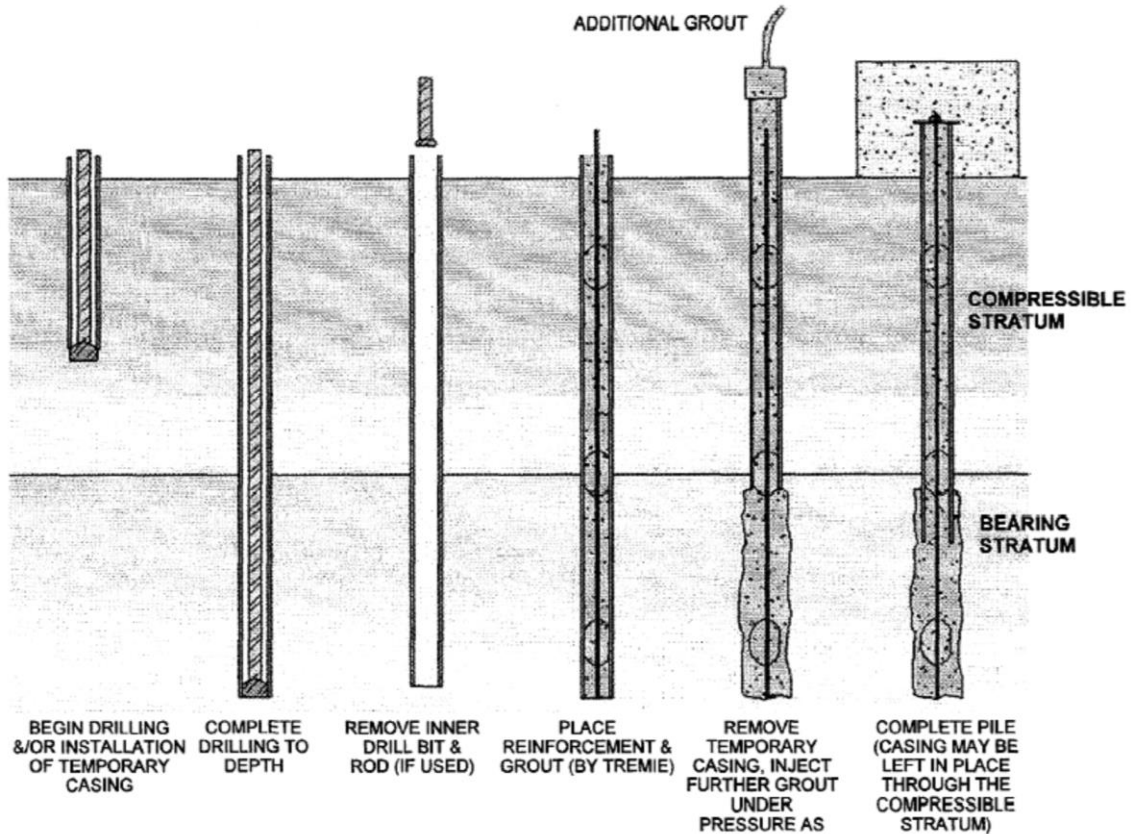


Figure 5-3 – Typical drilled micropiles construction sequence  
 (Ir. Shong, F. Chew Chung, 2003)

The installation of micropiles is done with the use of small rotary drilling rigs to open the hole. At the same time a temporary pipe is placed around the hole. When the drilling reached the desired depth, the drill bit is retrieved, and the drilling is filled with cement mortar.

Then the reinforcement is placed. It could be a central steel rod with a diameter from 25 mm to 50 mm or a more common “reinforced cage” and the embedding. The steel reinforcement occupies about 5% to 8% of the whole volume.

When the cement mortar is ready, the temporary pipe is removed, and additional pressure is applied. If the soil surrounding the foundation is divided in a soft layer and one with high strength characteristics. The temporary pipe can be kept in the soft layer.

The final and most important step is the connection between micropiles and structure.

According to the Federal Highway Administration (FHWA, 2005), there are two possible categories of micropiles based on:

- the behaviour or purpose of the micropile. Symbolized by a number.
- the method of grouting, which defines the grout- soil bond capacity. Symbolized by a letter.

In the classification based on the porpoise, there are two types:

- the CASE 1, when the micropiles are loaded directly as the main foundation system and they sustain the majority of the loads;
- the CASE 2, when the micropiles are used to reinforce the soil and increase the bearing capacity for an existing foundation system.

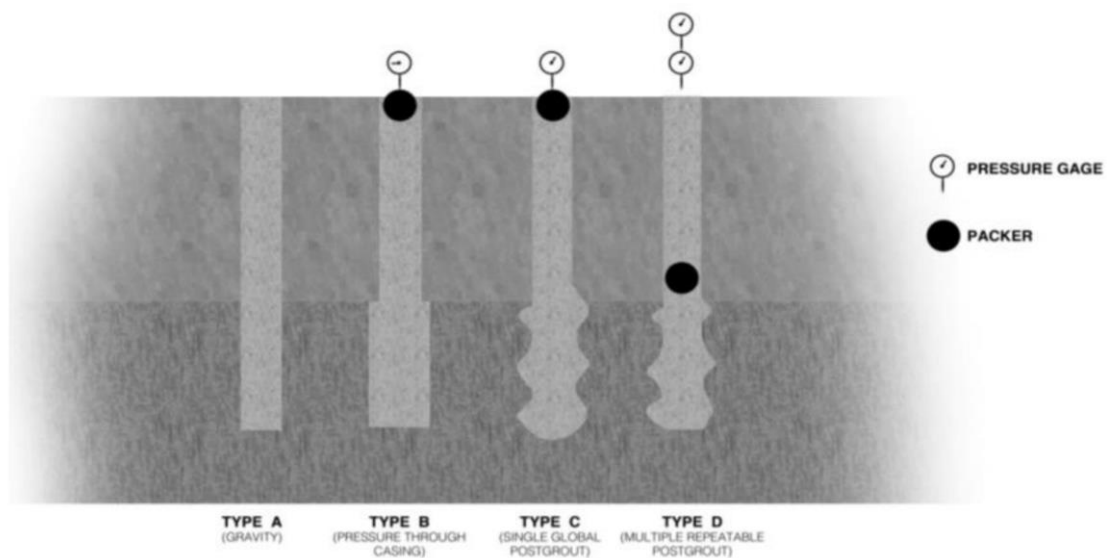


Figure 5-4 - Micropiles classification according to the types of grouting  
(A. Alnuaim, 2014)

In the classification based on the method in which the grouting is placed, there are four categories:

- type A: the grout is placed solely under gravity action from the top of the hole, with or without reinforcement;
- type B: the grout is placed by applying injection pressure, which is about 0,5 to 1 MPa, obtaining a high shaft friction due to the high penetration of the grout into the soil;
- type C: this system is performed in two steps. First the grout is placed under gravity head, as in the type A, and then after 15/25 minutes a sleeved grout pipe is used to inject similar grout at minimum 1 MPa

pressure. The pipe has valves at intervals of 1 m and the grout is injected the help of a special device. As for the type B, the shaft friction is high;

- type D: similar to the type B, but the additional grout of the second step is injected at a pressure of 2 to 8 MPa. To increase the friction capacity of the bond, a packer is use inside the sleeved pipe. The side friction is very high (more than the other types) and the grout- to grout bond is about 63% higher than type A.

The behaviour of the micropiles vary depending on the type of soil and the grouting method.

In terms of structural function, the resistance of the micropiles is mobilized by lateral friction of the soil, as they are often applied to poor quality soils. If the foundation is on solid rock and the micropiles are injected under pressure with an enlarged base being formed, they can work as ordinary piles.

They are mainly resistant to axial strength due to their small section. When they must resist to lateral loads, the micropiles can be executed in the spatial direction that favours the conversion of the lateral strength to axial strength.

The micropiles strongly mobilize the lateral friction of the foundation and allow the effective control of the settlements and the small movements of the building they support.

About the execution, they can be drilled, self- drilled or driven.

The first applications of the micropiles aimed at strengthening the foundations, controlling the excessive settlement of the building, raising the bearing capacity of the foundations to withstand an increase of the loads due to additional floors and strengthening existing structures against earthquakes.

They are also used to improve the ground, in embankments and retaining walls, where anchors cannot be used due to the characteristics of the soil or because the amount of material to be injected is difficult to estimate.

Their use in the new building construction consists of a deep foundation with a contribution to withstand the lifting due to high aquifer or a particularly bad soil condition. In both cases, in contrast to other techniques, the effect of the lateral friction of the micropiles leads to the mobilization of a satisfactory load (bearing capacity). They are also used in very thin foundations for their contribution against the earthquake.

In the restoration field, the micropiles have been used to support foundations with excessive settlement, where the ground resistance is not enough to withstand the load of the superstructure or an additional load. Such a load may be imposed on the construction due to additional floors or a change in the function of use of the building, when strengthening the foundation or improving the soil would be not economically feasible or when these methods result too complex to apply (high aquifer, soft ground, etc).

They are also used to enhance anti- seismic reinforcement of existing structures, for the expansion under existing structures and in neighbouring works that could affect the close existing foundations (excavations, tunnels, adjacent buildings whose foundations are at a lower level).

This method can be implemented in two ways:

- without underpinning, crossing the existing masonry elements, provided they are long and strong enough to anchor the micropile;
- with underpinning, using steps or plinths, helping the micropiles to connect to the existing foundations.

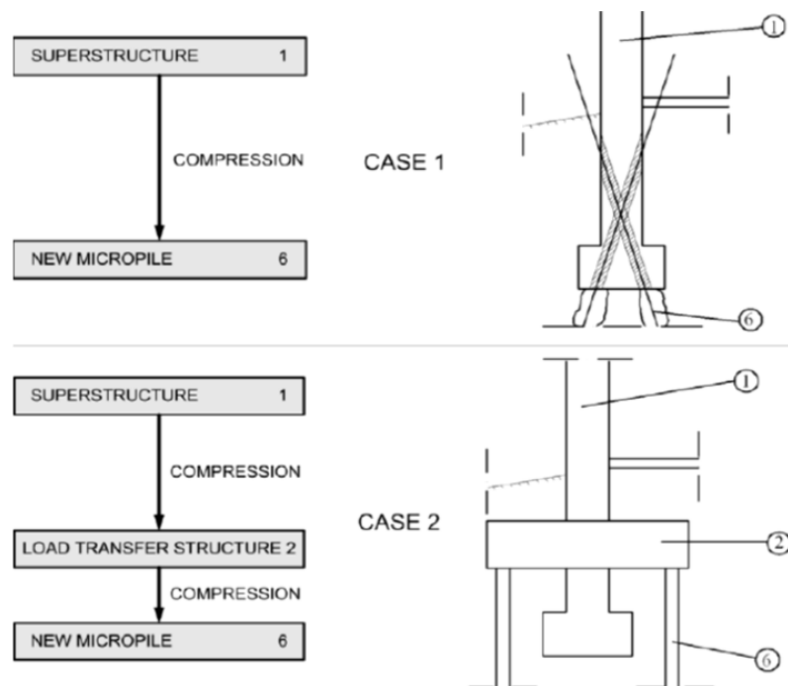


Figure 5-5 - Modalities of application of the micropiles without underpinning (top) and with underpinning (below)  
(T. R. S. Antunes, 2012)

The micropiles are often used when rehabilitation involves strengthening foundations.

They can be easily executed in relatively confined spaces with low ceiling. They have a small diameter. They do not usually require chambers to be created under the existing foundations and can be made to intersect existing foundations (being executed at a higher level avoids the need of prior excavation to the bottom of the existing foundation).

### 5.3 Simulation of micropiles and reinforcement results of the analysis

To simulate the micropiles in the model, the spring parameters are increased. This is achieved by increasing the value of the shear modulus by 50% as suggested by Professor Pitilakis. An example:

$$G = 159,837 \cdot 1,5 = 239,755$$

It is like having stiffer springs.

So the spring constants change as shown in the tables below.

Section	$k_z$	$k_y$	$k_x$	$k_{z, \text{uploaded}}$	$k_{y, \text{uploaded}}$	$k_{x, \text{uploaded}}$
$\tau\mu 1$	17395432,5	18877074,49	15055753	128855	8348,99	442816
$\tau\mu 2$	16842338,6	18339684,11	14695002	132617	8494,53	432206
$\tau\mu 3$	17395432,5	18877074,49	15055753	128855	8101,75	442816
$\tau\mu 4$	16842338,6	18339684,11	14695002	132617	8494,53	432206
$\tau\mu 5$	8603118,91	10428179,58	9213121	204836	14605,3	541948
$\tau\mu 6$	9473080,01	11265391,98	9807518	185747	13523,9	576913
$\tau\mu 7$	9473080,01	11265391,98	9807518	185747	13523,9	576913
$\tau\mu 8$	8603118,91	10428179,58	9213121	204836	14605,3	541948
$\tau\mu 9$	6961501	8806312,971	8055880	248625	19185,9	473875
$\tau\mu 10$	8910813,42	10725177,63	9424274	189592	14019,8	277185
$\tau\mu 11$	6961501	8806312,971	8055880	248625	19185,9	473875

Table 5-1 - Spring parameters after increasing the shear modulus  $G$  by 50%

These new values are applied to the model, as previously done in the chapter 3.3.5.

After the analysis, if smaller drifts and displacements will be registered, the micropiles method will be considered an effective measure of retrofit.

The periods with an increased value of the shear modulus are 0,413 s in the x-axis direction and 0,368 s in the y-axis direction.

While for the previous not increased value of the shear modulus, the periods were 0,43 s in the x-axis direction and 0,379 s in the y-axis direction.

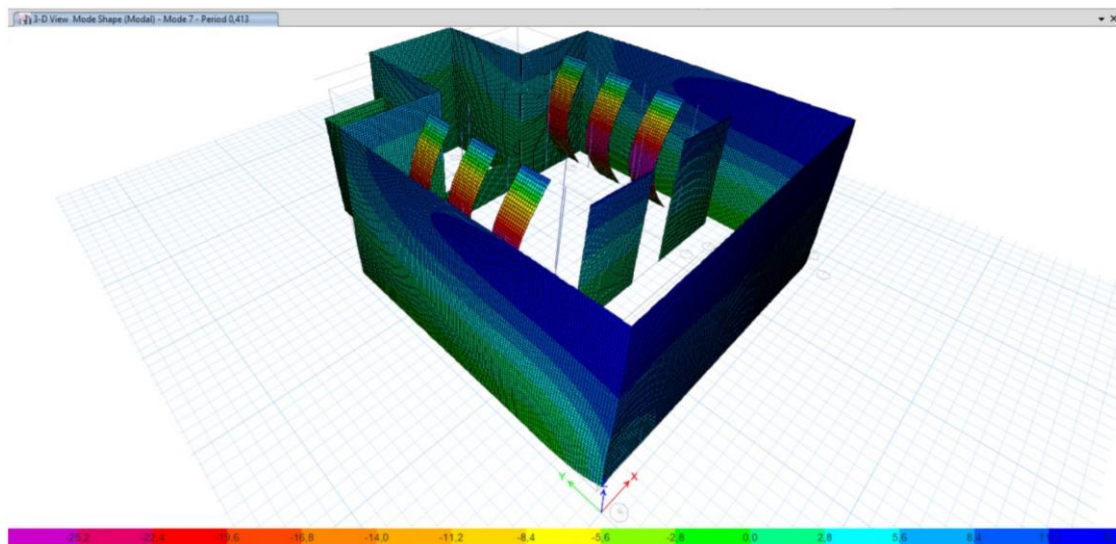


Table 5-2 - Modal analysis of the flexible model in x-axis direction with micropiles. The displacements values [mm] are quantitatively (based on colour) shown in the horizontal axis at the bottom of the image.



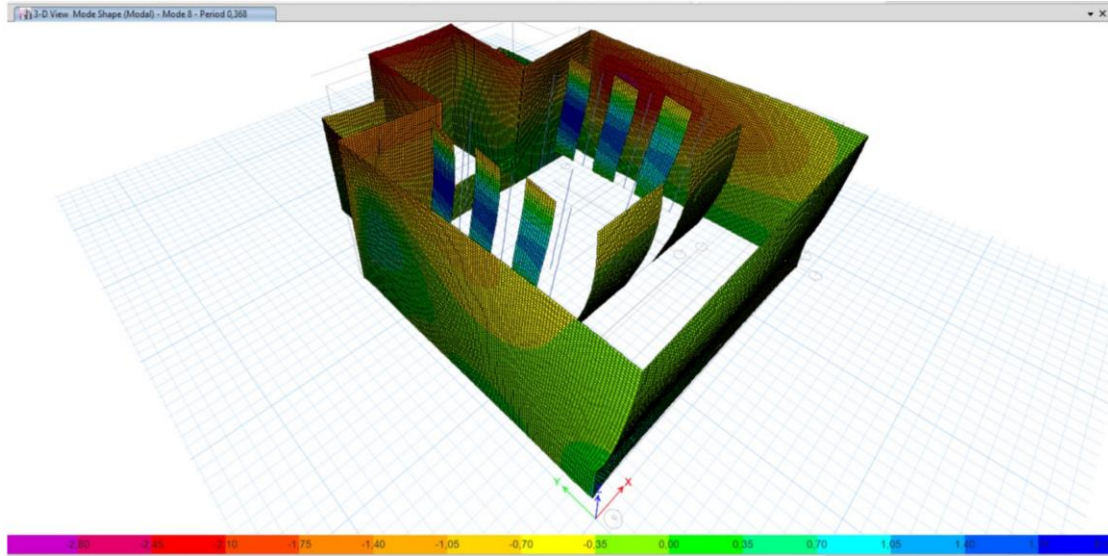


Table 5-3 - Modal analysis of the flexible model in y-axis direction with micropiles. The displacements values [mm] are quantitatively (based on colour) shown in the horizontal axis at the bottom of the image.

Thanks to the micropiles method application, the maximum displacements decrease in the majority of the studied points.

Flexible model with micropiles							
North - West				North - East			
Elevation	x	y	z	Elevation	x	y	z
12,5	-13,393	-15,16	-2,996	12,5	-10,035	-15,16	-2,439
0	-7,531	3,061	-3,214	0	-1,254	-6,865	-1,365
-4,5	-5,129	0,795	-1,119	-4,5	-0,359	-5,26	-0,522
South - West				South - East			
Elevation	x	y	z	Elevation	x	y	z
12,5	-13,393	17,278	2,36	12,5	-10,035	17,278	4,47
0	-7,84	2,663	2,1	0	1,154	2,295	2,633
-4,5	-6,005	-0,749	0,833	-4,5	-0,787	0,652	0,923

Table 5-4 - Maximum displacements at the four corners of the flexible model with micropiles at the top of the building, at the ground level and at the lowest point of the foundation. The values are given in mm.

Flexible model with micropiles			
Side	x	y	z
North (middle)	-9,231	-10,958	-0,465
West (middle)	-11,68	-13,329	-0,29
South (middle)	-10,982	11,26	0,212

Table 5-5 - Maximum displacements in the middle of each side of the flexible model with micropiles, except the side of the sanctuary. The values are given in mm.

The maximum principal and shear stresses distribution in the model with increased G are shown in the following images, respect to three walls of the building (at north, south and west). The maximum values are not simultaneous.

- Flexible model with micropiles: Principal stresses

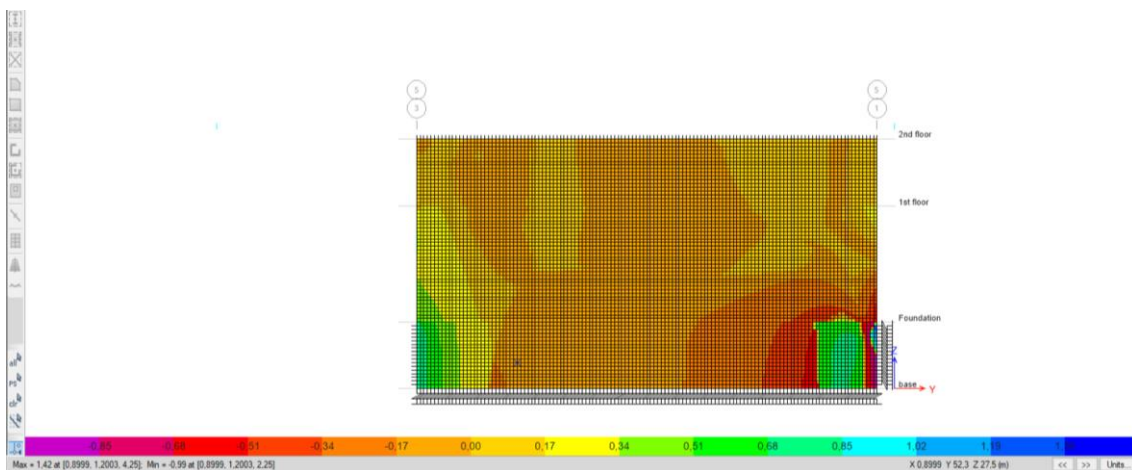


Figure 5-6 - Maximum principal stresses distribution in the north wall of the flexible model with micropiles. The principal stress values [MPa] are qualitatively shown based on colour in the horizontal axis at the bottom of the image.

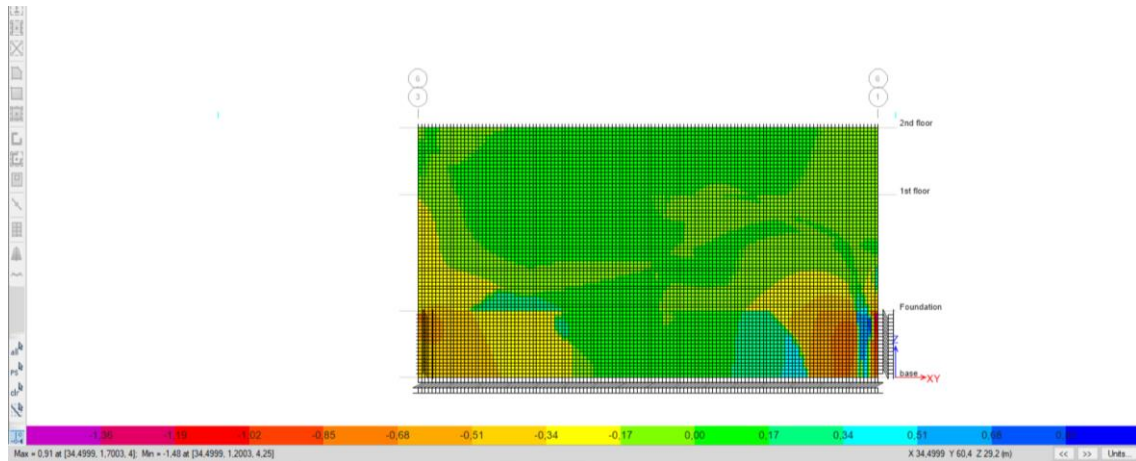


Figure 5-7 - Maximum principal stress distribution in the south wall of the flexible model with micropiles. The principal stress values [MPa] are qualitatively shown based on colour in the horizontal axis at the bottom of the image.

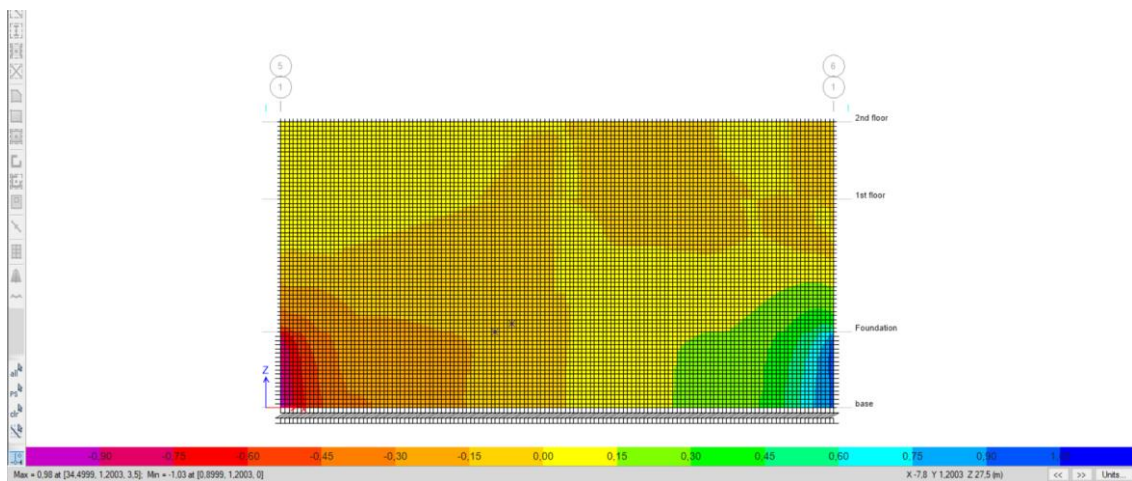


Figure 5-8 - Maximum principal stresses distribution in the west wall of the flexible model with micropiles. The principal stress values [MPa] are qualitatively shown based on colour in the horizontal axis at the bottom of the image.

In the model with micropiles, in the north wall the majority of the principal stresses are small and negative (orange colour), while at the junction with other walls, at the foundation height the values increase both on the positive and negative side.(green and red colour). On the south wall, on the contrary, there is mostly traction (green colour), but not at the junctions with other walls where they is small compression (yellow and orange colour). On the west wall the small stresses are both negative (orange colour) and positive (yellow colour)

in the majority of the structure, while on the left bottom the negative values (red colour) and on the right one the positive values (green colour) increase.

- Flexible model with micropiles: Shear stresses

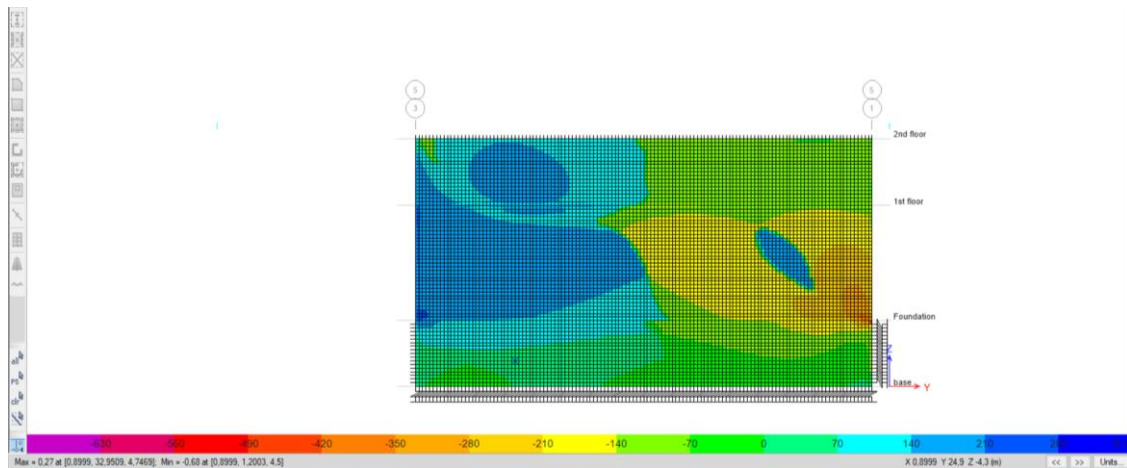


Figure 5-9 - Maximum shear stresses distribution in the north wall of the flexible model with micropiles. The shear stress values [MPa] are qualitatively shown based on colour in the horizontal axis at the bottom of the image.

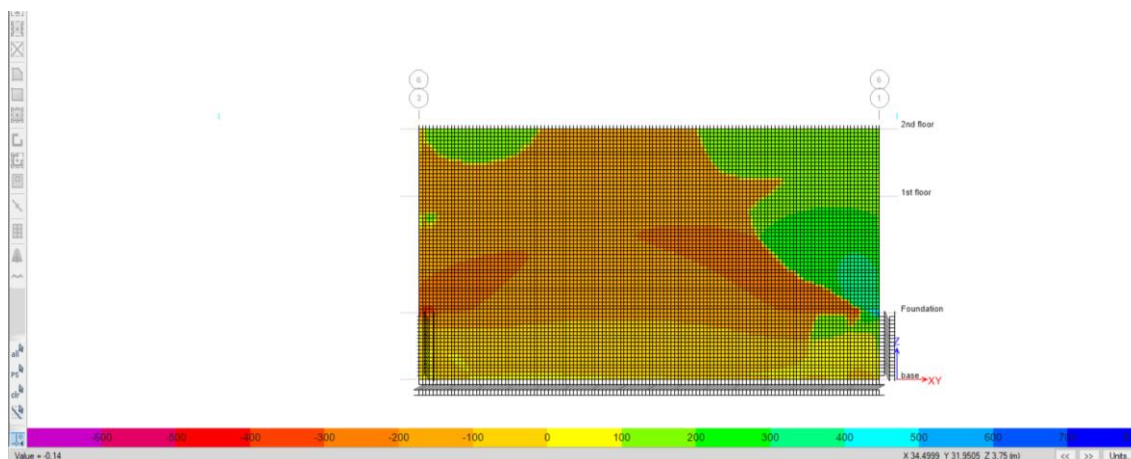


Figure 5-10 - Maximum shear stresses distribution in the south wall of the flexible model with micropiles. The shear stress values [MPa] are qualitatively shown based on colour in the horizontal axis at the bottom of the image.

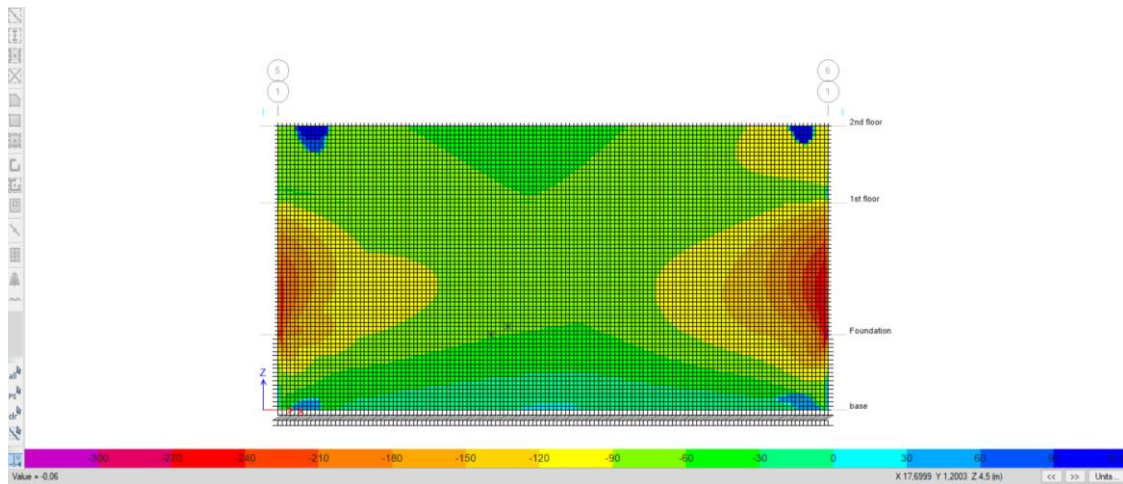


Figure 5-11 - Maximum shear stresses distribution in the west wall of the flexible model with micropiles. The shear stress values [MPa] are qualitatively shown based on colour in the horizontal axis at the bottom of the image.

In the north wall the developing trends are separated, being negative on the right (green, yellow and orange colour) and positive on the left (blue colour). On the south wall there is concentration of positive stresses at the right side (green colour), while the rest of the surface is dominated by negative values (orange colour). On the west wall the negative trends predominate (green colour) with higher values on the junctions with other walls (red colour)

From the results of the analysis on the reinforced model, the increased construction stiffness, the reduction of the oscillation period and of the displacements are registered, respect to the original flexible model. There is a more uniform distribution of principal stresses. Therefore the micropiles technique results to be effective.

# Chapter 6

## Conclusions

Examining the results from the analysis under seismic loads for both the flexible model and the fixed- base model, some conclusions are drawn regarding the building behaviour. Comparing the two models, there is an increase of the drift and maximum stresses of the construction in the flexible model with springs.

The maximum out- of- plane displacements occur in the middle of almost every wall cause here there are not constraints, which are at the extreme points of the structure.

It is observed that due to the introduction of springs, so due to the influence of the soil, the displacements increase by 60% along the x-axis direction and by 175% along the y-axis direction.

The influence of soil is visible even in the increase of the oscillation periods of the flexible model respect to the fixed- base one.

This indicates a higher risk of failure in the flexible simulation, so when the influence of the soil is taken into account.

The inclusion of soil influence is meaningful since the results can be very different. Without the soil influence, the model could seem resistant, while in a flexible base case the need of strengthening would appear.

The influence of dynamic soil- superstructure interaction plays an important role in the construction response. A proper simulation of the foundation cannot be merely based on a fixed- base model. Taking into account the interaction of the soil is necessary in the assessment of the vulnerability of the structure and while dealing with seismic hazard.

An important conclusion is that the reliability of the results depends on a very large extent on the assumptions and simplifications made during the modelling phase.

Finally, applying the micropiles technique to the model, by increasing the shear modulus by 50%, provides a visible improved result of the response of the construction.

The micropiles strengthening technique can be considered a valuable and effective method to reduce the damages on the building, while preserving its aesthetical and historical values.

## References

- T. Albanesi, C. Nuti. *Analisi statica non lineare (pushover)*. Dipartimento di strutture, Roma Tre (2007).
- M. Alexoudi, Th. Hatzigogos, K. Pitilakis. *Earthquake- hazard assessment in Thessaloniki, Greece: elevel 1: Probabilistic & deterministic approach*. Earthquake loss estimation and risk reduction (2002).
- S. Alfieri. *Il problema dell'interazione suolo struttura per gli edifici storici: il caso ghirlandina e del duomo di Modena*. PhD thesis at Università degli studi di Parma.
- A. Alnuaim. *Performance of micropiled raft in sand and clay- centrifuge and numerical studies*. Graduate program thesis at The University of Western Ontario (2014).
- T. R. S. Antunes. *Rehabilitation of foundations of old buildings using micropiles*. Master's dissertation at Tecnico Lisboa (2012).
- P.G. Asteris, M.G. Doubika, M. Apostolopoulou, A. Moropoulou. *Seismic and restoration assessment of monumental masonry structures*. Materials (2017).
- M. Basil, R. Kumar. *Earthquake resistant design of masonry buildings in Kashmir*. International Journal of Advanced Research in Education & Technology (2016).
- J. Bothara, S. Brzev. *A tutorial: improving the seismic performance of stone masonry buildings*. EERI (2011).
- F. Cakir, F. Kocygit. *Architectural and structural analysis of historical structures*. Gradevinar (2016).
- A.K. Chopra. *Dynamics of structures*. Prentice Hall International (1995).
- G. Croci. *General methodology for the structural restoration of historic buildings: the cases of the Tower of Pisa and the Basilica di Assisi*. Journal of Cultural Heritage 1 (2000).



M.J. DeJong. *Seismic assessment strategies for masonry structures*. Massachusetts institute of technology (2009).

A. Di Lernia, D. Boldini, A. Amorosi. *Interazione dinamica terreno- struttura: il caso di Lotung*. IARG (2015).

*Eurocode 8: Design of structures for earthquake resistance – Part 1: General rules, seismic actions and rules for buildings*.

A.W. Hendry, B.P. Sinha, S.R. Davies. *Design of masonry structures*. E & FN SPON (2004).

C. Ignatakis, Professor at School of Civil Engineering, Aristotle University of Thessaloniki, Greece. Personal communication.

A. Karatzetzou, D. Pitilakis, M. Krzan, V. Bosiljkov. *Soil- foundation- structure interaction and vulnerability assessment of the Neoclassical School in Rhodes, Greece*. Bull Earthquake (2015).

A. Karatzetzou, D. Pitilakis. *Reduction factors to evaluate acceleration demand of soil- foundation- structure systems*. Soil Dynamic and Earthquake Engineering 109 (2018).

C.G. Lai. *Interazione dinamica terreno struttura di edifici con fondazioni superficiali e profonde*. Eucentre (2011).

G. Magenes. *Edifici con struttura in muratura*. Dipartimento di Meccanica Strutturale, Università di Pavia (2003).

G. Magenes. *Masonry building design in seismic areas: recent experiences and prospects from a European standpoint*. First European Conference on Earthquake Engineering and Seismology (2006).

T. Paulay, M.J.N. Priestley. *Seismic design of reinforced concrete and masonry buildings*. John Wiley & Sons, Inc (1992).

D. Pitilakis, A. Karatzetzou. *Dynamic stiffness of monumental flexible masonry foundations*. Bull Earthquake Eng (2015).

D. Pitilakis, K. Iliou, A. Karatzetzou. *Shaking table tests on a stone masonry building: modelling and identification of dynamic properties including soil- foundation- structure interaction*. International Journal of Architectural Heritage (2018).

K.D. Pitilakis, A.J. Anastasiadis. *Soil and site characterization for seismic response analysis*. Proceeding of the XI ECEE, Paris 6-11 Sept. 1998, Inv. Lectures, pp.65-90.

K. Pitilakis, D. Raptakis, K. Lontzetidis, Th. Tika- Vassilikou, D. Jongmans. *Geotechnical and geophysical description of euro- seistest, using field, laboratory tests and moderate strong motion recordings*. Journal of earthquake engineering, Vol 3, No. 3 (1999), pp. 381-409

S. Prabhu, S. Atamturktur, D. Brosnan, P. Messier, R. Dorrance. *Foundation settlement analysis of Fort Sumter National Monument: Model development and predictive assessment*. Engineering Structures 65 (2014).

Ir. Shong, F. Chew Chung. *Design and construction of micropiles*. Gue & Partners Sdn Bhd, Kuala Lumpur (2003).

T. G. Sitharam. *Advanced Foundation Engineering*. Indian Institute of Science, Bangalore (2013).

K. Theoharidou. *The architecture of Hagia Sophia, Thessaloniki*. From its erection up to the Turkish conquest. BAR International Series 399, 1988

M. Todorovska, M. Trifunac. *Flexible versus rigid foundation models of soil- structure interaction: incident sh- waves*. Japan Workshop on Soil- Structure Interaction (2001).

A.I. Unay. *Evaluation of the structural safety of historical masonry buildings*. Architectural Science Review volume 50.1 (2006).

M. Ziyaeifar, H. Meshki, M. Rajaei. *Rehabilitation of historical buildings subjected to seismic hazards, a methodology*. 13<sup>th</sup> World Conference on Earthquake Engineering, Vancouver (2004).

[https://www.researchgate.net/publication/299413084\\_Chapter\\_15\\_MICROPILE\\_S\\_-\\_APPLICATION\\_AND\\_METHODS\\_OF\\_CALCULATION](https://www.researchgate.net/publication/299413084_Chapter_15_MICROPILE_S_-_APPLICATION_AND_METHODS_OF_CALCULATION)

<https://books.google.es/books?hl=it&lr=&id=2IUqVtspYKgC&oi=fnd&pg=PA65&dq=pitilakis+1999+wave+velocity&ots=Y1yCdQIdeZ&sig=jiL00DP4jPAIH2GPPeA8FNRyp1U#v=onepage&q=pitilakis%201999%20wave%20velocity&f=false>

<https://www.roush.com/wp-content/uploads/2015/09/Insight.pdf>

<https://www.sciencedirect.com/topics/engineering/standard-penetration-test>

<https://www.geologismiki.gr/Documents/SPTCorr/files/%7B3DDAFA3F-2547-4CF9-9E16-1B15C0659329%7D.htm>

<https://www.geosystemsbruce.com/v20/biblio/286%20-%20Micropile%20Installation%20Methods%20and%20Selection.pdf>